MULTIQUARK STATES
IN THE BAG MODEL

P. J. G. Mulders

MULTIQUARK STATES IN THE BAG MODEL

MULTIQUARK STATES IN THE BAG MODEL

PROEFSCHRIFT

Contents

In the last thirty years there has been a proliferation of the
strongly interacting subnuclear particles or hadrons, of which the
nucleons are the oldest known ones. The quark model, proposed in 1964
[Gel 64, Zwe 64] gave a natural explanation for the large number of
hadrons. It also explained the regularities in the quantum numbers
which had to be assigned to these hadrons in order to understand their
stability and their decay modes. The known hadron spectrum could be
satisfactory described by states consisting of a quark and an anti-
quark $(Q\bar{Q})$, the mesons, and by states consisting of three quarks (Q^3),
the baryons. States with such quantum numbers that could not be
realized by $Q\bar{Q}$ or Q^3 states were called *exotic* hadrons. No real exotics
were known; states like the deuteron or possible other candidates were
explained as bound states or resonances as the result of the (attrac-
tive) meson exchange forces between the hadrons.

In the last few years this situation has changed, for which two
main reasons can be pointed out. The first reason is the MIT bag model,
developed in 1974 [Cho 74], which made it possible to make quantitative
predictions for multiquark states. Jaffe [Jaf 77.2] convincingly showed
that the $J^{PC} = 0^{++}$ mesons, $\varepsilon(760)$, S*(980) and δ(980) are *crypto-exotic*
states; they are exotic because of their quark content $(Q^2\bar{Q}^2)$, but they
have non-exotic quantum numbers which can be also realized by $Q\bar{Q}$ mesons.
Jaffe [Jaf 77.1] also predicted (exotic) Q^6 states and indicated that
the $\Lambda(1405)$ is a possible crypto-exotic baryon [Jaf 76]. The second
reason is the experimental indications which exist for (real) exotic
Q^6 states in the baryon-baryon channels and exotic $Q^4\bar{Q}$ states with

exotic hypercharge Y = 2 (Z* resonances).

The MIT bag model is a phenomenological application of Quantum Chromo Dynamics (QCD), which describes the color interactions between the quarks. The fact that the quarks are (permanently) confined to the hadron might be a consequence of QCD. In anticipation of the proof of this a group of theorists at MIT developed a relativistic quark model with built-in confinement [Cho 74]. The model has been very successful in describing the masses and some of the static parameters of the light $Q\bar{Q}$ and Q^3 hadrons [DeG 75]. Also the calculation of the masses of the $Q^2\bar{Q}^2$ mesons [Jaf 77.2, Jaf 77.3] has been very successful and has proven that probably reliable calculations for multiquark states can be performed.

The description of orbitally excited hadrons by a bag containing one or more quarks in higher orbits has not been very successful [DeG 76]. This as contrasted with the phenomenological extension of the bag model to stringlike rotating bags [Joh 76]. For the actual calculations of those orbitally excited multiquark states slightly different approaches are possible. In the approaches followed by the MIT group [Jaf 78] and the Nijmegen group [Mul 78.2, Mul 79.1] the intercepts M_0 of the trajectories (the mass squared M_ℓ^2 versus the orbital angular momentum ℓ) are the masses of the physical $\ell = 0$ (s-wave) hadrons, for which the MIT bag model has proven to be successful. Our approach differs from the one by Jaffe in the treatment of the color interactions. Jaffe postulates straight parallel trajectories for *all* multiquark states with a certain color configuration; the color interactions become weaker for increasing orbital angular momentum. We postulate straight parallel trajectories for the multiquark states with a certain

2

color configuration when we neglect the color interactions. The splitting due to the color interactions is assumed to be independent of the orbital angular momentum; this is an assumption which follows more naturally. Our specific choice for the treatment of the color interactions has been confirmed by the behaviour of the trajectories for the orbitally excited Q^3 baryons.

The resulting mass operator enables us to determine the mass spectrum for all multiquark states without any other parameters than the quark masses and the three bag parameters which have been determined from the light $Q\bar{Q}$ and Q^3 hadron spectra. The proper calculation for the orbital excitations with small angular momentum ℓ (for the baryons those ones with $\ell = 1$) needs some phenomenological contributions.

In the past few years we have considered the following s-wave multiquark states and their orbital excitations: $Q\bar{Q}$ and $Q^2\bar{Q}^2$ mesons, Q^3 and $Q^4\bar{Q}$ baryons and Q^6 dibaryons. In addition to calculating their masses we have considered their stability and possible decay modes and we tried to assign them to experimental states. The classification of multiquark states has also led to an alternate classification of the ordinary Q^3 baryon resonances.

The results for the $Q\bar{Q}$, the $Q^2\bar{Q}^2$ and the s-wave Q^6 states were the subjects of the thesis of A.T. Aerts [Aer 79.1], while the Q^3, the s-wave $Q^4\bar{Q}$ and the Q^6 states are the subjects of this thesis.

The content of this thesis is as follows: this introduction is followed by a more extensive discussion of the MIT bag model and the underlying concepts. The second chapter deals with the phenomenological mass operator for multiquark states. As an example we treat the

3

trajectories for orbitally excited $Q\bar{Q}$ mesons. We also briefly discuss the stability of the multiquark states. The baryon resonances, Q^3 and $Q^4\bar{Q}$, are the subject of the third chapter and the dibaryon resonances are the subject of the fourth chapter.

1.1. Elementary particles

Whenever physicists have found symmetric patterns in nature, they have searched for an explanation. Usually the symmetry indicates a composite structure of the system in question: The SU(3) multiplets in which the nadrons can be arranged, arise in a natural way when these hadrons are composite. In 1964 three quarks (u, d, s) were proposed as mathematical basic states [Gel 64, Zwe 64]. Although these quarks have not been seen as free particles, there is at present little doubt of their existence as real constituents inside the hadrons. For a review of the developments in the past twenty years we refer the reader to the thesis of A.T. Aerts [Aer 79.1].

In this thesis we will consider the quarks and leptons as the "elementary" particles, as there are at present no indications - except maybe their number - for a composite structure. Five quarks are known. The properties in wnich these five quarks differ from each other are summarized in the flavor assigned to each quark. Next to these there are internal degrees of freedom. The quarks are fermions with spin 1/2. Two possible spin or helicity states are possible, in the latter case called left- and right-handed. Besides the ordinary electric charge, through which the quarks couple to the photon, the quarks have a "color" charge, through which they couple to gluons. There are three colors which are the basis of an SU(3) symmetry, referred to as color SU(3) or SU(3,C). A list of the quarks is given in table 1.1.

Quarks with different flavors are considered as different quarks, because the flavor of a quark is not affected by the strong interactions. This may be expressed by the association of a conserved quantum number to each flavor: isospin (I) and its third component (I_3),

quark	flavor	Q/e	I	I_3	Y	S	C	B
u	up	2/3	1/2	+1/2	+1/3	0	0	0
d	down	-1/3	1/2	-1/2	+1/3	0	0	0
s	strange	-1/3	0	0	-2/3	-1	0	0
c	charm	2/3	0	0	0	0	1	0
b	bottom	-1/3	0	0	0	0	0	1
(t	top	2/3)						

Table 1.1:   The quarks, their flavors, charges in multiples of e and
"flavor" quantum numbers.

strangeness (S) or equivalently hypercharge (Y), charm (C) and beauty
(B). Although flavor is not affected by the strong interactions, quarks
with different flavor do not behave completely the same with respect to
strong interactions because they have a different mass. This mass of
course is not the physical mass, as quarks have not been observed as
free particles, but it is model-dependent, e.g. the mass entering in
the Lagrangian which describes the interactions between the quarks.
The u- and d-quarks, who have the lightest masses, have very
similar properties and form the basic representation of the isospin
SU(2) symmetry group, referred to as SU(2,I). The s-quark is heavier
than the nonstrange (n) quarks, but it is still useful to introduce
flavor SU(3) as a symmetry, referred to as SU(3,F). In fact this
symmetry was introduced first to classify the hadrons [Gel 61, Nee 61,
Gel 62].

Next to the quarks, the leptons exist as physical "elementary"
particles. Three generations of leptons exist. The first generation
contains the electron e⁻ (and its antiparticle the positron e⁺) and

the electron-neutrino ν_e, a massless (m < 60 eV [PDG 78]) fermion which

has only a left-handed component (and its right-handed antiparticle $\bar{\nu}_e$).

The second generation differs from the first one only through the mass.

The muon μ^- is much heavier than the electron, but its corresponding

neutrino ν_μ is still massless. The third generation (τ^-) is still

heavier. The leptons only feel weak and electromagnetic interactions

and it is useful to classify them in representations of an SU(2) weak

isospin group, referred to as SU(2,W) [Gla 61]. The leptons are clas-

sified in the singlet and doublet representations of SU(2,W):

$$\text{singlets:} \quad e_R^- \quad , \quad \mu_R^- \quad , \quad \tau_R^- \quad ,$$

$$\text{doublets:} \quad \begin{pmatrix} \nu_e \\ e_L^- \end{pmatrix} \quad , \quad \begin{pmatrix} \nu_\mu \\ \mu_L^- \end{pmatrix} \quad , \quad \begin{pmatrix} \nu_\tau \\ \tau_L^- \end{pmatrix} \; .$$

The subscripts R and L stand for right- or left-handed respectively.

Also the quarks feel the weak interactions, which excellently are

described when the quarks are classified in singlet and doublet repre-

sentations of SU(2,W) in the following way:

$$\text{singlets:} \quad u_R \; , \; d_R \; , \; s_R \; , \; c_R \; , \; b_R \; , \; t_R \; ,$$

$$\text{doublets:} \quad \begin{pmatrix} u \\ d' \end{pmatrix}_L \quad , \quad \begin{pmatrix} c \\ s' \end{pmatrix}_L \quad , \quad \begin{pmatrix} t \\ b' \end{pmatrix}_L \quad ,$$

where approximately $d' \simeq d_c = \cos\theta_c \, d + \sin\theta_c \, s$, $s' \simeq s_c = -\sin\theta_c \, d$

$+ \cos\theta_c \, s$ and $b' \simeq b$. θ_c is called the Cabibbo angle, which from

experiments is determined to be $\sin\theta_c \simeq 0.22$. Clearly the top-quark,

included in table 1.1, is necessary to complete the third generation

of quarks.

1.2. Interactions of the elementary particles

Except for gravity, the interactions between the fundamental

particles are mediated by vector boson exchanges. This is well-known for electrodynamics where the photon is exchanged. The abelian U(1) gauge group for electrodynamics is generated by the charge operator and the photon is the gauge field, introduced to make the theory invariant under local gauge transformations.

Non-abelian gauge theories [Yan 54, Abe 73] are the generalization of the abelian U(1) gauge theory. The internal symmetry group is a Lie group generated by a number of generators, F^a, which do not commute;

$$[F^a, F^b] = i \ f^{abc} \ F^c \qquad (1.1)$$

f^{abc} are the structure constants. Gauge fields A^a_μ are introduced to make the theory locally gauge invariant. The non-abelian gauge theories [Gla 65] together with the mechanism of spontaneously broken symmetries [Hig 64, Kib 67] led to the Weinberg-Salam model [Wei 67, Sal 68]: the weak and electromagnetic interactions are unified in a non-abelian gauge theory in which the gauge group is $SU(2,W) \otimes U(1)$, generated by four generators T_i, $i = 1$ to 3 and Y. The four gauge particles are named $W^{\pm}_\mu$, W^0_μ and B_μ. The $SU(2,W) \otimes U(1)$ symmetry is broken down to a U(1) symmetry when the stable vacuum is only invariant under transformations generated by the charge operator $Q = T_3 + Y/2$. Three gauge bosons acquire a mass and one gauge boson, the photon A_μ, stays massless. Z_μ and A_μ are linear combinations of W^0_μ and B_L. The quarks and leptons couple to the photon field via the electric current

$$J^{em}_\mu = i \ \bar{\psi} \ \gamma_\mu \ Q \ \psi \qquad \qquad . \qquad (1.2)$$

They couple to e.g. the charged intermediate bosons W^+_μ via the weak current

$$J^{\pm}_\mu \sim i \ \bar{\psi} \ \gamma_\mu \ T^+ \ \psi \qquad \qquad , \qquad (1.3)$$

8

where $T^{\pm} = T_1 \pm i\, T_2$ and for doublets $T_i = \tau_i/2$ (τ_i are the Dirac matrices). The ψ-fields are the singlets or doublets discussed in section 1.1. Explicitly we get for lepton doublets, e.g. the electron and its neutrino, the leptonic current

$$j^+_{\mu,\ell} \sim i\, \bar{e}_L\, \gamma_\mu\, \nu_e \qquad , \qquad (1.4)$$

and for quarks, e.g. the u- and d'-quarks, the hadronic current

$$j^+_{\mu,n} \sim i\, \bar{u}_L\, \gamma_\mu\, d'_L \simeq i\, \bar{u}_L\, \gamma_\mu\, (\cos\upsilon_c\, d_L + \sin\theta_c\, s_L) \quad . \quad (1.5)$$

In Eqs 1.4 and 1.5 we have used the particle symbol for the field, e.g. e instead of ψ_e. Eq. 1.5 shows that the weak interactions do affect the flavor of the quarks. Up to now all experimental results concerning the weak interactions agree with the Weinberg-Salam model.

The strong interactions are also described in a non-abelian gauge theory [Fri 71]. The color-symmetry not only gives three extra degrees of freedom, e.g. necessary to solve the statistics problem for baryons [Gre 64] or to get the correct results for the ratio $R = \sigma(e^+e^- \rightarrow \text{hadrons})/\sigma(e^+e^- \rightarrow \mu^+\mu^-)$, the ratio $\Gamma(\tau \rightarrow e^-\bar{\nu}\nu)/\Gamma(\tau \rightarrow \text{all})$, and for $\Gamma(\pi^0 \rightarrow \gamma\gamma)$, but it also is the source for the strong interactions [Nam 66]. The interactions between the quarks are mediated by exchange of gluons, which are the gauge bosons in the non-abelian gauge theory for color SU(3), called Quantum Chromo Dynamics (QCD).

1.3. QCD [Mar 78]

In order to describe the interactions between the quarks in QCD, we write down the Lagrangian for the quarks and the gluons (see appendix A for conventions),

$$\mathcal{L}_{QCD} = -\frac{1}{4} G^a_{\mu\nu} G^{a,\nu} - \bar{\psi}(\not{D} + m)\psi \qquad , \qquad (1.6)$$

where $\not{D} = D_\mu \gamma^\mu$ and D_μ is the covariant derivative,

$$D_\mu = \partial_\mu - i g A^a_\mu F^a \qquad (1.7)$$

F^a, $a = 1$ to 8, are the representation matrices of the generators of SU(3,C), which satisfy the commutation relations of Eq. 1.1. For the quarks, which belong to the triplet representation of color ($c = \underline{3}$), $F^a = \lambda_a/2$ (λ_a are the eight Gell-Mann SU(3) matrices); for the anti-quarks $F^a = -\lambda^*_a/2$. The gluons also carry color; they belong to the octet representation ($c = \underline{8}$), for which $(F^a)^{bc} = -i f^{abc}$. The field-strength tensor $G^a_{\mu\nu}$ is given by

$$G^a_{\mu\nu} = \partial_\mu A^a_\nu - \partial_\nu A^a_\mu + g f^{abc} A^b_\mu A^c_\nu \qquad . \qquad (1.8)$$

The Lagrangian $\mathcal{L}_{QCD}$ is invariant under local SU(3) gauge transformations.

The hope is that QCD will be able to describe the strong interactions, just as QED does for the electromagnetic interactions. We mention some of the nice features of QCD.

1.3.1. Renormalizability. Non-abelian gauge theories can be quantized and in 1971 't Hooft has proven their renormalizability [Hoo 71].

1.3.2. Asymptotic freedom [Pol 73, Gro 73]. Although for high energies or zero quark-masses there is no dimension in $\mathcal{L}_{QCD}$ (g dimensionless), there is a typical scale $\Lambda \simeq 0.1$ to 1 GeV for QCD. This scale enters as an integration constant in the renormalized coupling constant $g(Q^2)$, where $Q^2 = -q^2 > 0$ are the typical momenta. $g(Q^2)$ follows from

$$\frac{\partial\, g(Q^2)}{\partial\, \ln Q^2} = \beta(g(Q^2)) \qquad . \qquad (1.9)$$

For SU(N) gauge theories with N_f fermions (= number of flavors) $\beta(g)$ can be calculated in perturbation theory,

$$\beta(g) = \frac{2 N_f - 11 N}{48 \pi^2} g^3 + \ldots \qquad . \qquad (1.10)$$

Then, provided N_f is not too large and $\beta < 0$,

$$\frac{g^2(Q^2)}{4\pi} \underset{Q^2 \text{ large}}{\simeq} \frac{1}{\frac{11 N - 2 N_f}{6\pi} \ln\left(\frac{Q^2}{\Lambda^2}\right)} \qquad , \qquad (1.11)$$

where $\ln \Lambda^2$ is the integration constant. This means that the coupling constant goes to zero for large momenta (or small distances); this is denoted asymptotic freedom. Asymptotic freedom is experimentally seen in deep inelastic scattering experiments, where the nucleon is probed by the photon or the intermediate bosons, exchanged between charged leptons and the nucleon. They reveal the quarks inside the hadron as almost free pointlike constituents.

1.3.3. Confinement. Asymptotic freedom allows perturbation theory for large Q^2. Troubles arise for low Q^2. The coupling constant grows and Eqs 1.10 and 1.11 are not valid anymore. The hope is that nonperturbative approaches to QCD will prove that it is impossible to split a colorless system into two colored fragments, at least beyond distances much larger than $\Lambda^{-1} \simeq 1$ fm.

1.3.4. Unification. When one is able to describe the strong interactions in QCD all the interactions with the exception of gravity are described by the gauge group

$$SU(3,C) \otimes SU(2,W) \otimes U(1)$$

This symmetry can be obtained from a simple Lie group by spontaneous symmetry breaking, where the smallest group which contains the color,

11

the weak isospin and the electromagnetic gauge groups is SU(5).

$$SU(5) \supset SU(3,C) \otimes SU(2,W) \otimes U(1) \supset SU(3,C) \times U(1,EM) \ .$$

The symmetry is consecutively broken down. Above the "grand unifica-tion" scale ($Q \gtrsim 10^{16}$ GeV) there is only one coupling constant. There are 24 gauge bosons in the case of SU(5). At the first stage of breaking 12 gauge bosons acquire masses of the order of 10^{16} GeV. These gauge bosons couple to leptons and quarks, and they violate baryon number converting quarks into leptons and vice versa. The second stage of breaking is that in the Weinberg-Salam model. Three gauge bosons ($W^{\pm}$,Z) acquire masses of the order of 10^2 GeV. The remain-ing symmetries are SU(3,C) (eight massless gluons) and U(1,EM) (one massless photon).

1.4. Hadrons

The picture that we have of the strongly interacting particles, called hadrons, is that of an extended object in which the "valence" quarks determine the flavor and spin properties. Color is the source for the strong interactions, which are mediated by gluon exchange. The colored quarks are confined to the hadron, which is colorless. This allows only $Q^m \bar{Q}^n$ states (states with m quarks and n antiquarks) with (m-n) a multiple of three, or equivalently an integer baryon number (quarks have baryon number $B = 1/3$, antiquarks have $B = -1/3$). The hadrons with $B = 0$ are the mesons, e.g. $Q\bar{Q}$ and $Q^2\bar{Q}^2$; baryons have $B = 1$, e.g. Q^3 and $Q^4\bar{Q}$; dibaryons have $B = 2$, e.g. Q^6.

Inside the hadron (at short distances) the interactions between the quarks are weak (asymptotic freedom). The quarks are almost free

and for large Q^2 perturbation theory is allowed in various reactions involving quarks, gluons and leptons. One has to remember that initial state quarks come from hadrons and that final state quarks recombine into jets which contain a number of aligned hadrons.

Properties concerning the hadron itself involve low Q^2 (large distances) where perturbation theory is not possible anymore. Such a property is e.g. the mass of the hadron. Still there are systematics in hadronic mass spectra. In the J-M^2 plane (J = total spin, M = mass) the hadrons lie on straight (Regge) trajectories with a universal slope α', $J \sim \alpha' M^2$. These trajectories and also the spectrum of bound states and resonances of a heavy quark and a heavy antiquark ($c\bar{c}$ or $b\bar{b}$) indicate that the energy in a quark-antiquark system is roughly linear in the quark-antiquark separation, with a tension $T \sim 0.2$ GeV^2 $\simeq 1$ GeV fm^{-1}. Other systematics are the N-Δ and Λ-Σ splittings which can be understood as arising from spin-spin interactions in one-gluon-exchange models [Ruj 75].

It is hoped that finally these and other low Q^2 properties will be explained by QCD. Now only phenomenological models based on QCD explain the low Q^2 properties.

1.5. The MIT bag model [Cho 74, Jaf 79.2]

In the MIT bag model the hadrons are described by a bag which contains quarks and gluons. The bag is a region of space - or better a tube in space-time - to which the quark and gluon fields are confined. Inside the bag a positive energy density B is added to the energy density of quark and gluon fields. The value of B determined from the light hadron spectrum is $B \simeq 59$ MeV fm^{-3} or $B^{1/4} = 0.145$ GeV. It

sets the scale in the bag model and can be compared with the QCD

parameter Λ in section 1.3. The introduction of the bag pressure B

leads to confinement as only systems with a finite volume have a

finite energy. No gluon fields exist outside the bag, so no color flux

can leave the bag, hence bags are color singlets: the model has built-

in color confinement.

The energy-momentum tensor for a bag becomes

$$T_B^{\mu\nu} = [T^{\mu\nu} - B \, g^{\mu\nu}] \, \theta_B \qquad , \qquad (1.12)$$

where $\theta_B(x) = 1$ inside the bag and $\theta_B(x) = 0$ outside the bag. $T^{\mu\nu}$ is

the energy-momentum tensor for quarks and gluons, described by $\mathcal{L}_{QCD}$

in eq. 1.6,

$$T^{\mu\nu} = \frac{1}{2} \, \bar{\psi} \, \gamma^\mu \, \overleftrightarrow{D}^\nu \, \psi - G^{a\mu\rho} \, \partial^\nu \, A_\rho^a + [-\frac{1}{4} \, G_{\rho\sigma}^a \, G^{a\rho\sigma}] \, g^{\mu\nu} \qquad . \qquad (1.13)$$

Translation invariance requires conservation of the energy-momentum

tensor

$$\partial_\mu \, T_B^{\mu\nu} = [\partial_\mu \, T^{\mu\nu}] \, \theta_B + [n_\mu \, T^{\mu\nu} - Bn^\nu] \, \delta_B = 0 \qquad (1.14)$$

where δ_B is the δ-function at the boundary of the bag (S) defined by

$$\int d^4x \, \delta_B(x) \, f(x) = \int_S d^3x \, f(x) \qquad (1.15)$$

in a covariant way. n^μ is the inward directed unit vector, normal to

the boundary S. Inside the bag one therefore finds the ordinary

equations of motion for fermion and vector fields

$$(\not{D} + m)\psi = 0 \qquad , \qquad (1.16)$$

$$D_\mu \, G^{a\mu\nu} = -i g \, \bar{\psi} \, \gamma^\nu \, F^a \, \psi \qquad , \qquad (1.17)$$

or explicitly

$$(\not{\partial} + m)\psi = i g \, \gamma^\mu \, F^a \, \psi \, A_\mu^a \qquad , \qquad (1.18)$$

14

$$- \partial_\mu G^{a\mu\nu} = i g \bar{\psi} \gamma^\nu F^a \psi + g f^{abc} A^b_\mu G^{c\mu\nu} \qquad (1.19)$$

Besides these equations a set of boundary conditions emerges,

$$n_\mu T^{\mu\nu} - Bn^\nu = 0 \qquad . \qquad (1.20)$$

On the surface they require:

$$\not{n} \psi = - \Gamma \psi \qquad , \qquad (1.21a)$$

$$n_\mu G^{a\mu\nu} = 0 \qquad , \qquad (1.21b)$$

$$- \frac{1}{4} G^a_{\mu\nu} G^{a\mu\nu} + \frac{1}{2} n^\mu \partial_\mu (\bar{\psi} \Gamma \psi) - B = 0 \qquad . \qquad (1.21c)$$

The most general form for the matrix Γ is

$$\Gamma = e^{i \alpha \gamma_5} \qquad , \qquad (1.22)$$

where α is an arbitrary real number. From eq. 1.21a follows that $\bar{\psi}\not{n} = \bar{\psi}\Gamma$ and therefore $\bar{\psi}\Gamma\psi\big|_S = 0$. The boundary conditions 1.21 are sufficient to assure also the conservation of the other currents, required by invariance under U(1,EM) transformations,

$$J^\mu_{em} = i \bar{\psi} \gamma^\mu Q \psi \qquad , \qquad (1.23)$$

invariance under Lorentz transformations,

$$M^{\mu\rho\sigma} = x^\rho T^{\mu\sigma} - x^\sigma T^{\mu\rho} + \frac{1}{2} \bar{\psi} (\gamma^\mu \sigma^{\rho\sigma} + \sigma^{\rho\sigma} \gamma^\mu) \psi$$
$$+ G^{\mu\sigma} A^\sigma - G^{\mu\sigma} A^\rho \qquad , \qquad (1.24)$$

and invariance under SU(3,C) transformations,

$$J^{a\nu} = i g \bar{\psi} \gamma^\nu F^a \psi + g f^{abc} A^b_\mu G^{c\mu\nu} \qquad . \qquad (1.25)$$

Also the current associated with the U(1) symmetry $\psi \to e^{i\alpha}\psi$ (phase factor),

$$J^\mu = i \bar{\psi} \gamma^\mu \psi \qquad , \qquad (1.26)$$

is conserved. Noteworthy is that the transformation

$$\psi \rightarrow e^{i \alpha \gamma_5} \psi \qquad (1.27)$$

$$(\bar{\psi} \rightarrow \bar{\psi} e^{i \alpha \gamma_5})$$

gives other, equivalent boundary conditions. Generally it is not a symmetry as m $\bar{\psi} \psi$ is not invariant under such a transformation. However in the case of massless fermions, it becomes a U(1) symmetry with a conserved current

$$J_5^\mu = i \bar{\psi} \gamma^\mu \gamma_5 \psi \qquad . \qquad (1.28)$$

This chiral symmetry is broken when one chooses a specific value for α for doing calculations. This does not matter for chirally invariant operators like $\int dV \, T^{\mu\nu}(x)$, but it does for non-invariant operators like $\int dV \, \bar{\psi}(x) \, \psi(x)$. For instance the spectrum, determined from the Hamiltonian $H = \int dV \, T^{00}(x)$ is invariant under a change of choice for α. As we are mainly interested in spectra, we will not discuss possible solutions which have been proposed to restore the chiral symmetry [Cho 75, Ino 75, Joh 79.2, Bro 79].

Eqs 1.18, 1.19 and 1.21 describe both the quark and gluon fields inside the bag and the surface of the bag. The quark and gluon fields are already determined completely by the equations 1.18 and 1.19 with the homogeneous boundary conditions 1.21a and 1.21b. E.g. in the case that there are only gluons in the bag, neglecting the self-coupling ($g \rightarrow 0$) we find for the color-electric and color-magnetic fields, which are the components of the field-strength tensor $G^a_{\mu\nu}$,

$$\left. \begin{array}{l} \vec{\nabla} \cdot \vec{E}^a = 0 \\[2mm] \vec{\nabla} \times \vec{B}^a = 0 \end{array} \right\} \qquad \text{inside the bag} \qquad , \qquad (1.29)$$

$$\hat{n} \cdot \vec{E}^a = 0$$

$$\hat{n} \times \vec{B}^a = 0 \qquad \Big\} \qquad \text{on the surface.} \qquad (1.30)$$

These equations are analogous to those for electromagnetic fields in a cavity surrounded by a superconducting medium, but with the roles of $\vec{E}$ and $\vec{B}$ reversed. The eqs 1.29 and 1.30 uniquely determine a solution. The inhomogeneous boundary condition in eq. 1.21c may be understood as a pressure balancing. The pressure of the quarks and gluons is balanced by B, which acts as a pressure exerted from the outside on the bag.

1.6. The spherical bag approximation [DeG 75]

A general solution of the MIT bag model, outlined in the previous section does not exist (in four dimensions). Approximate solutions exist in certain cases, when some assumptions have been made. The first assumption implies that after subtraction of the confining part, which is responsible for the existence of the bag, only weak color interactions remain. We then can start with free quarks and afterwards incorporate the weak color interactions as a perturbation.

Still no general solution exists. However, if as a next step the bag is approximated by a static sphere ($n^\mu = (0, -\hat{r})$), a solvable set of equations is obtained,

$$(\not{\partial} + m)\ \psi_1 = 0 \qquad\qquad \text{inside the bag} \qquad (1.31)$$

$$\hat{r} \cdot \vec{\gamma}\ \psi_1 \Big|_S = \psi_1 \qquad\qquad (1.32a)$$

$$-\frac{\partial}{\partial r}\ (\sum_1 \bar{\psi}_1 \psi_1) \Big|_S = 2\ B \qquad , \qquad\qquad (1.32b)$$

where 1 labels the fermions in the bag. These approximations are thought to be valid for light (relativistic) quarks. The quarks are moving with velocities close to c. They can reach the surface where

they are bounced off. Eq. 1.32b, which implies that the bag pressure is balanced only by the pressure of the quarks, can be used. Heavy quarks have a different behaviour. They act as a static source for the color fields, through which they interact with the bag. In that case (see section 1.8) the pressure of the gluon fields also has to be included in the quadratic boundary condition.

The only static classical solution of the Dirac equation in a spherical bag satisfying eqs 1.31 and 1.32 are the $j = 1/2$ solutions. This is the consequence of the restriction to *static* solutions in *spherical* bags. The positive parity solutions are

$$\psi(\vec{r},t) = \frac{N}{\sqrt{4\pi}} \begin{bmatrix} \sqrt{\frac{\alpha+\mu}{\alpha}} \; J_0(kr)\chi \\ i\sqrt{\frac{\alpha-\mu}{\alpha}} \; J_1(kr)(\vec{\sigma}\cdot\hat{r})\chi \end{bmatrix} e^{-iEt} \quad . \quad (1.33)$$

Instead of energy $E = p^0$, momentum $k = |\vec{p}|$ and quark mass m, we often will use the dimensionless quantities $\alpha = ER$, $x = kR$ and $\mu = mR$ $(\alpha^2 = x^2 + \mu^2)$. The energy spectrum is discrete, due to the linear boundary condition, which allows positive and negative energy eigenvalues α/R, a well-known feature of the Dirac equation. The negative parity solutions are $\gamma_5\psi^*(-\vec{r},t)$ with energy eigenvalues $-\alpha/R$. The energy eigenvalue α/R, depends on the product of the fermion mass and the bag radius, $x = x(\mu)$ and $\alpha = \alpha(\mu)$. For the lowest mode $x(\mu) \xrightarrow[\mu=0]{} 2.043$ and $x(\mu) \xrightarrow[\mu\to\infty]{} \pi$.

In terms of the classical solutions the energy of a bag is

$$E = \int_B dV \; T^{00}(x) = \int_B dV \left[\sum_1 \frac{1}{2} \bar{\psi}_1 \gamma^0 \overset{\leftrightarrow}{\partial_3}{}^0 \psi_1 + B \right]$$
$$= \sum_1 \frac{\alpha_1(R)}{R} \int_B dV \; \psi_1^+\psi_1 + \frac{4\pi}{3} BR^3 \qquad (1.34)$$

With the use of this expression for the energy the quadratic boundary

condition in eq. 1.32b can be rewritten

$$\frac{\partial E}{\partial R} = 0 \qquad (1.35)$$

The mass operator for a bag with free quarks and antiquarks is the
quantized formulation of eq. 1.34,

$$M_0(R) = \sum_1 N_1 \frac{\alpha_1(R)}{R} - \frac{Z_0}{R} + \frac{4\pi}{3} BR^3 \qquad . \qquad (1.36)$$

N_1 is the number operator, which counts the numbers of quarks and
antiquarks with energy $\alpha_1(R)/R$. If all quarks are in the lowest bag
mode, 1 labels the flavors in the bag and $\alpha_1(R) = \alpha(m_1 R)$. The term
$- Z_0/R$ is introduced to account for the correct zero-point energy and
the subtraction of the center of mass motion. It has been shown that a
$1/R$ contribution (independent of the number of quarks in the bag) is
present in the zero-point correction [DeG 75] and for the subtraction
of the center of mass motion [Don 79], although also other terms may
contribute [Ben 76]. From these contributions terms proportional to R^3
can be included in the volume term $\frac{4\pi}{3} BR^3$. As the contributions have
not yet been calculated, they have to be included in a phenomenological
way, and in order to make the number of parameters not larger than
strictly necessary, only the parameter Z_0 is introduced.

The mass operator M_0 in eq. 1.36 depends on the bag radius which
is determined by minimizing the expectation value with respect to R,

$$< \frac{\partial M_0}{\partial R} > = 0 \qquad (1.37)$$

1.7. The color interactions [DeG 75]

Color interactions are included as a perturbation by adding to
the energy density for fermions those terms, which contain the (static)

gluon fields,

$$T^{00} = T^{00}_{quarks} - J^a_\mu A^{a\mu} + \frac{1}{4} G^a_{\mu\nu} G^{a,\nu} \qquad . \qquad (1.38)$$

In lowest order (α^2_c) the only contributions are given by the diagrams

which are the interactions arising from eignt abelian fields $\vec{E}^a$ and
$\vec{B}^a$, whose sources are the quarks. The fields can be considered as
abelian fields as there are no gluon self-couplings to this lowest
order.

1.7.1. The color-electric interactions

The color-electric field generated by the color-charge of a quark
is given by Gauss' law;

$$\vec{\nabla} \cdot \vec{E}^a = J^{a0} = g \, \psi^+ \, F^a \, \psi \qquad . \qquad (1.39)$$

This gives at tne surface of a spherical bag,

$$\vec{E}^a = \frac{g \, F^a}{4\pi} \cdot \frac{\vec{R}}{R^3} \qquad (1.40)$$

Provided the quarks in tne bag couple to a color-singlet, $\sum_i F^a_i = 0$,
the color-electric fields satisfy the homogeneous boundary condition

$$\sum_i \hat{n} \cdot \vec{E}^a_i = 0 \qquad (1.41)$$

Neglecting the self-energy contribution the color-electric interactions
contribute

$$\Delta E_e = \sum_{i \neq j} \left[-\frac{1}{2} \int_B dV \, \vec{E}_i(x) \cdot \vec{E}_j(x) + \int_B dV \, J^0_i(x) \, A^0_j(x) \right]$$

$$= \frac{1}{2} \sum_{1 \neq j} \int_B dV \ \vec{E}_1(x) \cdot \vec{E}_j(x) + \sum_{1 \neq j} (\hat{n} \cdot \vec{E}_1) \ A_j^0 \Big|_S$$

By assumption almost the complete color-electric effects are already included in the volume term, e.g. the higher order (confining) parts or in the mass terms for the quarks, e.g. the self-energy contribution. For a number of identical quarks, coupling to a color-singlet, it is assumed that $\Delta E_e = 0$. This can be obtained by adding a part of the self-energy diagram to the color-electric energy. Then ΔE_e can be written

$$\Delta E_e = \frac{1}{2} \sum_{1,j} \int_B dV \ \vec{E}_1(x) \cdot \vec{E}_j(x)$$

$$= \sum_{1,j} \alpha_c \ \frac{E_{1j}(R)}{R} \ F_1 \cdot F_j \qquad , \qquad (1.42)$$

where $F_1 \cdot F_j = \sum_a F_1^a F_j^a$ (summation over group indices) and $\alpha_c = g^2/4\pi$. For identical quarks ΔE_e is proportional to the quadratic Casimir operator of color $SU(3)$

$$F_c^2 = (\sum_1 F_1^a)(\sum_j F_j^a) = \sum_{1,j} F_1 \cdot F_j \qquad , \qquad (1.43)$$

which for color-singlets has the eigenvalue $f_c^2 = 0$ (see appendix B). If there are different quarks in the bag a small contribution is left, due to the flavor-dependence of the functions $E_{1j}(R)$. The values of the functions $E_{1j}(R) = E(m_1 R, m_j R)$ can be found in ref [DeG 75], e.g. $E(0,0) = 0.139$ and for $\mu = mR \simeq 1.4$, which is a typical value for a strange quark in a baryon the values are $E(0,\mu) \simeq 0.163$ and $E(\mu,\mu) \simeq 0.185$. In this thesis we restrict ourselves to the light quarks (u, d, s), for which the contribution ΔE_e is of the order of or smaller than 5 MeV. Therefore the color-electric energy contribution is neglected.

1.7.2. The color-magnetic interactions

The color-magnetic field, generated by the color current of a quark is found from Maxwells equation

$$\vec{\nabla} \times \vec{B}^a = \vec{j}^a = g \, \psi^+ \, \vec{\alpha} \, F^a \, \psi \qquad (1.44)$$

A solution satisfying the boundary condition $\hat{n} \times \vec{B}_i = 0$ for each quark can be found. Neglecting the self-energy contribution the color-magnetic interactions contribute

$$\Delta E_m = \sum_{i \neq j} \left[\frac{1}{2} \int_B dV \, \vec{B}_i(x) \cdot \vec{B}_j(x) - \int_B dV \, \vec{j}_i(x) \cdot \vec{A}_j(x) \right]$$

$$= -\frac{1}{2} \sum_{i \neq j} \int_B dV \, \vec{B}_i(x) \cdot \vec{B}_j(x)$$

$$= - \sum_{i > j} \alpha_c \frac{M_{ij}(R)}{R} \, (F_i \sigma_i) \cdot (F_j \sigma_j) \qquad , \qquad (1.45)$$

where $(F_i \sigma_i) \cdot (F_j \sigma_j) = \sum_a (F_i^a F_j^a)(\vec{\sigma}_i \cdot \vec{\sigma}_j)$ is the summation over the group-indices. The values of the functions $M_{ij}(R) = M(m_i R, m_j R)$ can be found in ref [DeG 75], e.g. $M(0,0) = 0.177$ and for $\mu \simeq 1.4$, $M(0,\mu) \simeq 0.142$ and $M(\mu,\mu) \simeq 0.118$.

Including the color interactions between the quarks, the mass operator between the quarks becomes

$$M(R) = M_0(R) + \Delta E_e(R) + \Delta E_m(R) \qquad (1.46)$$

and the quadratic boundary condition requires

$$< \frac{\partial M}{\partial R} > = 0 \qquad (1.47)$$

1.8. The light hadron spectrum

In order to apply the mass formula eq. 1.46 to the light baryon

particle	$F_i \cdot F_j$	Δ_{nn}	Δ_{ns}	Δ_{ss}	M_B[GeV]	M_{exp}[GeV]
N	−2/3	−2	−	−	0.938	0.939
Δ		+2	−	−	1.233	1.232
Λ		−2	−	−	1.105	1.116
Σ		+2/3	−8/3	−	1.144	1.193
Σ*		+2/3	+4/3	−	1.382	1.385
Ξ		−	−8/3	+2/3	1.289	1.318
Ξ*		−	+4/3	+2/3	1.529	1.533
Ω		−	−	+2	1.672	1.672
π	−4/3	−4	−	−	0.280	0.138
η_n		−4	−	−	0.280	+)
ρ		+4/3	−	−	0.783	0.776
ω		+4/3	−	−	0.783	0.783
$K, \bar{K}$		−	−4	−	0.497	0.496
$K*, \bar{K}*$		−	+4/3	−	0.928	0.892
η_s		−	−	−4	0.695	+)
φ		−	−	+4/3	1.068	1.020

+ $\eta_n = n\bar{n}$ and $\eta_s = s\bar{s}$ are the ideally mixed combinations which
    contain only nonstrange or only strange quarks (exp m_η = 0.549
    GeV and $m_{\eta'}$ = 0.958 GeV).

Table 1.2. The eigenvalues of the operators $F_i \cdot F_j$, Δ_{nn}, Δ_{ns} and Δ_{ss}
        (eq. 1.48), the bag masses calculated by the MIT group,
        and the experimental masses.

and meson spectra one has to evaluate the expectation values of the
two-particle operators $F_i \cdot F_j$ and $\sigma_i \cdot \sigma_j$ (see appendix B). ΔE_m is divided
in three parts, namely tne interactions between nonstrange, between
strange and between nonstrange and strange quarks,

$$\Delta E_m = \frac{\alpha_c}{R} \left[M_{nn}(R) \sum_{n_1 > n_2} (F_{n_1} \cdot F_{n_2})(\sigma_{n_1} \cdot \sigma_{n_2}) \right.$$

$$+ M_{ss}(R) \sum_{s_1 > s_2} (F_{s_1} \cdot F_{s_2})(\sigma_{s_1} \cdot \sigma_{s_2}) + M_{ns}(R) \sum_{n,s} (F_n \cdot F_s)(\sigma_n \cdot \sigma_s) \Bigg]$$

$$- \frac{\alpha_c}{R} \Bigg[M_{nn}(R) \, \Delta_{nn} + M_{ss}(R) \, \Delta_{ss} + M_{ns}(R) \, \Delta_{ns} \Bigg] \qquad (1.48)$$

The eigenvalues of the operators Δ_{nn}, Δ_{ns} and Δ_{ss} have been given in table 1.2 for the light baryons and mesons. The masses obtained from eqs 1.46 and 1.47 are compared with the experimental masses. The parameters B, Z_0, α_c and m_s ($m_n = 0$) have been determined from the masses of the N, Δ, Ω^- and ω [DeG 75]. They are $B^{1/4} = 0.145$ GeV, $Z_0 = 1.84$, $\alpha_c = 2.20$ and $m_s = 0.279$ GeV.

One of the nicest features of the color-magnetic interaction is that it correctly explains the splittings between the light hadrons. It is a strong argument in favor of color-dependent interactions. E.g. a spin-spin interaction due to an interaction between ordinary magnetic moments, instead of color-magnetic moments, would render the nucleon heavier than the delta. The dependence of the color-magnetic interactions on the quark-masses causes the Λ-Σ splitting, although its magnitude $M_\Lambda - M_\Sigma = \frac{8}{3} (M_{nn} - M_{ns})$ is too small.

The results for the baryons and the vector mesons are satisfying. The color-magnetic splittings are roughly of the order of 20 % of the unperturbed mass. This justifies treating the color-magnetic interactions as a perturbation, although the (effective) coupling constant α_c seems rather large. For the pseudoscalars the agreement between the bag masses and the experimental masses is worse. The η and η' are not ideally mixed, as predicted by the bag mass operator. They have a strong mixing due to annihilation effects. Also the pion mass comes out wrong. This, however, is not remarkable, as the color-magnetic contri-

bution is more than half the unperturbed mass. Johnson [Joh 79.2] has shown that also the subtraction of the center of mass motion is different for the pion.

1.9. Stringlike bag configurations

In the spherical bag approximation only the quarks are important. They provide the pressure necessary to balance the bag pressure at the boundary. As already noted in section 1.6 this will be different for heavy quarks, which act as a static source for the color fields. The color fields now provide the pressure at the boundary. This means that

$$- \frac{1}{4} G^a_{\mu\nu} G^{a\mu\nu} = B \qquad , \qquad (1.49)$$

or

$$\frac{1}{2} (\vec{E}^a \cdot \vec{E}^a - \vec{B}^a \cdot \vec{B}^a) = B \qquad . \qquad (1.50)$$

In the (instantaneous) rest frame of the bag and the quarks $(\vec{B}^a = 0)$ eq. 1.50 becomes

$$\frac{1}{2} \vec{E}^a \cdot \vec{E}^a = B \qquad (1.51)$$

The linear boundary condition requires

$$\hat{n} \cdot \vec{E}^a = 0 \qquad . \qquad (1.52)$$

Assuming that the quarks only act as a source for the color-electric fields, a stringlike solution exist between the (two) sources (fig. 1.1) with a cross section A. Using Gauss' law (from eq. 1.19), $|\vec{E}^a|A = g F^a$, we get

$$\frac{1}{2} \vec{E}^a \cdot \vec{E}^a = 2\pi \alpha_c f^2_c / A^2 \qquad , \qquad (1.53)$$

which shows that it is impossible to separate the color sources by
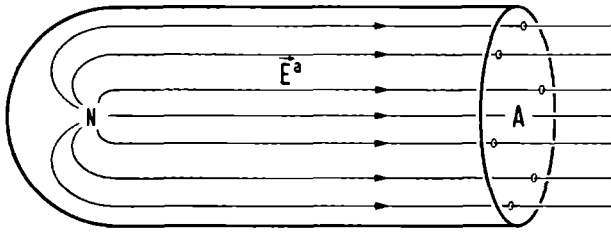
Fig. 1.1. Stringlike solution between two separated color sources.

squeezing the bag $(A \to 0)$, because the energy density becomes infinite. Eliminating the cross section of the bag from eqs 1.51 and 1.53 and multiplying it with the energy density $\frac{1}{2} \vec{E}^a \cdot \vec{E}^a + B = 2B$ we find a constant linear energy density

$$T_0 = (8\pi \, \alpha_c \, B \, f_c^2)^{1/2} \qquad . \qquad (1.54)$$

Using the bag parameters the result for two sources, one belonging to the color irreducible respresentation (irrep) $\underline{3}$ and the other to the conjugate irrep $\underline{3}^*$, is

$$T_0 \simeq 0.18 \text{ GeV}^2 \qquad . \qquad (1.55)$$

The stringlike "solution" of the bag is not only applicable to heavy quarks, but also in the case of rotating bags. In the rotating bag the quarks, acting as sources reside at the ends and the color forces provide the centripetal forces.

The value of T_0 in eq. 1.55 is reasonable both for bags containing heavy quarks and for rotating bags. In the former case it is the tension in the linear potential between two heavy quarks; in the latter case it is related to the slope, $\alpha' = (2\pi T_0)^{-1}$, of the Regge trajectories.

26

The MIT bag model nicely reproduces the masses of the light (s-wave) baryons and mesons (section 1.8). We want to retain these success-ful features in a mass operator which is applicable to both the s-wave hadrons and the orbitally excited hadrons. In order to do this we must make some further approximations in the spherical bag approximation which allow the generalization to orbitally excited hadrons. Moreover we require that the connection remains between the intercepts of the trajectories for orbitally excited hadrons and the spherical bag s-wave or $\ell = 0$ states. This is achieved through the assumption that the spherical bag states are the intercepts of the trajectory, when the color-magnetic interactions are neglected (section 1.6).

For orbitally excited hadrons a stringlike bag is assumed in which the quarks reside at the ends in two clusters. These clusters of quarks are the color sources; this leads to a constant linear energy density (section 1.9). A classical relativistic calculation shows that with quarks which are light compared to the total energy of the bag, the trajectories are linear in the $M^2-\ell$ plane; the slope depends on the color irrep to which the clusters at the ends of the bag couple.

The color-magnetic interactions in a spherical bag (section 1.7) explain the splittings in the mass spectra of the light hadrons. This is called the fine structure of the spectra. The (short range) inter-actions between each pair of quarks depend on their color and spin. The strength depends on the flavor of these quarks. The averaging of this strength renders a factorization of the flavor-dependent strength and the color- and spin-dependent group-theoretical factor Δ. This is

an approximation that makes hadrons with the same flavor configuration, but with different isospins, degenerate, e.g. the s-wave baryons (1116) and Σ(1193).

For the orbital excitations it is assumed that the interactions between quarks at different ends vanish for large x values. This is satisfied for the multiquark systems where it can be checked, namely the orbitally excited $Q-\bar{Q}$ mesons and $Q-Q^2$ baryons, already for $\ell = 1$ the strength of the interaction between quarks at different ends is largely reduced.

The color-magnetic interaction within the clusters is assumed to factorize like it does in a spherical bag. The group-theoretical factors for the clusters, Δ_1 and Δ_2, can be evaluated; the strength, however, is unknown. We assume that the expression found for the strength in (colorless) spherical bags is also applicable for a (colored) cluster of quarks, i.e. that the strength depends on the flavor and the number of quarks in the same way. Our treatment of the multiquark hadrons is summarized in table 2.1 and described in detail in sections 2.1 - 2.4.

Our method of calculation for the masses of multiquark states does not need other parameters than those from ref. [DeG 75] introduced in the spherical bag approximation and determined from the light (s-wave) baryon and meson spectra. The calculation for other s-wave and all orbitally excited multiquark states is $parameter$-$free$. Our way of calculation is rather similar to the one by Jaffe [Jaf 77.2, Jaf 77.3]. In the spherical bag approximation we use a slightly different averaging procedure for the strength of the color-magnetic interactions. We also make some other approximations; we use a radius for a bag

	Ground-state	orbital excitations
shape of the bag	spherical (radius $R = r_0 N^{1/3}$)	stringlike
quarks	almost free in the bag	at ends; sources for color fields
mass without color interactions (multiplet mass)	$M_0 = \frac{4\pi}{3} BR^3 - \frac{z_0}{R}$ $+ \sum_i N_i \frac{\alpha_i(R)}{R}$ [2.1]	$M_\ell^2 = M_0^2 + (1/\alpha')\ell$ $(1/\alpha') = 2\pi T_0$ [2.3]
color-magnetic contribution	$M_m = m\Delta$ [2.2] $m = m(N;N_i)$ [2.2.1] $\Delta = \Lambda(c,s,cs)$ [2.2.2]	$M_m = m_1\Delta_1 + m_2\Delta_2$ [2.4] $m_1 = m(N_1;N_i)$ [2.4.1] $\Delta_1 = \Delta(c_1,s_1,c_1s_1)$ [2.4.2]

Table 2.1: Mass operator for multiquark states. The equations are explained in the sections indicated within square brackets.

which depends on the number of quarks and antiquarks in it and which is independent of the flavor, spin and color of the quarks and anti-quarks.

Jaffe proposed the following mass formula for the orbital excitations [Jaf 78]:

$$M^2 = (M_0 + M_m)^2 + (1/\alpha')\ell \tag{2.1}$$

where M_m only includes the color-magnetic interactions between quarks in the same cluster; he adds this contribution to the intercept mass M_0. The mass $M_0 + M_m$ is the result of the spherical bag calculation. We think that it is more natural to add the color-magnetic interaction to the multiplet masses M_ℓ:

$$M = \lceil M_0^2 + (1/\alpha')\ell \rceil^{1/2} + M_m \qquad .\qquad (2.2)$$

The difference with the approach of Jaffe is that we must make assumptions about the strength of the color-magnetic interactions beyond the spherical bag approximation. While Jaffe gets straight parallel trajectories for all multiquark states, we only find parallel trajectories for the multiplet masses. The inclusion of the color-magnetic interactions causes the trajectories to diverge slightly.

Another approach has been proposed by Chan et al. [Cha 77, Cha 78]. Their mass formula has the same structure as eq. 2.2. They, however, treat the intercepts and the strength of the color-magnetic interactions as free parameters. This strength is fixed using the light hadrons. The intercept of each trajectory is fixed by assigning one of the states on it to an experimental candidate. The relation between the intercept mass M_0 and the physical $\ell = 0$ states is lost in this way. We think that it is premature to extract parameters from assignments in the present situation where for multiquark states other than $Q\bar{Q}$ and Q^3 states all candidates still need confirmation or at least clarification.

The content of this chapter is as follows. We discuss in detail the spherical and stringlike bags and the fine structure. As an example we consider the $Q-\bar{Q}$ mesons. Next we mention two phenomenological contributions to the mass, namely the exchange contributions and the hyperfine structure. We finally discuss the connection between the predicted multiquark states and physically observed resonances.

2.1. The spherical bag

The mass of a spherical bag without color interactions is given by eq. 1.36:

$$M_0(R) = \frac{4\pi}{3} BR^3 - \frac{z_0}{R} + \sum_i N_i \frac{\alpha_i(R)}{R} \qquad . \qquad (2.3)$$

This equation is valid for light quarks, as discussed in section 1.6. The actual mass is found by minimizing the expectation value of M_0 with respect to the bag radius R. This gives

$$R^4 = (4-B)^{-1} \left[\sum_i N_i (\alpha_i(R) - R \frac{\partial \alpha_i}{\partial R}) - z_0 \right] \qquad (2.4)$$

As long as a linear approximation for $\alpha_i(R) = \alpha(m_i R)$ is valid we can write

$$R \simeq (4\pi B)^{-1/4} [N\alpha(0) - z_0]^{1/4} \qquad , \qquad (2.5)$$

where $\alpha(0) = \alpha_n = 2.043$. This can be accurately parametrized by (see table 2.2):

$$R \simeq r_0 N^{1/3} \quad \text{with} \quad r_0 = 3.63 \text{ GeV}^{-1} \qquad . \qquad (2.6)$$

N	multiquark system	R_{min} [GeV^{-1}] eq. 2.5	$r_0 N^{1/3}$ [GeV^{-1}]
2	$Q\bar{Q}$	4.48	4.57
3	Q^3	5.27	5.24
4	$Q^2\bar{Q}^2$	5.81	5.76
5	$Q^4\bar{Q}$	6.23	6.20
6	Q^6	6.58	6.60
9	Q^9	7.39	7.55
12	Q^{12}	7.99	8.31

Table 2.2: Parametrization of eq. 2.5 by $R = r_0 N^{1/3}$. The parameters in eq. 2.5 are $B^{1/4} = 0.145$ GeV and $Z_0 = 1.84$. The radius $r_0 = 3.63$ GeV^{-1}.

The result is that the mass of the ground state, which depends on the bag radius (R) and the quark flavors (N_1), only depends on the flavors so $M_0(R;N_n,N_s,...) = M_0(N;N_n,N_s,...)$. When we only consider the (light) u, d and s quarks (for which the approach is valid) we can write

$$M_0 = M_0(N;N_s) \qquad . \qquad (2.7)$$

The results up to N = 6 are given in table 2.3.

N \ N_s	0	1	2	3	4	5	6
2	.673	.833	.992				
3	1.092	1.255	1.418	1.581			
4	1.463	1.628	1.794	1.960	2.125		
5	1.804	1.972	2.140	2.307	2.475	2.643	
6	2.125	2.295	2.464	2.634	2.803	2.973	3.142

Table 2.3: The masses $M_0(N;N_s)$ in GeV for the spherical bags neglecting color interactions.

2.2. Fine structure in the spherical bag

In a spherical bag the color-magnetic interaction has the form

$$M_m = - \sum_{i>j} \alpha_c \frac{M_{ij}(R)}{R} (F\sigma)_i \cdot (F\sigma)_j \qquad (2.8)$$

For simple systems like $Q\bar{Q}$ and Q^3 it is not difficult to separately evaluate all nonstrange-nonstrange, nonstrange-strange and strange-strange contributions (section 1.8). This soon becomes complicated if the number of quarks and antiquarks (N) is larger than three, however, because more than one color configuration is possible. While in the Q^3 system the Q^2 subsystem necessarily belongs to the color irrep

32

$\underline{c} = \underline{3}^*$, there are two possibilities in the $Q^2\bar{Q}^2$ system, $\underline{c} = \underline{3}^*$ and $\underline{c} = \underline{6}$. A simplification [Jaf 77.2] is taking an average value for the strength of the interactions,

$$M_{ij}(R) \simeq M_{av}(R) \qquad , \qquad (2.9)$$

and obtaining factorization of the color-magnetic contribution. We choose the following averaging procedure;

$$M_{av}(R) = \frac{\frac{1}{2} N_n(N_n-1)M_{nn}(R) + \frac{1}{2} N_s(N_s-1)M_{ss}(R) + N_n N_s M_{ns}(R)}{\frac{1}{2} N(N-1)} \quad , \quad (2.10)$$

and get

$$M_m = \alpha_c \frac{M_{av}(R)}{R} \sum_{i>j} - (F\sigma)_i \cdot (F\sigma)_j \qquad . \qquad (2.11)$$

The price of this averaging is that all multiquark states with the same flavor configuration, i.e. the same number of strange quarks, but with different isospins, are degenerate. Eq. 2.11 is exact for hadrons which belong to a totally symmetric flavor irrep, e.g. $\underline{f} = \underline{10}$ for the baryons. An estimate of the errors made for mixed symmetric flavor irreps, e.g. $\underline{f} = \underline{8}$ for the baryons, can be readily obtained from the values of the functions $M_{ij}(R)$ for nonstrange and strange quarks (section 1.8). This gives errors $\lesssim$ 15 % in the color-magnetic contribution as compared with the values obtained from eq. 2.8. Thereby we have to keep in mind that eq. 2.8 did not give the correct isospin splitting between the Λ and Σ [DeG 75].

We make one other approximation. We do not minimize the eigen-value of the mass operator $M = M_0 + M_m$ with respect to the bag radius, but we use the radius $R = r_0 N^{1/3}$ to evaluate the color-magnetic contribution. Only a small error is introduced in this way. Although the color-magnetic contribution may give a reasonably large energy

shift, it only causes a small shift in the radius. The approximate

radius in eq. 2.6 gives a minimum value for the expectation value

$<M_0(R)>$ and it gives a value for $<M(R)>$ which is still in the neigh-

borhood of the minimum value. An estimate of the error made by taking

the value of R in eq. 2.5, independent of flavor, color and spin,

instead of minimizing gives

$$\Delta M \simeq \frac{1}{2} \quad \frac{M_{in}}{M_0} \quad M_m \qquad (2.12)$$

For a typical example, the nonstrange baryons N and Δ, we find

$\Delta M \simeq 10$ MeV. This shows that this approximation does not seriously

influence the results of ref. [DeG 75].

2.2.1. The strength of the color-magnetic interactions

Using the radius $R = r_0 \, N^{1/3}$ the strength of the color-magnetic

interactions becomes

$$m(R;N_n,N_s) = m(N;N_s) = \alpha_c \left. \frac{M_{av}(R;N_n,N_s)}{R} \right|_{R=r_0 N^{1/3}} \qquad (2.13)$$

The values up to N = 6 have been given in table 2.4. These results

can be parametrized in the following way;

$$m(N;N_s) \simeq a \, N^{-1/3} - b \, N_s N^{-1} \qquad , \qquad (2.14)$$

with a = 107 MeV and b = 28 MeV; this parametrization is exact for

$N_s = 0$.

2.2.2. The group-theoretical factor Δ

The calculation of Δ,

$$\Delta = - \sum_{i>j} (F\sigma)_i \cdot (F\sigma)_j \qquad , \qquad (2.15)$$

requires group-theoretical methods. Operators associated with SU(3,C)

and SU(2,S) appear in Δ. Using the quadratic Casimir operators F_c^2 for

$N \backslash N_s$	0	1	2	3	4	5	6
2	85.1	70.2	58.2				
3	74.4	64.3	55.5	47.9			
4	67.6	60.1	53.3	47.0	41.2		
5	62.7	56.8	51.2	46.0	41.3	36.9	
6	59.0	54.1	49.5	45.1	40.9	37.0	33.4

Table 2.4: The strength $m(N;N_s)$ for the color-magnetic interactions.

$SU(3,C)$, S^2 for $SU(2,S)$ and A^2_{cs} for $SU(6,CS)$ (see appendix B) Δ can be rewritten [Jaf 77.3]

$$\Delta = 2N + \frac{1}{2} A^2_{cs}(tot) - \frac{1}{3} S^2(tot) - \frac{1}{2} F^2_c(tot)$$
$$+ F^2_c(Q) + \frac{2}{3} S^2(Q) - A^2_{cs}(Q)$$
$$+ F^2_c(\bar{Q}) + \frac{2}{3} S^2(\bar{Q}) - A^2_{cs}(\bar{Q}) \qquad . \qquad (2.16)$$

In parentheses is indicated whether the color, spin and color-spin for quarks (Q), antiquarks $(\bar{Q})$ or for the entire system (tot) is meant.

The quark and antiquark parts of the expression in eq. 2.16 can be simplified. Consider a system of N quarks with a symmetric spatial wave function (all quarks are in s-waves). The wave function of the Q^N-system is completely antisymmetric with respect to $SU(3,F)$ $\otimes$ $SU(2,S)$ $\otimes$ $SU(3,C)$ or with respect to $SU(3,F)$ $\otimes$ $SU(6,CS)$. This means that the product of the permutation operators

$$P^{cs}_{ij} P^f_{ij} = - 1 \qquad \qquad (2.17)$$

for all quark pairs, or if we only consider nonstrange quarks

$$P^{cs}_{ij} P^l_{ij} = - 1 \qquad \qquad (2.18)$$

This leads to a relation between the color-spin SU(6,CS) and the flavor SU(3,F) Casimir operators A^2_{cs} and F^2_f,

$$A^2_{cs} + 2 F^2_f = \frac{1}{2} N(18 - N) \qquad , \qquad (2.19)$$

or in the case of nonstrange quarks to a relation between the color-spin SU(6,CS) and the isospin SU(2,I) quadratic Casimir operators A^2_{cs} and I^2,

$$A^2_{cs} + 2 I^2 = \frac{2}{3} N(12 - N) \qquad\qquad (2.20)$$

For a state containing only quarks (or only antiquarks) the color-spin operators can be replaced by flavor operators $\Delta(N;c,s,cs) = \Delta(N;c,s,f)$:

$$\Delta = -\frac{1}{4} N(10 - N) + \frac{1}{3} S^2 + F^2_f + \frac{1}{2} F^2_c \qquad , \qquad (2.21)$$

or for nonstrange quarks $\Delta(N,c,s,cs) = \Delta(N;c,s,1)$:

$$\Delta = -\frac{1}{3} N(6 - N) + \frac{1}{3} S^2 + I^2 + \frac{1}{2} F^2_c \qquad . \qquad (2.22)$$

As an example consider the color-magnetic splitting of the baryons or the $(Q^3)_1$ system. By $(Q^N)_c$ we indicate an N-quark system coupling to the color irrep $\underline{c}$. The $(Q^3)_1$ system is totally antisymmetric. The color irrep is $\underline{1}$ and the corresponding Young diagram is $[1^3]$. The Young diagram corresponding to the flavor-spin irrep is the associate diagram [3] (the rows of the associate diagram are the columns of the original diagram). The flavor-spin irrep for the $(Q^3)_1$ system therefore

$\underline{f}$	s	Δ
$\underline{10}$	3/2	+ 2
$\underline{8}$	1/2	- 2
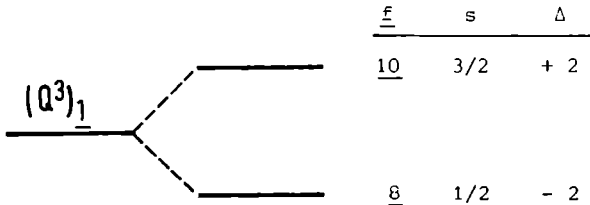
Fig. 2.1: The color-magnetic splitting of the s-wave baryons.

36

is the symmetric irrep {56} (see appendix B4). For each $(\underline{f},s)$ multiplet Δ can be calculated from eq. 2.21. The splitting is given in fig. 2.1. The masses of the s-wave baryons, $M_0 + m\Delta$, can be calculated using tables 2.3 and 2.4 and they can be compared with the results of ref. [DeG 75] and the experimental results (table 2.5).

particle	M_B [GeV]	M [GeV]	M_{exp} [GeV]
N	0.938	0.943	0.939
Δ	1.233	1.241	1.232
Λ	1.105	1.126	1.116
Σ	1.144	1.126	1.193
Σ^*	1.382	1.384	1.385
Ξ	1.289	1.307	1.318
Ξ^*	1.529	1.529	1.533
Ω	1.672	1.677	1.672

Table 2.5: Comparison between the baryon masses M_B from [DeG 75], M using our mass operator, and the experimental masses M_{exp}.

In tables 2.6 and 2.7 the splitting of the colorless $(Q^3)_1$ and $(Q^6)_1$ states is given (using eq. 2.21). For multiquark states containing both quarks and antiquarks eq. 2.16 is needed and the situation is more complex. Δ depends on the colorspin, color and spin of the quarks, the antiquarks and the entire system. For a $Q^m\bar{Q}^n$ state Λ is in general neither diagonal in the states $|Q^m\bar{Q}^n;[cs],\underline{c},s>$ nor in the direct product states $|Q^m;[cs],\underline{c},s> \otimes |\bar{Q}^n;[cs],\underline{c},s>$; we have to know the Clebsch-Gordan coefficients for this product in order to evaluate Δ. For the $(Q\bar{Q})_1$ states evaluation of Δ is no problem and the results are

given in table 2.8. For the $(Q^4\bar{Q})_1$ states the calculation is possible, when certain Clebsch-Gordan coefficients are known. Consider for instance the first two states in table 2.9. ϕ_1 and ϕ_2 are the direct product states, $\phi_1 = |Q^4;[31],\underline{3},0\rangle \otimes |\bar{Q};[1^5],\underline{3}^*,1/2\rangle$ and $\phi_2 = |Q^4;[31],\underline{3},1\rangle \otimes |\bar{Q};[1^5],\underline{3}^*,1/2\rangle$. The product states, which must be colorless, can belong to the color-spin irreps [21] or [421^3] when the total spin is s = 1/2. They are

$$
\begin{bmatrix} |[21],\underline{1},1/2\rangle \\ |[421^3],\underline{1},1/2\rangle \end{bmatrix} = \begin{bmatrix} -1/2 & \sqrt{3/4} \\ \sqrt{3/4} & 1/2 \end{bmatrix} \begin{bmatrix} \phi_1 \\ \phi_2 \end{bmatrix} \qquad . \qquad (2.23)
$$

Using eq. 2.23 it is possible to evaluate Δ; the eigenvalues and eigenstates expressed in the basis states ϕ_1 and ϕ_2 are given in table 2.9. Also for the $(Q^2\bar{Q}^2)_1$ states [Aer 79.1, Aer 79.2] the eigenvalues and eigenstates of Δ have been given (table 2.10).

$(Q^3)_1$	f	s	Δ
B	$\underline{8}$	1/2	-2
D	$\underline{10}$	3/2	2

Table 2.6: Eigenvalues of Δ for $(Q^3)_1$ states belonging to the fs irrep {56}.

ERRATA

List of Abbreviations:

HE = haematoxylin eosin stain.

page 101: 23rd line: Fig. 38 should be Fig. 37

page 166 should be read before page 165

page 178: 1. should be exchanged with 3.

page 206: DIPASQUA should be DIPASQUALE

$(Q^2\bar{Q}^2)_1$	Q^2				$\bar{Q}^2$								$(Q\bar{Q})_1(Q\bar{Q})_1$ recoupling	
	f	cs	c	s	f	cs	c	s	cs	s	Δ	eigenstates		
ϕ_1	$\underline{3}^*$	$[2]$	$\underline{3}^*$	0	$\underline{3}$	$[2^5]$	$\underline{3}$	0	$[1^6]$	0	-10.84	$\begin{bmatrix} .582 & .813 \\ .813 & -.582 \end{bmatrix}\begin{bmatrix} \phi_1 \\ \phi_2 \end{bmatrix}$	PP	VV
ϕ_2			$\underline{6}$	1			$\underline{6}^*$	1	$[42^4]$	0	-0.49		PP	VV
ϕ_3									$[21^4]$	1	-4		PV	VV
ϕ_4									$[42^4]$	2	$8/3$			VV
ϕ_5	$\underline{3}^*$	$[2]$	$\underline{3}^*$	0	$\underline{6}^*$	$[1^4]$	$\underline{3}$	1	$[21^4]$	1	$-10/3$	$\begin{bmatrix} \sqrt{2/3} & \sqrt{1/3} \\ -\sqrt{1/3} & \sqrt{2/3} \end{bmatrix}\begin{bmatrix} \phi_5 \\ \phi_6 \end{bmatrix}$	PV	VV
ϕ_6			$\underline{6}$	1			$\underline{6}^*$	0	$[31^3]$	1	$8/3$		PV	VV
ϕ_7	$\underline{6}$	$[1^2]$	$\underline{3}^*$	1	$\underline{3}$	$[2^5]$	$\underline{3}$	0	$[21^4]$	1	$-10/3$	$\begin{bmatrix} \sqrt{2/3} & \sqrt{1/3} \\ -\sqrt{1/3} & \sqrt{2/3} \end{bmatrix}\begin{bmatrix} \phi_7 \\ \phi_8 \end{bmatrix}$	PV	VV
ϕ_8			$\underline{6}$	0			$\underline{6}^*$	1	$[3^2 2^3]$	1	$8/3$		PV	VV
ϕ_9	$\underline{6}$	$[1^2]$	$\underline{6}$	0	$\underline{6}^*$	$[1^4]$	$\underline{6}^*$	0	$[1^6]$	0	-4.84	$\begin{bmatrix} .582 & .813 \\ .813 & -.582 \end{bmatrix}\begin{bmatrix} \phi_9 \\ \phi_{10} \end{bmatrix}$	PP	VV
ϕ_{10}			$\underline{3}^*$	1			$\underline{3}$	1	$[2^2 1^2]$	0	5.51		PP	VV
ϕ_{11}									$[21^4]$	1	0		PV	VV
ϕ_{12}									$[2^2 1^2]$	2	$8/3$			VV

Table 2.10: Eigenvalues and eigenstates of Δ for $(Q^2\bar{Q}^2)_1$ states and the recoupling to color-singlet meson-meson channels (see table 2.8).

2.3. The stringlike bag

We have considered stringlike bag configurations in section 1.9.
The characteristic feature is a constant linear energy density
$T_0 = (8\pi \alpha_c B f_c^2)^{1/2}$ in the instantaneous rest frame of the string.

As long as the motion is non-relativistic the Schrodinger equation
with a linear potential seems to be the best description of this system
of two separated color sources. However, if the system consists of
light quarks, it is certainly relativistic. This can be treated
classically and such a classical model will be our starting point; in
the non-relativistic limit of heavy quarks the quantum mechanical
result is recovered introducing a quantum defect [Joh 79.1].

Consider a string with masses m_1 and m_2 at the ends and a linear
energy density T_0 in the rest frame. If this string rotates with an
angular frequency ω the energy density becomes $T = T_0/\sqrt{1-v^2}$. This also
happens in the stringlike bag where the energy density comes from the
color-electric and color-magnetic fields and the bag pressure. In the
rest frame the linear energy density is ($\frac{1}{2} \vec{E}^2 + B$) A_0, which using
the boundary condition $\frac{1}{2} \vec{E}^2 = B$ (eq. 1.51) can be rewritten to

$$T_0 = (B + B) A_0 = 2B A_0 \qquad , \qquad (2.24)$$

from which the cross section of the bag (A_0) can be eliminated using
Gauss' law. In the rotating system the linear energy density becomes
$T = (\frac{1}{2} \vec{E}^2 + \frac{1}{2} \vec{B}^2 + B)$ A, which using $\vec{B} = \vec{v} \times \vec{E}$ and the boundary
condition $\frac{1}{2} (\vec{E}^2 - \vec{B}^2) = B$ can be rewritten to

$$T = \left(\frac{1}{1-v^2} B + \frac{v^2}{1-v^2} B + B \right) A_0 \sqrt{1-v^2} = \frac{T_0}{\sqrt{1-v^2}} \qquad . \qquad (2.25)$$

In the string the velocity v can be used as a coordinate. The

velocities of the ends, v_1 and v_2 are determined by the equation

$$T_0 \sqrt{1-v_1^2} = m_1 v_1 \omega / \sqrt{1-v_1^2} \qquad . \qquad (2.26)$$

The energy of the string is given by

$$
\begin{aligned}
E &= \frac{m_1}{\sqrt{1-v_1^2}} + \frac{m_2}{\sqrt{1-v_2^2}} + \frac{T_0}{\omega} \int_{-v_1}^{v_2} dv \, \frac{1}{\sqrt{1-v^2}} \\
&= \frac{T_0}{\omega} \left[\frac{\sqrt{1-v_1^2}}{v_1} + \arcsin v_1 + \frac{\sqrt{1-v_2^2}}{v_2} + \arcsin v_2 \right] \quad , \qquad (2.27)
\end{aligned}
$$

and the orbital angular momentum is given by

$$
\begin{aligned}
\ell &= \frac{m_1 v_1^2}{\omega \sqrt{1-v_1^2}} + \frac{m_2 v_2^2}{\omega \sqrt{1-v_2^2}} + \frac{T_0}{\omega^2} \int_{-v_1}^{v_2} dv \, \frac{v^2}{\sqrt{1-v^2}} \\
&= \frac{T_0}{2\omega^2} \left[v_1 \sqrt{1-v_1^2} + \arcsin v_1 + v_2 \sqrt{1-v_2^2} + \arcsin v_2 \right] \quad . \qquad (2.28)
\end{aligned}
$$

We want to consider three limiting cases

2.3.1. m_1 and m_2 non-relativistic; $E \simeq m_1, m_2$

Introducing $M = m_1 + m_2$ and $\mu = m_1 m_2 / (m_1 + m_2)$ we find the following relation between the energy E and the orbital angular momentum ℓ,

$$E = M + \frac{3}{2} \left(\frac{T_0^2}{\mu} \right)^{1/3} \ell^{2/3} \qquad . \qquad (2.29)$$

This is exactly the result for the Bohr quantized linear potential $V(r) = T_0 r$. The quantum mechanical result for orbitally and radially excited levels is reproduced rather precisely by a replacement of the argument

$$M(n_r, \ell) = E(\ell + \ell_0 + \gamma n_r) \qquad . \qquad (2.30)$$

The constant ℓ_0 is called the quantum defect; γ is a factor by which the radial quantum number n_r has to be multiplied. For the linear potential, $\ell_0 \simeq 1.376$ and $\gamma \simeq 1.8$. A comparison with the exact levels for the linear potential is given in table 2.11. In the cases of the

Coulomb potential and the harmonic oscillator the replacement in eq. 2.30 is exact. For the Coulomb potential $\ell_0 = \gamma = 1$ and for the three-dimensional harmonic oscillator $\ell_0 = 3/2$, $\gamma = 2$.

level $(n_r+1)\ell$	$\frac{2}{3}\left(\frac{T_0}{\mu}\right)^{-1/3} E$	$(\ell + \ell_0 + \gamma n_r)^{2/3}$
1s	1.237	1.237
1p	1.779	1.781
2s	2.163	2.161
1d	2.248	2.250
2p	2.585	2.593
1f	2.673	2.675

Table 2.11: Comparison between the exact levels for a linear potential and the levels with the use of a quantum defect $\ell_0 = 1.376$ and radial factor $\gamma = 1.8$.

2.3.2. m_1 non-relativistic, m_2 relativistic; $E \simeq m_1 \gg m_2$

The relation between E and ℓ becomes (with $m \simeq m_1$)

$$E = m + (\pi\, T_0\, \ell)^{1/2}\left[1 + \frac{2}{\pi^2} \cdot \frac{(\pi\, T_0\, \ell)^{1/2}}{m} + \ldots\right] \qquad . \quad (2.31)$$

This intermediate case is e.g. applicable to the charmed mesons [Joh 79.1].

2.3.3. m_1 and m_2 relativistic; $E \gg m_1, m_2$

In this case the velocities of the ends approach the velocity of light. The limits of eqs 2.27 and 2.28 are $E \simeq \pi\, T_0/\omega$ and $\ell \simeq \pi\, T_0/2\omega^2$. The relation between E and ℓ is

$$E^2 = 2\pi\, T_0\, \ell = (1/\alpha')\, \ell \qquad , \qquad (2.32)$$

which form linear trajectories in the M^2-ℓ plane. If we assume that the
same procedure as has been followed in section 2.3.1 gives the correct
quantum mechanical result, we find

$$
\begin{aligned}
M_\ell^2 &= (1/\alpha')(\ell + \ell_0) \\
&= M_0^2 + (1/\alpha')\ell
\end{aligned}
\tag{2.33}
$$

This yields linear trajectories with an intercept $\ell = -\ell_0$ or
$M_0^2 = (\ell_0/\alpha')$. Taking this intercept mass M_0 to be the (average) mass
of the s-wave states calculated in the spherical bag approximation
neglecting the color-magnetic interactions, is an assumption that takes
account of the connection between the s-wave states and the orbitally
excited states, as is experimentally observed for baryon-meson and
meson-meson resonances.

The slope of the trajectories

$$
(1/\alpha') = 2\pi \ (8\pi \ \alpha_c \ B \ f_c^2)^{1/2}
\tag{2.34}
$$

calculated from the bag parameters $\alpha_c = 2.20$ and $B^{1/4} = 0.145$ GeV
yields $1/\alpha' \simeq 1.1$ GeV^2 and is in excellent agreement with the experi-
mental slope of baryon and meson trajectories. In this case, Q-$\bar{Q}$ or
Q-Q^2, the color structure is $\underline{3}$-$\underline{3^*}$ (the color irreps to which the quarks
at the ends belong are $\underline{c} = \underline{3}$ and $\underline{c} = \underline{3^*}$) and $f_c^2 = 4/3$. For multiquark
states with $N > 3$ not only the color structure $\underline{3}$-$\underline{3^*}$, but also $\underline{6}$-$\underline{6^*}$
and $\underline{8}$-$\underline{8}$ are possible, e.g. $(Q^2)_6$-$(\bar{Q}^2)_{6^*}$ and $(Q\bar{Q})_8$-$(Q\bar{Q})_8$. Orbital
excitations with such color structures have different slopes. The slope
$1/\alpha'$ is proportional to the square root of the eigenvalue of the
quadratic Casimir operator f_c^2. For a $\underline{6}$-$\underline{6^*}$ structure $f_c^2 = 10/3$ and
$(1/\alpha_6') = \sqrt{5/2} \ (1/\alpha_3')$; for a $\underline{8}$-$\underline{8}$ structure $f_c^2 = 3$ and $(1/\alpha_8') =$
$3/2 \ (1/\alpha_3')$

2.3.4. Other bag-shapes

One could ask why a stringlike configuration is preferred above other configurations, e.g. starlike configurations. Classically there is an argument in favor of a linear string. Consider a starlike configuration with n arms. At each end there is a cluster with the (smallest) color charge $\underline{3}$ or $\underline{3}^*$. The linear energy density in each arm is $T_0 = 1/2\pi\alpha_3'$. For large ℓ (or light clusters) it immediately follows (analogous to eqs 2.27 and 2.28) that $E = n\pi T_0/2\omega$ and $\ell = n\pi T_0/4\omega^2$, and we find

$$E^2 = n \ (1/2\alpha_3') \ \ell \qquad\qquad (2.35)$$

This shows that starlike configurations $(n > 2)$ are heavier than the stringlike configuration $(n = 2)$

2.4. Fine structure in the stringlike bag

While in the spherical bag the strength of the color-magnetic interactions can be calculated, one has to make assumptions in a stringlike bag. The first assumption is that the color-magnetic spin-spin interactions between the color-magnetic moments of two quarks vanishes if the two quarks are spatially separated at different ends of the stringlike bag, i.e. for large ℓ. We can write

$$M_m = m_1\Delta_1 + m_2\Delta_2 + V_{12} \qquad\qquad . \qquad\qquad (2.36)$$

The part $m_1\Delta_1$ (or $m_2\Delta_2$) is the color-magnetic interaction contribution of the cluster 1 (or 2) at the end of the bag. The average strength of the interaction is m_1 (or m_2). Δ_1 (or Δ_2) is the group-theoretical factor

$$\Delta_1 = \Lambda_1(N_1, c_1, s_1, c_1 s_1) = - \sum_{i_1 > j_1} (F\sigma)_{i_1} \cdot (F\sigma)_{j_1} \qquad , \qquad (2.37)$$

46

where the summation is over quarks in cluster 1. V_{12} contains the
interactions between the color-magnetic moments of two quarks at
different ends of the bag. It also contains interactions between the
color-magnetic moments of the quarks and the color fields in the
stringlike bag. It causes the hyperfine splitting of the mass spectrum
(section 2.6.2). Neglecting V_{12}, the color-magnetic interaction is the
sum of two contributions from the quark clusters at the ends of the
bag. The masses of orbitally excited multiquark states are obtained by
adding the color-magnetic contribution to the multiplet mass M_ℓ.

2.4.1. The strength of the color-magnetic interactions in a cluster

The strength of the color-magnetic interactions in a stringlike
bag cannot be calculated like in the spherical bag, nor can it be taken
as a free parameter in cases other than the baryon resonances; for
multiquark states with $N > 3$ only very few candidates with well-estab-
lished quantum numbers exist. We simply use the strength in a spherical
bag to estimate the strength in a cluster. We assume the strength to
be given by $m(N, N_s)$ from eq. 2.13 or table 2.4 the strength of the
color-magnetic interaction for a cluster depends on the number and
flavor of the quarks in it, but it is independent of the color of the
cluster.

2.4.2. The group theoretical factors Δ_1, Δ_2

The factors Δ_1 and Δ_2 are evaluated as described in section 2.2.2.
All formulae derived in this section can be applied for clusters
$(Q^m \bar{Q}^n)_c$; in section 2.2.2 tables have been given for the colorless
clusters $(Q^3)_1$, $(Q^6)_1$, $(Q\bar{Q})_1$, $(Q^4\bar{Q})_1$ and $(Q^2\bar{Q}^2)_1$.

As an example of a colored cluster we consider the color-magnetic
splitting of the $(Q^2)_{3*}$ clusters. The wave function is totally anti-

symmetric. The color part ($\underline{c}$ = $\underline{3}^*$) is antisymmetric (Young diagram
[1^2]). The flavor-spin irrep is symmetric, fs = {21} (Young diagram
[2]). For each ($\underline{f}$,s) multiplet Δ can be calculated from eq. 2.21. The
splitting is given in fig. 2.2.

The splittings of the $(Q^2)_{3*}$, $(Q^2)_6$, $(Q^3)_8$, $(Q^4)_3$, $(Q^4)_{6*}$ and
$(Q^5)_{3*}$ cluster are given in tables 2.12 - 2.17. Like in the colorless
case the colored clusters containing quarks and antiquarks are more
difficult to evaluate than the clusters containing quarks only. For
the simplest clusters namely $(Q\bar{Q})_8$ and $(Q^2\bar{Q})_3$ the splittings are given
in tables 2.18 and 2.19.

$\underline{f}$	s	Λ
$\underline{6}$	1	+ 2/3
$\underline{3}^*$	0	- 2

$|Q^2|_{\underline{3}*}$
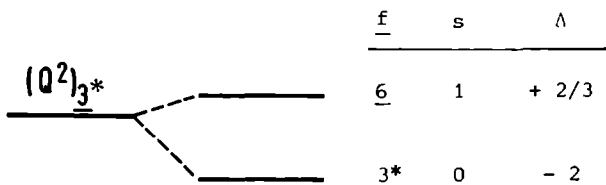
Fig. 2.2: The color-magnetic splitting of the $(Q^2)_{3*}$ cluster.

$(Q^2)_{3*}$	$\underline{f}$	s	Δ
T_0	$\underline{3}^*$	0	- 2
T_1	$\underline{6}$	1	2/3

Table 2.12:
eigenvalues of Δ for the $(Q^2)_{3*}$
clusters, belonging to the fs irrep
{21}.

$(Q^2)_6$	$\underline{f}$	s	Λ
ϕ_1	$\underline{3}^*$	1	- 1/3
ϕ_2	$\underline{6}$	0	1

Table 2.13:
eigenvalues of Δ for the $(Q^2)_6$
clusters, belonging to the fs irrep
{15}.

48

$(Q^3)_8$	f	s	Δ
ϕ_1	1	1/2	$-7/2$
ϕ_2	8	1/2	$-1/2$
ϕ_3	8	3/2	1/2
ϕ_4	10	1/2	5/2

Table 2.14: eigenvalues of Δ for the $(Q^3)_8$ clusters, belonging to the fs irrep {70}.

$(Q^4)_3$	f	s	Λ	$(Q^3)_1(Q)_3$ recoupling	
ϕ_1	$\underline{3}$	0	-4	BQ	
φ_2	$\underline{3}$	1	$-10/3$	BQ	
ϕ_3	$\underline{6}^*$	1	$-4/3$	BQ	
ϕ_4	$\underline{15}$	0	0	BQ	
φ_5	$\underline{15}$	1	2/3	BQ	DQ
ϕ_6	$\underline{15}$	2	2		DQ
ϕ_7	$\underline{15}_s$	1	14/3		DQ

Table 2.15: eigenvalues of Δ for the $(Q^4)_3$ clusters belonging to the fs irrep {210$_1$} and recoupling to the baryon-quark channels (see table 2.6).

$(Q^4)_{6*}$	f	s	Δ
ϕ_1	$\underline{3}$	1	$-7/3$
ϕ_2	$\underline{6}$*	0	-1
ϕ_3	$\underline{6}$*	2	1
ϕ_4	$\underline{15}$	1	$5/3$
ϕ_5	$\underline{15}_s$	0	5

Table 2.16: eigenvalues of Δ for the $(Q^4)_{6*}$ clusters, belonging to the fs irrep $\{105_2\}$.

$(Q^5)_{3*}$	f	s	Δ	$(Q^3)_1 (Q^2)_{3*}$ recoupling			
ϕ_1	$\underline{3}$*	1/2	-4	BT_0	BT_1		
ϕ_2	$\underline{3}$*	3/2	-3		BT_1		
ϕ_3	$\underline{6}$	1/2	-2	BT_0	BT_1		
ϕ_4	$\underline{6}$	3/2	-1		BT_1	DT_0	
ϕ_5	$\underline{15}$*	1/2	0	BT_0	BT_1		DT_1
ϕ_6	$\underline{15}$*	3/2	1		BT_1		DT_1
ϕ_7	$\underline{15}$*	5/2	8/3				DT_1
ϕ_8	$\underline{24}$	1/2	3		BT_1		DT_1
ϕ_9	$\underline{24}$	3/2	4		BT_1	DT_0	DT_1
ϕ_{10}	$\underline{21}$	1/2	8				DT_1

Table 2.17: eigenvalues of Δ for the $(Q^5)_{3*}$ clusters belonging to the fs irrep $\{420\}$ and recoupling to baryon-diquark channels (see tables 2.6 and 2.12).

$(Q\bar{Q})_8$	Q				$\bar{Q}$				cs	s	Δ
	f	cs	c	s	f	cs	c	s			
ϕ_1	$\underline{3}$	$[1]$	$\underline{3}$	$1/2$	$\underline{3^*}$	$[1^5]$	$\underline{3^*}$	$1/2$	$[21^4]$	0	$1/2$
ϕ_2										1	$-1/6$

Table 2.18: *eigenvalues of* Δ *for the* $(Q\bar{Q})_8$ *clusters.*

$(Q^2\bar{Q})_{\underline{3}}$	Q^2						Δ	eigenstate	$(Q\bar{Q})_1 (Q)_3$ recoupling	
	f	cs	c	s	cs	s				
ϕ_1	$\underline{3^*}$	$[2]$	$\underline{3^*}$	0	$[1]$	$1/2$	-5.42	$\begin{bmatrix} .582 & -.813 \\ .813 & .582 \end{bmatrix}\begin{bmatrix} \phi_1 \\ \phi_2 \end{bmatrix}$	PQ	VQ
ϕ_2			$\underline{6}$	1	$[31^4]$	$1/2$	-0.25		PQ	VQ
ϕ_3					$[31^4]$	$3/2$	$4/3$			VQ
ϕ_4	$\underline{6}$	$[1^2]$	$\underline{6}$	0	$[1]$	$1/2$	-2.42	$\begin{bmatrix} -.582 & .813 \\ .813 & .582 \end{bmatrix}\begin{bmatrix} \phi_4 \\ \phi_5 \end{bmatrix}$	PQ	VQ
ϕ_5			$\underline{3^*}$	1	$[2^2 1^3]$	$1/2$	2.75		PQ	VQ
ϕ_6					$[2^2 1^3]$	$3/2$	$4/3$			VQ

Table 2.19: *eigenvalues of* Δ *for the* $(Q^2\bar{Q})_{\underline{3}}$ *clusters and the recoupling to meson-quark channels (see table 2.8).*

2.5. An example: the orbitally excited $Q-\bar{Q}$ mesons

For $Q-\bar{Q}$ mesons the mass operator

$$M = M_\ell + m_1 \Delta_1 + m_2 \Lambda_2 \qquad (2.38)$$

reduces to $M = M_\ell$ as there is one particle at each end, so $\Delta_1 = \Lambda_2 = 0$. For nonstrange orbitally excited $Q-\bar{Q}$ mesons the multiplet masses M_ℓ, found from $M_\ell^2 = M_0^2 + (1/\alpha_3')\ell$ with $M_0(2;0) = 0.673$ GeV and $1/\alpha_3' = 1.1$ GeV^2, are compared with the experimental masses in table 2.20. As

ℓ	M_ℓ[GeV]	J^{PC}	M_{exp} [GeV]	
			I = 1	I = 0
0	0.67	0^{-+}	π(0.138)	η(0.549)
		1^{--}	ρ(0.776)	ω(0.783)
1	1.25	1^{+-}	B(1.231)	
		0^{++}	δ'(~1.27)	ϵ'(~1.3)
		1^{++}	A_1(1.28)	D(1.276)
		2^{++}	A_2(1.312)	f(1.271)
2	1.63	2^{-+}	A_3(~1.64)	
		1^{--}	ρ'(~1.60)	
		2^{--}		
		3^{--}	g(1.688)	ω(1.668)
3	1.94	3^{+-}		
		2^{++}	~ 1.95	
		3^{++}		
		4^{++}	~ 1.98	h(2.04)

Table 2.20. Predicted and experimental $Q\bar{Q}$ mesons. The experimental masses are taken from refs [PDG 78], [Oza 78] and [Dau 79].

expected the color-magnetic interaction between the quark and the anti-
quark, which reside at different ends, vanishes and the ρ- and π-
trajectories become degenerate in the $M^2-\ell$ plane. Already for $\ell = 1$
they are very close. The $Q\bar{Q}$ $\ell = 1$ states containing nonstrange quarks
all lie around 1.25 GeV. For almost all of these states candidates
exist in this region. The scalar mesons ($J^{PC} = 0^{++}$) $\varepsilon(700)$, $S^*(980)$
and $\delta(980)$ do not belong to the $^3P_0$ $Q\bar{Q}$ nonet. They have a very natural
explanation as $\ell = 0$ $Q^2\bar{Q}^2$ states [Jaf 77.2]. From tables 2.3, 2.4 and
2.10 it is found that the lowest $Q^2\bar{Q}^2$ s-wave states have $J^{PC} = 0^{++}$
and $\Delta = -10.84$. The $n^2\bar{n}^2$ (I = 0) state has a mass $M \simeq 0.7$ GeV; the
two (degenerate) $ns\bar{n}\bar{s}$ (I = 0 and 1) states have a mass $M \simeq 1.2$ GeV
(n = nonstrange quark, s = strange quark). The shift of the position
of the two degenerate states to the $K\bar{K}$ threshold at 0.98 GeV is due
to the strong coupling of the states to the $K\bar{K}$ channel [Jaf 79.1,
Som 80].

2.6. Phenomenological contributions

2.6.1. Exchange contribution

    In this section we discuss the first of two possible contributions
to the mass, namely the exchange contribution. Quarks reside at the
ends of the stringlike bag but their wave functions nevertheless may
overlap. For a system of identical particles the wave functions must
have a definite symmetry. This leads to exchange contributions which
depend on the symmetry of the spatial part of the wave function. These
contributions are absent in the $Q-\bar{Q}$ system as the wave function need
not have a definite symmetry; they are present in a bag with more
quarks or antiquarks, but will vanish for large ℓ values when the

quarks at different ends are spatially separated.

To find a (first-order) expression for the exchange contributions we neglect all splittings due to color, flavor and spin interactions. For each quark two spatial wave functions are possible, $|1>$ or $|2>$, indicating whether the quark belongs to the cluster at end 1 or at end 2. For an N-quark state $Q^{N_1}-Q^{N_2}$ the spatial part of the wave function for the Q^{N_1} system belongs to the symmetric irrep of $S(N_1)$, the symmetric or permutation group of N_1 objects. This irrep is represented by the Young diagram $[N_1]$ (see appendix B). The symmetry of the Q^{N_2} system is given by the Young diagram $[N_2]$. The spatial part of the total wave function then belongs to the reducible representation of $S(N)$ given by the product of these symmetric irreps of $S(N_1)$ and $S(N_2)$. The reduction of this representation in its (N_2+1) irreducible components (say $N_2 \leq N_1$) is given by

$$[N_1] \otimes [N_2] = \sum_{\nu=0}^{N_2} [N_1+N_2-\nu,\nu] = \sum_{\nu=0}^{N_2} [N-\nu,\nu] \quad . \tag{2.39}$$

These irreps can be simply labeled by $\nu = 0$ to N_2. As the mass operator M_0 (eq. 2.3) is a scalar operator under permutations, it can be written as

$$M_0 = \sum_{\nu} h_{\nu} P_{\nu} \quad , \tag{2.40}$$

where h_{ν} is the eigenvalue of M_0 for states whose (spatial) wave functions belong to the irrep $[N-\nu,\nu]$ of $S(N)$ and P_{ν} is the projection operator on this irrep. The eigenvalues h_{ν} can be expressed in terms of (N_2+1) exchange integrals. The simplest two are the direct matrix element

$$<12\ldots|M_0|12\ldots> - M_d \tag{2.41}$$

54

and the two-quark interchange matrix element

$$\langle 12 \ldots | M_0 | 21 \ldots \rangle = - M_e \qquad . \qquad (2.42)$$

When we assume that all other (more-quark) exchange matrix elements do
not contribute, M_0 can be expressed in M_d and M_e:

$$M_0 = M_d - M_e \sum_\nu \{ (N_1 - \nu)(N_2 - \nu) - \nu \} P_\nu \qquad (2.43)$$

The minus sign in eq. 2.42 and 2.43 is introduced because we expect a
negative contribution of the exchange integrals in the case of the
baryonic Q-Q^2 excitations. In this case eq. 2.43 becomes

$$M_0 = M_d - M_e (2 P_0 - P_1) \qquad (2.44)$$

The exchange integral is analogous to the one in the Helium atom, but
the sign is different. In the Helium atom the exchange contribution
comes from the electric interaction between the two electrons
$\sim (-e)^2 > 0$. In our case it comes from the color interaction between
two quarks $\sim g^2 F_1 \cdot F_2$, which for two quarks coupling to a color irrep
$\underline{3}^* \subset \underline{3} \otimes \underline{3}$ equals $- 2 g^2/3 < 0$. It also follows that M_e can be positive
or negative when the number of quarks and antiquarks is larger than
three since a two-quark subsystem can then also couple to a color irrep
$\underline{6} \subset \underline{3} \otimes \underline{3}$ for which $g^2 F_1 \cdot F_2 = g^2/3$.

   The total wave function of an N-quark system is antisymmetric. A
spatial wave function with a symmetry given by the Young diagram
$[N-\nu, \nu]$ is uniquely combined with a color-spin-flavor (csf) wave
function with a symmetry given by the associated diagram $[2^\nu, 1^{N-\nu}]$.
P_ν therefore also projects out the allowed color $\otimes$ spin $\otimes$ flavor
representations.

   For baryon resonances the projection operators P_ν even project out

flavor-spin SU(6) irreps since for Q^3 baryons the color part is completely antisymmetric ($[1^3]$). States for which the flavor-spin part belongs to the symmetric irrep $\{56\} = [3]$ or the mixed symmetric irrep $\{70\} = [2,1]$ have a spatial part belonging to the symmetric irrep $[3]$ ($\nu = 0$) or the mixed symmetric irrep $[2,1]$ ($\nu = 1$) respectively. Using the projection operators P_{56} and P_{70} on the 56- and 70-dimensional representations of flavor-spin SU(6) we can write eq. 2.44 as [Cut 77]

$$M = M_d - M_e \ (2 \ P_{56} - P_{70}) \qquad .\qquad\qquad (2.45)$$

We expect that the exchange contributions are not very important for bags with a color $\underline{3}$-$\underline{3}^*$ structure and masses above 2 GeV. This is based on the observation that for $\ell = 2$ Q^2-Q baryons with $M \simeq 1.9$ GeV the exchange contributions are already rather small compared to the $\ell = 1$ Q^2-Q baryons ($M \simeq 1.5 - 1.8$ GeV). The cross section of a bag only depends on the color structure $\underline{c}$-$\underline{c}^*$. The separation of the ends therefore does not depend on the angular momentum ℓ, but rather on the mass. This leads to the expectation that the mass is a criterion for the exchange contributions and that these contributions can be neglected above 2 GeV.

2.6.2. Hyperfine structure

The color-magnetic interactions in a spherical bag or in the clusters of a stringlike bag are responsible for splittings in the mass spectra of multiquark states which we call the fine structure. Other effects due to color interactions we will call the hyperfine structure. One contribution is the color-magnetic interaction between the magnetic moments of two quarks at different ends of the bag. This residual color-magnetic interaction is written as

$$M_m^{(res)} = m_{12} \Lambda_{12} \qquad , \qquad (2.46)$$

where m_{12} is the strength and Λ_{12} is the group-theoretical factor

$$\Lambda_{12} = - \sum_{1_1, 1_2} (F\sigma)_{1_1} \cdot (F\sigma)_{1_2} \qquad , \qquad (2.47)$$

where the summation is over pairs of quarks at different ends. The factor Δ_{12} is the difference between Δ and $\Lambda_1 + \Delta_2$,

$$\Delta_{12} = \Delta - \Delta_1 - \Delta_2 \qquad , \qquad (2.48)$$

and depends on the color-spin, color and spin of the clusters and the entire system. Other interactions in (stringlike) orbitally excited bags may be spin-orbit- and tensor-like interactions.

The exchange and hyperfine interaction terms can be included in a phenomenological way. We will only consider them when we discuss our results obtained from the mass formula in table 2.1 and when the experimental mass spectrum requires the inclusion of them.

2.7. Resonant behavior of multiquark states

The masses of multiquark states are calculated in a zero-width approximation. A set of quarks and antiquarks is confined to a bag. If their number is larger than three there are color-singlet subsystems in such a bag, e.g. $(Q\bar{Q})_1 (Q\bar{Q})_1 \subset (Q^2\bar{Q}^2)_1$, $(Q^3)_1 (Q\bar{Q})_1 \subset (Q^4\bar{Q})_1$, and $(Q^3)_1 (Q^3)_1 \subset (Q^6)_1$. These subsystems need not be confined, the multiquark bag can very easily fission into two bags, and very large widths are expected.

Jaffe and Low [Jaf 79.1] argued that the zero-width approximation is not valid and that one has to use a new method of analyzing the data; the masses calculated in the bag model are the positions of poles

in the P-matrix.

The P-matrix is related to the S-matrix via

$$P = \sqrt{k} \ [I'(x_0) + O'(x_0)S][I(x_0) + O(x_0)S]^{-1} \ \sqrt{k} \quad , \qquad (2.49)$$

where $I(x)$ and $O(x)$ are the incoming and outgoing waves. We use dimen-
sionless wave functions $u(x) = u(r)/\sqrt{k}$, $x = kr$, $x_0 = kb$, where b is the
distance beyond which the color-singlet subsystems are free. If no
long-range potentials like the Coulomb-potential are present $O(x)$ and
$I(x)$ become for an ℓ-wave channel and large x:

$$O(x) \ \to \ x \ h_\ell^{(1)}(x) \ \to \ (-1)^{\ell+1} \ e^{1x} \quad , \qquad (2.50a)$$

$$I(x) \ \to \ x \ h_\ell^{(2)}(x) \ \to \ (1)^{\ell+1} \ e^{-1x} \quad . \qquad (2.50b)$$

The relation between P and K-matrices is

$$P = \sqrt{k} \ [F'(x_0) + G'(x_0)K][F(x_0) + G(x_0)K]^{-1} \ \sqrt{k} \qquad (2.51)$$

where $F(x)$ and $G(x)$ are tne regular and irregular solutions which when
no long-range potentials are present become:

$$F(x) \ \to \ x \ j_\ell(x) \ \to \ \sin(x - \ell\pi/2) \quad , \qquad (2.52a)$$

$$G(x) \ \to \ - \ x \ n_\ell(x) \ \to \ \cos(x - \ell\pi/2) \quad . \qquad (2.52b)$$

The P-matrix is in general a multichannel matrix, I, O, and $\sqrt{k}$ being
diagonal matrices; it is real for real energies, symmetric and it has
fewer singularities than the K-matrix. The P-matrix equals

$$P = \sqrt{k} \ \psi'(x_b) \ \psi^{-1}(x_b) \ \sqrt{k} \quad . \qquad (2.53)$$

In a potential-scattering problem it has poles at the energy values
$E = E_n$ where E_n are the eigenvalues in the problem when we impose the
boundary condition $\psi(x_b) = 0$. The P-matrix formalism naturally applies
to multiquark states as the $(Q^2\bar{Q}^2)_1$ states are the solutions in the

$(Q\bar{Q})_1 (Q\bar{Q})_1$ channel after imposing the bag model boundary conditions.

The one-dimensional P-matrix for an ℓ-wave channel is found from eq. 2.51 and $K_\ell = \tan \delta_\ell$:

$$\tan (\delta_\ell - \phi_\ell) = \text{Im } L_\ell / (P_\ell/k - \text{Re } L_\ell) \qquad , \qquad (2.54)$$

where

$$\phi_x = - F_\ell(x_0)/G_\ell(x_0) \quad \text{and} \quad L_\ell = O'_\ell(x_0)/O_\ell(x_0) \quad . \quad (2.55)$$

L_ℓ and ϕ_ℓ can be obtained from the recursion relations

$$\text{Im } L_\ell = x \text{ Im } L_{\ell-1}/[(\ell/x - \text{Re } L_{\ell-1})^2 + (\text{Im } L_{\ell-1})^2] \qquad (2.56a)$$

$$\text{Re } L_\ell = - \ell/x + x(\ell/x - \text{Re } L_{\ell-1})/[(\ell/x - \text{Re } L_{\ell-1})^2$$
$$+ (\text{Im } L_{\ell-1})^2] \qquad (2.56b)$$

$$\phi_x = \phi_{\ell-1} + \tan^{-1} [\text{Im } L_{\ell-1}/(\ell/x - \text{Re } L_{\ell-1})] \qquad . \qquad (2.56c)$$

The explicit expressions for $\ell = 0$ and $\ell = 1$ become

$$P_0/k = \cot (x_0 + \delta_0) \qquad , \qquad (2.57)$$

$$P_1/k = [-1 + x_0^2 \cot (x_0 + \delta_1 - \tan^{-1} x_0)]/(1 + x_0^2). \quad (2.58)$$

The residues of the poles in the P-matrix are proportional to the projection operators on the channels in which the poles occur. Like for the S-matrix a small residue gives a rapid variation in the phase shift ($x_0 = kb$ is approximately constant in the neighborhood of the resonance momentum k_R), while a large residue gives a smooth variation in the phase shift.

We discern a few possibilities. First consider an unstable state, which easily fissions in an S-wave. From eq. 2.57 it follows that the relation $k_R b + \delta_0 = \pi$ holds for the first pole. This means that this state gives a positive (attractive) phase shift when $k_R b < \pi$ and that

it gives a negative (repulsive) phase shift when $k_R b > \pi$.

An example is the $\epsilon(700)$; this is the lowest $Q^2 \bar{Q}^2$ state ($J^{PC} = 0^{++}$, $I^G = 0^+$) coupling to the $I = 0$ $\pi\pi$ S-wave. It causes a strong attraction ($k_R \simeq 0.32$ GeV and with a reasonable value $b \simeq 6$ GeV^{-1} we find $k_R b \simeq 2.9 < \pi$). A P-matrix analysis [Jaf 79.1] of the $I = 0$ $\pi\pi$ S-wave gives a pole at 0.69 GeV. In S-matrix analyses the ϵ meson corresponds to a pole far from the real axis [Pro 79], $M = (0.66 - 0.32 \text{ i})$ GeV and therefore appears as a wide resonance [Nag 75] with $M = 0.76$ GeV and $\Gamma = 0.64$ GeV.

These unstable states which fission into open channels generally will not show up as (clear) S-matrix poles but contribute to the background, especially when the positions of the poles are near $k = \pi/b$. For instance if we have P-matrix poles at positions $n\pi/b$ (n integer) with residues $2\pi^2/b^3$ there is no contribution to the phase shift. Eq. 2.57 and the expansion

$$x \cot x = 1 + \sum_{n=1}^{\infty} \frac{2x^2}{x^2 - n^2\pi^2} \tag{2.59}$$

even shows that δ might be zero. A nice example is the lowest exotic $I = 2$ meson, a $Q^2 \bar{Q}^2$ state with $\Delta = -4.84$ predicted at 1.14 GeV coupling to the $I = 2$ $\pi\pi$ S-wave ($k_R = 0.55$ GeV). This $\pi\pi$-wave shows a negative phase shift. There is no pole in the S-matrix, but the P-matrix analysis [Jaf 79.1] shows a pole at 1.04 GeV.

When there is a barrier which prohibits the decay, the states are more stable and usually will show up in the S-matrix. Examples of such barriers are weak coupling and angular momentum barriers for decays in L-waves with $L \neq 0$.

Consider the ρ meson as a first example. The ρ meson is (mainly)

a $Q\bar{Q}$ meson and for the coupling to the I = 1 $\pi\pi$ P-wave creation of a quark-antiquark pair is necessary. The coupling to $(Q\bar{Q})_1 (Q\bar{Q})_1$ is therefore suppressed and the P- and S-matrix poles almost coincide.

Another example is the S* predicted at 1.2 GeV. This is a $Q^2\bar{Q}^2$ state which couples strongly to $K\bar{K}$, the coupling to $\pi\tau$ is suppressed as this requires annihilation of an $s\bar{s}$ pair and the creation of an $n\bar{n}$ pair. A two-channel P-matrix analysis of the I = 0, $\pi\pi$-$K\bar{K}$ S-wave shows a pole at 1.04 GeV. The one-channel (reduced) P-matrix analysis shows a pole at the $K\bar{K}$ threshold at 0.98 GeV, which (as expected) lies below the pole in the full P-matrix analysis. In a coupled-channel S-matrix analysis [Som 80] the poles which in zero-width approximation lie above the $K\bar{K}$ threshold also shift to the $K\bar{K}$ threshold when the coupling between the bag and the decay channels is increased.

Excited baryons are described under the assumption that the quarks are confined to a stretched bag. For the simplest (three-quark) baryon resonances two quarks, referred to as the diquark, reside in one end and the third quark resides at the other end. The excitation energy for orbital excitations comes from the color fields inbetween the color sources, which are the quarks. The color-electric field lines are collimated in a flux tube [Joh 76], which leads to the constant linear energy density $T_0 = (8\pi\alpha_c B f_c^2)^{1/2}$. In case of three-quark baryons the color structure must be $(Q^2)_{3*}-(Q)_3$ and $f_c^2 = 4/3$, but for four-quark-one-antiquark baryons different color structures are possible, e.g. $(Q^2\bar{Q})_3-(Q^2)_{3*}$ and $(Q^2\bar{Q})_{6*}-(Q^2)_6$.

The essential difference between this model and quark-shell models [Hor 73] is that the gluons play an important role in the excited states. For the ground state baryons containing light quarks in a spherical bag [DeG 75] the gluons can be discarded, but for heavy quarks or high orbital angular momenta the color-electric and color-magnetic fields dominate the bag energy. The quarks are only the sources of these fields and their wave functions are no longer impor-tant. In this case the bag is stringlike [Joh 76]. An intermediate case is the bag which contains light quarks and has small angular momentum. This system can be approximately described by a bag with quarks in higher waves taking into account surface deformations [Reb 76, DeG 78]. The system can also be approximately described by a stringlike bag taking into account the possibility of the exchange of quarks between the ends [Mul 78.4, Mul 79.1], which is discussed in this chapter and

which links up better with our general treatment of the multiquark states.

The Q^3 ground states belong to the multiplet $[56,0^+]$ in the SU(6,FS) × O(3) classification. Many baryon resonances have been found, which can be also classified in flavor-spin multiplets but these assignments are not always definite. For instance, a nucleon resonance with $J^P = 3/2^-$ can belong to the $[70,1^-]$, $[56,1^-]$ or $[70,3^-]$ multi-plets. Often one tries to make a more definite assignment by consider-ing the mass or the coupling to decay channels. For instance a nucleon with $J^P = 3/2^-$ belonging to the $[70,3^-]$ multiplet has spin s = 3/2 and decouples from the ΛK channel.

In combining three quarks one generally finds the flavor-spin multiplets

$$\{6\} \otimes \{6\} \otimes \{6\} = \{56\} \oplus \{70\} \oplus \{70\} \oplus \{20\} \qquad (3.1)$$

and in a quark model where the quarks reside in orbitals $(n_r+1)\ell$ with energies $E_{1s} < E_{1p} \leq E_{2s} \leq E_{1d} < \ldots$ (harmonic oscillator, linear potential) one finds (after elimination of spurious states) multiplets $[56,0^+]$, $[70,1^-]$, $[56,0^+]$, $[56,2^+]$, $[70,2^+]$, $[70,0^+]$, $[20,1^+]$, $[70,3^-]$ $[56,1^-]$, ... The ordering of the multiplets depends on the form of the potential [Fag 79, Dal 79].

In the stringlike bag the flavor-spin content is determined by the product of the irreps to which the quarks at the ends belong. The diquark belongs to the antisymmetric color irrep $\underline{3}^*$ and the symmetric flavor-spin irrep $\{21\}$. Therefore the flavor-spin content for baryon resonances is

$$\{21\} \otimes \{6\} = \{56\} \oplus \{70\} \qquad . \qquad (3.2)$$

The eigenstates for the baryons, however, do not purely belong to one

of the flavor-spin irreps {56} or {70} except for trivial cases like
$\Delta(3/2)$, i.e. a Δ resonance with spin 3/2, and $\Omega(3/2)$ which only appear
in the irrep {56} or $N(3/2)$, $\Delta(1/2)$, $\Lambda(3/2)$ and $\Omega(1/2)$ which only
appear in the irrep {70}. The other states are mixtures of the irreps
{56} and {70}. For small ℓ values the exchange contributions, due to
the tunneling of a quark from one end to the other, are large and the
mixing is small. For large ℓ values the exchange terms vanish and the
fine structure splitting, which breaks flavor-spin symmetry, remains;
in this case the mixing is strong. We mention here that even for s-wave
baryons, indications exist that in the decay the flavor-spin symmetry
is broken [Zra 79].

The number of flavor-spin multiplets in the case of stringlike
(excited) bags is considerably smaller than the number of them in the
quark-shell model if we restrict ourselves to excitations of the bag
in which the quarks are not excited. For instance all flavor-spin
irreps {20} are absent.

Baryons ($B = 1$) with more than three quarks are also possible,
e.g. s-wave $Q^4\bar{Q}$ states [Jaf 76, Mul 78.2, Som 78, Str 79], s-wave
$Q^5\bar{Q}^2$ states [Str 79] and their orbital excitations [Mul 78.2, Mul 78.3,
Fuk 78, Høg 78]. Except when they have a very low mass or when the
decay to open channels is inhibited by some barrier these states will
not show a clear resonance behavior.

The content of this chapter is as follows. In section 3.1 we apply
the multiquark mass formula of chapter 2 to the Q^3 and $Q^4\bar{Q}$ baryons. For
the low-lying Q^3 baryons the phenomenological contributions can be
included as many experimental candidates are present. In section 3.2
we consider the nonstrange baryons. For $\ell \geq 2$ the mass formula gives

a good description of the mass spectrum without the phenomenological contributions. For $\ell = 1$ a good description can be obtained when these contributions are included. In section 3.3 we consider the strange baryons. In the sections 3.2 and 3.3 we also discuss the possibility of $Q^4\bar{Q}$ baryon resonances. In section 3.4 we discuss the (exotic) $Y = 2$ baryon resonances.

Q^3 baryon resonances can decay in baryon-meson channels via quark-antiquark creation. The coupling of the resonances to the decay channels in the $^3P_0$ model is treated in section 3.5 and applied to the nonstrange baryons in section 3.6.

3.1. The masses of baryon resonances

3.1.1. The multiquark mass formula

Using the mass formula for multiquark states discussed in chapter 2, we find the masses from

$$M = M_0 + m \, \Delta \tag{3.3}$$

for the $(Q^3)_1$ and $(Q^4\bar{Q})_1$ states and from

$$M = [M_0^2 + (1/\alpha')\ell]^{1/2} + m_1 \Delta_1 + m_2 \Delta_2 \tag{3.4}$$

for orbitally excited systems. While for the three-quark system only one configuration is possible, namely $(Q^2)_{3*}-(Q)_3$, there are more possibilities for the four-quark-one-antiquark system, namely

$(Q^2\bar{Q})_3-(Q^2)_{3*}$, $(Q^3\bar{Q})_{3*}-(Q)_3$, $(Q^4)_3-(\bar{Q})_{3*}$, $(Q^2\bar{Q})_{6*}-(Q^2)_6$ and $(Q^3)_8(Q\bar{Q})_8$.

In the baryon sector the presence of Q^3 states makes the detection of the far more unstable $Q^4\bar{Q}$ states difficult. We will therefore mainly concentrate on the Q^3 states.

The fine structure of the spectrum is determined by the color-magnetic interactions between the quarks in the clusters. For Q^2-Q baryons the fine structure is therefore determined by the splitting of the diquark (see fig. 2.2), $\Delta = -2$ for the T_0-diquark and $\Delta = +2/3$ for the T_1-diquark. The most natural way to classify the baryon resonances is therefore according to their diquark content. We distinguish A states, consisting of a T_0-diquark and a quark, and B states, consisting of an T_1-diquark and a quark. As the strength of the color-magnetic interaction also depends on the number of strange quarks in the diquark, there are small differences in the color-magnetic contributions for the A and B states (table 3.1). Another possible classification is the usual classification in $SU(6,FS)$ and $SU(3,F)$ multiplets.

type	diquark f(y,l)s	Resonances and their spin s				M_m [MeV]
A(nn-n)	$\underline{3}^*$(2/3,0)0	N(1/2)				− 170
B(nn-n)	$\underline{6}$ (2/3,1)1	N(1/2)	N(3/2)	Δ(1/2)	Δ(3/2)	+ 57
A(nn-s)	$\underline{3}^*$(2/3,0)0	Λ(1/2)				− 170
A(ns-n)	$\underline{3}^*$(−1/3,1/2)0	Λ(1/2)		Σ(1/2)		− 140
B(ns-n)	$\underline{6}$ (−1/3,1/2)1	Λ(1/2)	Λ(3/2)	Σ(1/2)	Σ(3/2)	+ 47
B(nn-n)	$\underline{6}$ (2/3,1)1			Σ(1/2)	Σ(3/2)	+ 57
A(ns-s)	$\underline{3}^*$(−1/3,1/2)0	Ξ(1/2)				− 140
B(ss-n)	$\underline{6}$ (−4/3,0)1	Ξ(1/2)	Ξ(3/2)			+ 39
B(ns-s)	$\underline{6}$ (−1/3,1/2)1	Ξ(1/2)	Ξ(3/2)			+ 47
B(ss-s)	$\underline{6}$ (−4/3,0)1	Ω(1/2)	Ω(3/2)			+ 39

Table 3.1. $(Q^2)_{3^*}-(Q)_3$ orbitally excited baryons, diquark-quark basis states and the color-magnetic energy. The spin s has to be combined with the orbital angular momentum ℓ to find the total spin J.

The flavor-spin basis and the diquark-quark bases are related via the unitary transformation given in table 3.2.

3.1.2. Exchange contributions

The Q^2-Q baryon resonances are the lowest orbitally excited states and we may expect exchange contributions. Effectively the wave function for the Q^2-Q system is

$$\psi \sim \chi(Q_1^2,Q_2)\ R_B(r_{12})\ Y_m^{(\ell)}(\hat{r}_{12}) \qquad (3.5)$$

where the part $\chi(Q_1^2,Q_2)$ describes which quarks reside in end 1 or end 2 and the degrees of freedom like flavor, color and spin of the quarks.

y = 1 (N/Δ)	{56}, $\underline{8}$, N(1/2)	{70}, $\underline{8}$, N(1/2)	{70}, $\underline{8}$, N(3/2)	{70}, $\underline{10}$, Δ(1/2)	{56}, $\underline{10}$, Δ(3/2)
A(nn-n) N(1/2)	$\sqrt{1/2}$	$-\sqrt{1/2}$			
B(nn-n) N(1/2)	$\sqrt{1/2}$	$\sqrt{1/2}$			
B(nn-n) N(3/2)			1		
B(nn-n) Δ(1/2)				1	
B(nn-n) Δ(3/2)					1

y = 0 (Λ/Σ)	{56}, $\underline{8}$, Λ(1/2)	{70}, $\underline{1}$, Λ(1/2)	{70}, $\underline{8}$, Λ(1/2)	{70}, $\underline{8}$, Λ(3/2)	{56}, $\underline{8}$, Σ(1/2)	{70}, $\underline{8}$, Σ(1/2)	{70}, $\underline{10}$, Σ(1/2)	{56}, $\underline{10}$, Σ(3/2)	{70}, $\underline{8}$, Σ(3/2)
A(nn-s) Λ(1/2)	$\sqrt{1/3}$	$\sqrt{1/3}$	$-\sqrt{1/3}$						
A(ns-n) Λ(1/2)	$-\sqrt{1/6}$	$\sqrt{2/3}$	$\sqrt{1/6}$						
B(ns-n) Λ(1/2)	$-\sqrt{1/2}$	0	$-\sqrt{1/2}$						
B(ns-n) Λ(3/2)				1					
A(ns-n) Σ(1/2)					$\sqrt{1/2}$	$-\sqrt{1/2}$	0		
B(nn-s) Σ(1/2)					$\sqrt{1/3}$	$\sqrt{1/3}$	$\sqrt{1/3}$		
B(ns-n) Σ(1/2)					$-\sqrt{1/6}$	$-\sqrt{1/6}$	$\sqrt{2/3}$		
B(nn-s) Σ(3/2)								$\sqrt{1/3}$	$\sqrt{2/3}$
B(ns-n) Σ(3/2)								$\sqrt{2/3}$	$-\sqrt{1/3}$

(table 3.2)

69

y = −1 (Ξ)	{56}, $\underline{8}$, $\Xi(1/2)$	{70}, $\underline{8}$, $\Xi(1/2)$	{70}, $\underline{10}$, $\Xi(1/2)$	{56}, $\underline{10}$, $\Xi(3/2)$	{70}, $\underline{8}$, $\Xi(3/2)$
A(ns-s) $\Xi(1/2)$	$\sqrt{1/2}$	$-\sqrt{1/2}$	0		
B(ns-s) $\Xi(1/2)$	$\sqrt{1/6}$	$\sqrt{1/6}$	$\sqrt{2/3}$		
B(ss-n) $\Xi(1/2)$	$-\sqrt{1/3}$	$-\sqrt{1/3}$	$\sqrt{1/3}$		
B(ns-s) $\Xi(3/2)$				$\sqrt{2/3}$	$\sqrt{1/3}$
B(ss-n) $\Xi(3/2)$				$\sqrt{1/3}$	$-\sqrt{2/3}$

y = −2 (Ω)	{70}, $\underline{10}$, $\Omega(1/2)$	{56}, $\underline{10}$, $\Omega(3/2)$
B(ss-s) $\Omega(1/2)$	1	
B(ss-s) $\Omega(3/2)$		1

Table 3.2: The unitary transformation matrices between the diquark-quark basis and the flavor-spin basis for Q^6 baryons.

The part $R_B\, Y_m^{(\ell)}$ describes the spatial wave function of the bag; $\vec{r}_{12}$ gives the relative position of the ends (1 and 2) of the bag. Neglecting the color, flavor and spin of the quarks χ reduces to $|112\rangle$, $|121\rangle$ or $|211\rangle$, indicating which quarks reside at end 1 and which quark resides at end 2. It is easily seen from

$$|112\rangle\, R_B(r_{12})\, Y_m^{(\ell)}(\hat{r}_{12}) \xrightarrow{\text{tunneling}} |122\rangle\, R_B(r_{12})\, Y_m^{(\ell)}(\hat{r}_{12})$$

$$= (-)^{\ell} \; |211\rangle \; R_B(r_{12}) \; Y_m^{(\ell)} \; (\hat{r}_{12}) \qquad (3.6)$$

that the tunneling of a quark gives an exchange contribution. The tunneling of a quark is proportional to the exchange of the other two quarks. With the factor $(-)^{\ell}$ and using eq. 2.45 we can write

$$M_T = (-)^{\ell+1} \; M_e \; (2 \; P_{56} - P_{70}) \qquad (3.7)$$

From eq. 2.45 we see that next to the exchange contribution in eq. 3.7 also a constant contribution, which we denote as ΔM, may be present.

3.1.3. Hyperfine structure

Three types of hyperfine interactions have been discussed in section 2.6.2. We have not included spin-orbit and tensor-like interactions. The spin-orbit term is not needed in the nonstrange baryon spectrum and the inclusion of tensor-like contributions creates difficulties because we do not have explicit expressions for quark wave functions like in quark-shell models [Isg 77, Rei 78].

For small ℓ values we do include a term for the residual color-magnetic interactions (eq. 2.46). This corresponds to the contact term $\vec{S}_1 \cdot \vec{S}_j \; \delta^3(r_{ij})$ in refs [Isg 77]. The strength of the color-magnetic interactions between quarks at different ends, m_{12}, is taken as a parameter and the group-theoretical factor Δ_{12} can be written as

$$\Delta_{12} = \frac{2}{3} \, \vec{S}_1 \cdot \vec{S}_2 + 2 \, \vec{I}_1 \cdot \vec{I}_2 \qquad . \qquad (3.8)$$

3.2. The mass spectrum of nonstrange baryons

For each ℓ ($\neq 0$) the Q^2-Q baryon resonances belong to the flavor-spin representation $\{21\} \otimes \{6\}$; this representation can be decomposed into the flavor-spin irreps $\{56\} \oplus \{70\}$. From table 3.2

we see that the nonstrange baryons can be labeled $N_A(1/2)$, $N_B(1/2)$, $N_B(3/2)$, $\Delta_B(1/2)$ and $\Delta_B(3/2)$ in the diquark-quark basis or $N_{56}(1/2)$, $N_{70}(1/2)$, $N_{70}(3/2)$, $\Delta_{70}(1/2)$ and $\Lambda_{56}(3/2)$ in the flavor-spin basis; the subscripts of $N(3/2)$, $\Delta(1/2)$ and $\Delta(3/2)$ even can be omitted. Between parentheses the spin s of a state is given. Actually such a state stands for a multiplet of states with total angular momentum $J = |\ell-s|$, $|\ell-s|+1,..,|\ell+s|$, and parity $P = (-)^\ell$. Often we use instead of J^P the notation L 2I 2J indicating the Nπ-wave to which a resonance couples, the isospin and the total angular momentum.

We will separately discuss the mass spectra for orbitally excited Q^2-Q baryon resonances with $\ell = 1$, $\ell = 2$ and large ℓ ($\ell > 2$); also other possible baryon resonances, namely $Q^4\bar{Q}$ states and radially excited baryon resonances are discussed.

3.2.1. $\ell^P = 1^-$ Q^2-Q baryon resonances

Using the multiquark mass formula eq. 3.4 we calculate the masses by adding the color-magnetic splitting (table 3.1) to the multiplet mass $M_1 = 1.514$ GeV. The A-states are predicted at 1.344 GeV, the B-states at 1.573 GeV. There is a large discrepancy between these masses and the experimental negative parity baryon resonances. To explain the experimental mass spectrum we include some phenomenological terms; the mass operator becomes (section 3.1)

$$M = M_\ell + \Delta M + (-)^{\ell+1} M_e (2 P_{56} - P_{70}) + m \Delta + m_{12}\Delta_{12} . \qquad (3.9)$$

M_ℓ and m are calculated and ΔM, M_e and m_{12} are parameters. From table 3.2 the mass operator can be evaluated between the basis states in the diquark-quark or the flavor-spin basis. Except for the exchange term (M_T) the mass operator is diagonal in the diquark-quark basis.

M in GeV

0	50	100	150	M_e
130	163	206	253	ΔM

in MeV

Δ(3/2)   N(1/2)   N(3/2)   Δ(1/2)   N(1/2)
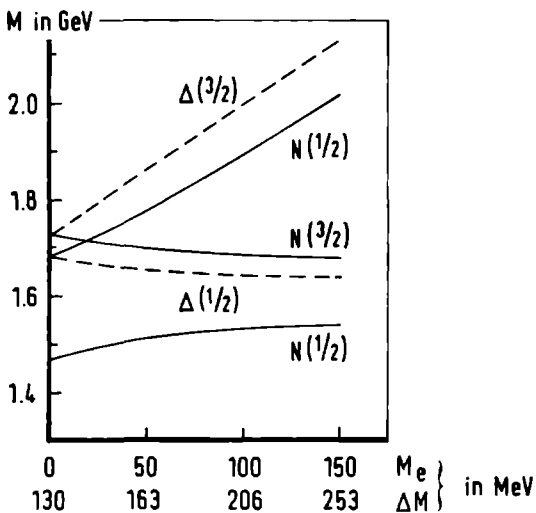
Fig. 3.1:

Masses of the $\ell^P = 1^-$

nucleon and delta

resonances as a function

of M_e. ΔM is determined

to fit the lowest

N(1/2), Δ(1/2) and

N(3/2) states.

To illustrate the effect of the exchange term we consider the nucleon and Δ resonances. Well established [Höh 78, Cut 79] are the N(1/2) states, S11(1.53) and D13(1.52), the Δ(1/2) states, S31(1.61) and D33(1.72), and the N(3/2) states, S11(1.67), D13(1.70), and D15(1.68). The parameter m_{12} follows from the difference between the N(3/2) and Δ(1/2) states which equals $M_{N(3/2)} - M_{\Delta(1/2)} = 4\,m_{12}$. So m_{12} is small. From a fit of the above resonances it follows that the values of M_e and ΔM are strongly correlated. This is shown in fig. 3.1 where the spectrum of the $\ell = 1$ N and Δ resonances has been plotted as a function of M_e. The best value of ΔM has been given below the values of M_e. To decide on the value of M_e we need the other N(1/2) and Δ(3/2) states, for which one- and two-star resonances exist as candidates [Höh 78, Cut 79]. For the N(1/2) states, candidates are the S11(1.88) and D13(1.83) resonances; for the Δ(3/2) states, candidates are the

73

S31(1.89), D33(2.01), and D35(1.91) resonances. A fit of these resonan-
ces from the analyses of the Karlsruhe-Helsinki group [Höh 78] and
the CMU-LBL group [Cut 79] yields the following parameters for $\ell = 1$;

$$\Delta M = 1.83 \text{ MeV} \quad , \quad M_e = 83 \text{ MeV} \quad , \quad m_{12} = 10.1 \text{ MeV} \quad .$$

It leads to the masses in table 3.3. In table 3.4 these masses are
compared with the experimental masses. It is noteworthy that there
are indications, although sometimes very weak, for all the predicted
resonances. Moreover, there are no indications for more negative
parity resonances in the region 1.5 - 1.9 GeV.

Mass	Eigenstate
1.509	$\begin{bmatrix} N_1(1/2) \\ N_2(1/2) \end{bmatrix} = \begin{bmatrix} -0.901 & 0.433 \\ 0.433 & 0.901 \end{bmatrix}\begin{bmatrix} N_A(1/2) \\ N_B(1/2) \end{bmatrix} = \begin{bmatrix} -0.331 & 0.944 \\ 0.944 & 0.331 \end{bmatrix}\begin{bmatrix} N_{56}(1/2) \\ N_{70}(1/2) \end{bmatrix}$
1.829	
1.684	$N(3/2)$
1.644	$\Lambda(1/2)$
1.934	$\Delta(3/2)$

*Table 3.3: The masses (in GeV) and eigenstates of the $\ell = 1$ nonstrange
baryon resonances.*

3.2.2. s-wave $Q^4\bar{Q}$ states

Other possible baryon resonances with negative parity are the
$Q^4\bar{Q}$ states. We think that they do not strongly influence the Q^3 baryon
mass spectrum, although the Q^3 baryons do contain $Q^4\bar{Q}$ admixtures. This
can be readily seen from the part H_{QPC} in the Hamiltonian responsible
for the creation of a quark-antiquark pair (with quantum numbers
$J^P = 0^+$);

(wave) J^P		M_{calc}	M_{exp} [Höh 78]	M_{exp} [Cut 79]
Nucleon resonances:				
$N_1(1/2)$	(S11) $1/2^-$	1509	1526 ± 7	1540 ± 20
	(D13) $3/2^-$	1509	1519 ± 4	1525 ± 15
N (3/2)	(S11) $1/2^-$	1684	1670 ± 8	1640 ± 30
	(D13) $3/2^-$	1684	1731 ± 15	1670 ± 25
	(D15) $5/2^-$	1684	1679 ± 8	1680 ± 15
$N_2(1/2)$	(S11) $1/2^-$	1829	1880 ± 20	
	(D13) $3/2^-$	1829		1830 ± 50
Delta resonances:				
Δ (1/2)	(S31) $1/2^-$	1644	1610 ± 7	1620 ± 20
	(D33) $3/2^-$	1644	1680 ± 70	1730 ± 30
Δ (3/2)	(S31) $1/2^-$	1934	1908 ± 30	1850 ± 35
	(D33) $3/2^-$	1934		2010 ± 100
	(D35) $5/2^-$	1934	1901 ± 15	1930 ± 20

Table 3.4: Comparison of the calculated mass spectrum and the experimental masses for $\ell = 1$. All masses are in MeV.

$$H_{QPC} \, |Q^3> = \epsilon \, |(Q^3)(Q\bar{Q})_{0^+}> = \sum_\alpha \epsilon_\alpha |(Q^4\bar{Q})_\alpha> \qquad (3.10)$$

certainly does not vanish, as it is involved in the decay of a baryon. We will more extensively discuss the $Q^4\bar{Q}$ admixtures in section 3.6.1. The predicted nonstrange $Q^4\bar{Q}$ states and their masses (using tables 2.3, 2.4 and 2.9) are given in table 3.5. Although some assignments could be made, there is no general agreement between the predicted $Q^4\bar{Q}$ states and the experimental negative parity baryons. Especially the

I			II		
(wave) J^P		mass	(wave) J^P		mass
nucleon resonances:			nucleon resonances:		
(S11)	$1/2^-$	1.51	(S11)	$1/2^-$	1.68
(D13)	$3/2^-$	1.62	(S11)	$1/2^-$	1.90
(S11)	$1/2^-$	1.71	(D13)	$3/2^-$	1.99
(D13)	$3/2^-$	1.83	(D13)	$3/2^-$	2.06
(S11)	$1/2^-$	1.98	(S11)	$1/2^-$	2.06
(D13)	$3/2^-$	2.01	(S11)	$1/2^-$	2.07
(D15)	$5/2^-$	2.01	(D13)	$3/2^-$	2.16
delta resonances:			(S11)	$1/2^-$	2.28
(D33)	$3/2^-$	1.62	(D13)	$3/2^-$	2.31
(S31)	$1/2^-$	1.71	(D15)	$5/2^-$	2.31
(S31)	$1/2^-$	1.98	delta resonances:		
(D33)	$3/2^-$	2.01	(D33)	$3/2^-$	1.99
(D33)	$3/2^-$	2.01	(S31)	$1/2^-$	2.07
(D35)	$5/2^-$	2.01	(S31)	$1/2^-$	2.28
(S31)	$1/2^-$	2.26	(D33)	$3/2^-$	2.31
I = 5/2 resonances:			(D33)	$3/2^-$	2.31
	$3/2^-$	2.01	(D35)	$5/2^-$	2.31
	$1/2^-$	2.26	(S31)	$1/2^-$	2.52

Table 3.5: The predicted $Y = 1$ $Q^4\bar{Q}$ states, for states containing only nonstrange quarks (I) and for states containing a strange quark-antiquark pair (II). All masses are in GeV.

clustering in (ℓ,s) multiplets is absent for $Q^4\bar{Q}$ states.

In section 2.7 it has been explained that the $Q^4\bar{Q}$ states generally will not appear as resonances in baryon-meson channels, but only as poles in the P-matrix. In the low-energy region, where the only open channel is $N\pi$, we can use the one-dimensional P-matrix (eq. 2.54), which for the S-wave is $P_0 = k \cot (kb + \delta_0)$. This means that in the low-energy region a $Q^4\bar{Q}$ state gives attraction in the baryon-meson channel when $k_R b < \pi$, and that it gives repulsion when $k_R b > \pi$. Examples are the $N\pi$ S11-wave, where the phase shift for low energies is positive and the $N\pi$ S31-wave, where the phase shift for low energies is negative. The lowest $Q^4\bar{Q}$ state $(Y = 1)$ lies at 1.51 GeV $(k_R = 0.45$ GeV$)$ for the S11-wave and at 1.71 GeV $(k_R = 0.59$ GeV$)$ for the S31-wave. With a typical value for $b \simeq 6$ GeV^{-1} the phase shift behavior can be explained since $k_R(S11)b = 2.7 < \pi < 3.5 = k_R(S31)b$. This is also an indication that the calculations for the lowest $Q^4\bar{Q}$ resonances are trustworthy. While the $Q^4\bar{Q}$ states give slowly rising or falling background contributions to the phase shift, the Q^3 resonances, which appear as poles in the S-matrix, give a more rapid (smaller width) increase of the phase shift. A P-matrix analysis of the baryons is complicated because, except for very low energies, it will meet with a large inelasticity [Roi 79].

3.2.3. $\ell^P = 2^+$ Q^2-Q baryon resonances

The calculation of the masses of the $\ell = 2$ Q^2-Q baryon resonances gives a satisfactory result without the inclusion of any of the phenomenological terms in eq. 3.9 containing the parameters ΔM, M_e and m_{12}. The result of this calculation (I) is given in table 3.6 and the comparison with the experimental masses in table 3.8.

Mass (I)	Eigenstate (I)
1.672	$\begin{bmatrix} N_A(1/2) \\ N_B(1/2) \end{bmatrix} = \begin{bmatrix} 0.707 & -0.707 \\ 0.707 & 0.707 \end{bmatrix} \begin{bmatrix} N_{56}(1/2) \\ N_{70}(1/2) \end{bmatrix}$
1.899	
1.899	$N(3/2)$
1.899	$\Lambda(1/2)$
1.899	$\Lambda(3/2)$

Table 3.6: The masses (in GeV) and eigenstates of the $\ell = 2$ nonstrange baryon resonances from the mass operator without phenomenological contributions.

If one includes the phenomenological contributions one finds the following parameters for $\ell = 2$:

$$\Delta M = 42 \text{ MeV} \quad , \quad M_e = 34 \text{ MeV} \quad , \quad m_{12} = 27 \text{ MeV} \quad .$$

This leads to the masses (II) given in table 3.7. The values of the parameters ΔM and M_e confirm our expectation that the parameters will vanish for large ℓ. The fact that the parameter $m_{12}(\ell)$ is larger for

Mass (II)	Eigenstate (II)
1.681	$\begin{bmatrix} N_1(1/2) \\ N_2(1/2) \end{bmatrix} = \begin{bmatrix} 0.957 & 0.289 \\ -0.289 & 0.957 \end{bmatrix} \begin{bmatrix} N_A(1/2) \\ N_B(1/2) \end{bmatrix} = \begin{bmatrix} 0.881 & -0.473 \\ 0.473 & 0.881 \end{bmatrix} \begin{bmatrix} N_{56}(1/2) \\ N_{70}(1/2) \end{bmatrix}$
1.866	
2.011	$N(3/2)$
1.902	$\Delta(1/2)$
1.909	$\Delta(3/2)$

Table 3.7: The masses (in GeV) and eigenstates of the $\ell = 2$ nonstrange baryon resonances from the mass operator with phenomenological contributions.

	(wave) J^P	$M_{calc}(I)$	$M_{calc}(II)$	M_{exp}[Höh 79]	M_{exp}[Cut 79]
nucleon resonances:					
$N_1(1/2)$	(P13) $3/2^+$	1672	1681	1710 ± 20	1740 ± 80
	(F15) $5/2^+$	1672	1681	1684 ± 3	1680 + 15 (B)
$N_2(1/2)$	(P13) $3/2^+$	1899	1866		
	(F15) $5/2^+$	1899	1866	1882 + 10	
$N(3/2)$	(P11) $1/2^+$	1899	2011	2050 + 20 (A)	
	(P13) $3/2^+$	1899	2011		
	(F15) $5/2^+$	1899	2011		
	(F17) $7/2^+$	1899	2011	2005 ± 150	1970 + 80 (B)
delta resonances:					
$\Delta(1/2)$	(P33) $3/2^+$	1899	1902	(see $\Delta(3/2)$)	
	(F35) $5/2^+$	1899	1902	(see $\Delta(3/2)$)	
$\Delta(3/2)$	(P31) $1/2^+$	1899	1909	1888 ± 20	1920 ∓ 50 (B)
	(P33) $3/2^+$	1899	1909	1868 ± 10	1960 ∓ 80 (B)
	(F35) $5/2^+$	1899	1909	1905 ± 20	1920 ± 30 (B)
	(F37) $7/2^+$	1899	1909	1913 ± 8	1950 ± 20

(A) This resonance might be also explained as a (3s) radial excitation.

(B) Additional resonances possible.

Table 3.8: Comparison of the calculated mass spectra and the experimental masses for $\ell = 2$. All masses are in MeV.

$\ell = 2$ than for $\ell = 1$ is understandable, because we try to fit a small contribution, while other comparable contributions, like spin-orbit and tensor contributions have been neglected.

In the case of $\ell = 2$ it is less evident than for $\ell = 1$ that almost

all states are present because the B states are (almost) degenerate. The only resonances for which there are still no indications are the two (degenerate) (P13) 3/2$^+$ nucleon resonances. For some of the experimentally found resonances indications exist that additional resonances are present [Cut 79].

3.2.4. Radially excited Q^3 baryon resonances

In addition to the positive parity resonances discussed in the previous section, a number of other low-lying (M $\lesssim$ 2.0 GeV) positive parity resonances exist. The P11 (1.42) and P33 (1.52) resonances can be identified as the nonstrange members of a $[56,0^+]$ multiplet. The P11 (1.72) resonance is a possible member of the lowest $[70,0^+]$ multiplet. For two other resonances, P13 (1.54) and P31 (1.55), which could be the other two nonstrange members of the $[70,0^+]$ multiplet, there exist only very weak indications [PDG 78].

In the quark-shell model excited hadrons contain quarks which reside in higher waves. The N = 2 excitations contain a $[56,0^+]$ and a $[70,0^+]$ multiplet. The physical states are linear combinations of the $(1s)^2(2s)$ and $(1s)(1p)^2$ configurations. The other linear combinations (also a $[56,0^+]$ and a $[70,0^+]$ multiplet) have to be eliminated, being spurious states [Kar 68]. In a harmonic oscillator scheme all N = 2 levels are degenerate, but anharmonic contributions will split the multiplets. The $[56,0^+]$ generally will have the lowest energy.

In the bag model quarks can be also placed in orbits. For radial excitations, however, the static spherical bag approach does not apply. The $(1s)^2(2s)$ excitations couple to breathing excitations of the surface through the boundary conditions (eqs 1.21) in the bag model [DeG 78]. Using section 1.6 with one of the (nonstrange) quarks in the

Mass	Eigenstate

$$1.399 \quad \begin{bmatrix} N_1(1/2) \\ N_2(1/2) \end{bmatrix} = \begin{bmatrix} 0.974 & 0.228 \\ -0.228 & 0.974 \end{bmatrix} \begin{bmatrix} N_A(1/2) \\ N_B(1/2) \end{bmatrix} = \begin{bmatrix} 0.850 & -0.527 \\ 0.527 & 0.850 \end{bmatrix} \begin{bmatrix} N_{56}(1/2) \\ N_{70}(1/2) \end{bmatrix}$$

1.727

$1.682 \quad N(3/2)$

$1.782 \quad \Delta(1/2)$

$1.537 \quad \Lambda(3/2)$

Table 3.9: The masses (in GeV) and eigenstates for the nonstrange radially excited baryons.

2s mode (x_{2s} = 5.396) a multiplet mass $M(nn-n^*)$ = 1.684 GeV is found. The surface oscillations can be introduced in a phenomenological way and lower the mass of the $[56,0^+]$ multiplet [DeG 78, Bow 79].

We have tried to use the mass formula for orbital excitations also for radial excitations;

$$M = M_{0*} - M_e(2 P_{56} - P_{70}) + m \lambda + m_{12} \lambda_{12} \qquad . \qquad (3.11)$$

This is possible because all terms preserve their meaning for a radially excited baryon, which also constitutes a Q^2-Q system. For m we use the value from table 2.4; M_{0*}, M_e and m_{12} are determined from the resonances P11 (1.42), P33 (1.52) and P11 (1.72). This yields the parameters

$$M_{0*} = 1.610 \text{ GeV} \quad , \quad M_e = 48 \text{ MeV} \quad , \quad m_{12} = -25 \text{ MeV} \quad ,$$

and gives the masses and eigenstates in table 3.9. The two (P11) $1/2^+$ resonances are mixtures of the flavor-spin irreps {56} and {70}. The $N_1(1/2)$ couples stronger to photons than the $N_2(1/2)$ [Bow 77], in agreement with the experimental couplings of the P11 (1.42) and P11

(1.72).

3.2.5. Orbitally excited $Q^4\bar{Q}$ resonances

Low-lying orbitally excited $Q^4\bar{Q}$ states ($\varkappa = 1$) also lead to positive parity baryons. The lowest $(Q^2\bar{Q})_3 - (Q^2)_{3*}$ state consists of an $n^2\bar{n}$ cluster with $\Delta = -5.42$ and $(\iota,s) = (1/2,1/2)$ and an n^2 cluster with $\Delta = -2$ and $(\iota,s) = (0,0)$ (a nonstrange T_0-diquark). The color-magnetic energy equals $M_m = -0.57$ GeV and (without phenomenological contributions) we find two nucleon resonances with $J^P = 1/2^+$ and $3/2^+$ at 1.52 GeV. The $n^2\bar{n}$ cluster recouples to a pion or ρ-meson and a nonstrange quark (table 2.19); this nonstrange quark recombines with the nonstrange T_0-diquark to a nucleon. The states therefore can decay in πN P-waves. They can also decay in $\pi\pi N$ S-waves after quark-antiquark creation. There are also low-lying $(Q^3\bar{Q})_{3*} - (Q)_3$ states but these are even more unstable because the $(Q^3\bar{Q})_{3*}$ cluster has two colorless sub-systems, namely $(Q^3)_1 (\bar{Q})_{3*}$ and $(Q\bar{Q})_1 (Q^2)_{3*}$, while a $(Q^2\bar{Q})_3$ cluster has only one colorless subsystem, namely $(Q\bar{Q})_1 (Q)_3$.

There might be some candidates for orbitally excited $Q^4\bar{Q}$ states, namely the narrow mass enhancements produced in $\pi N \rightarrow \tau(\pi N)$ and $\pi N \rightarrow \pi(\pi\pi N)$ [PDG 78, Hir 79] and also the P13 (1.54) and P31 (1.55) observed in $\pi N \rightarrow \pi\pi N$ [Lon 77], which we already mentioned in section 3.2.4.

3.2.6. Baryon resonances with large ℓ ($\ell > 2$)

We will only consider Q^2-Q baryons. For $\ell > 2$ we assume that the phenomenological contributions vanish. The structure of the baryon spectrum then is determined by the fine structure of the diquark and

$$M = M_\ell + m(2;0) \left\{ \frac{1}{3} s_1 (s_1+1) + \iota_1 (\iota_1+1) - 2 \right\} \quad , \qquad (3.12)$$

predicted		experimental		
		(wave) J^P	mass	ref.
$\ell=3$ $N_A(1/2)$	1.95	(D15) 5/2 $^-$	1.92	[Sax 80]
$N_B(1/2)$, $N(3/2)$	2.18	(D13) 3/2 $^-$	2.08	[Aye 76,Höh 78,Cut 79]
		(D15) 5/2 $^-$	2.23	[Aye 76,Höh 78]
		(G17) 7/2 $^-$	2.14	[Aye 76,Höh 78]
		(G19) 9/2 $^-$	2.27	[Aye 76,Höh 78]
$\Delta(1/2)$, $\Delta(3/2)$	2.18	(D35) 5/2 $^-$	2.31	[Höh 78]
		(G37) 7/2 $^-$	2.22	[Höh 78]
		(G39) 9/2 $^-$	2.17	[Aye 76]
$\ell=4$ $N_A(1/2)$	2.20	(H19) 9/2 $^+$	2.21	[Aye 76,Höh 78]
$N_B(1/2)$, $N(3/2)$	2.42			
$\Delta(1/2)$, $\Delta(3/2)$	2.42	(F37) 7/2 $^+$	2.43	[Höh 78]
		(H39) 9/2 $^+$	2.22	[Höh 78]
		(H3,11) 11/2 $^+$	2.42	[Aye 76,Höh 78]
$\ell=5$ $N_A(1/2)$	2.42			
$N_B(1/2)$, $N(3/2)$	2.64	(G19) 9/2 $^-$	2.79	[Höh 78]
		(I1,11) 11/2 $^-$	2.58	[Höh 78]
$\Delta(1/2)$, $\Delta(3/2)$	2.64	(G39) 9/2 $^-$	2.47	[Hoh 78]
		(I3,13) 13/2 $^-$	2.79	[Höh 78]
$\ell=6$ $N_A(1/2)$	2.62	(K1,13) 13/2 $^+$	2.61	[Höh 78]
$N_B(1/2)$, $N(3/2)$	2.85			
$\Delta(1/2)$, $\Delta(3/2)$	2.85	(K3,15) 15/2 $^+$	2.99	[Höh 78]
$\ell=7$ $N_A(1/2)$	2.81			
$N_B(1/2)$, $N(3/2)$	3.04		3.03	[PDG 78]
$\Delta(1/2)$, $\Delta(3/2)$	3.04			
$\ell=8$ $N_A(1/2)$	2.99			
$N_B(1/2)$, $N(3/2)$	3.22			
$\Delta(1/2)$, $\Delta(3/2)$	3.22		3.23	[PDG 78]

Table 3.10: Predicted nonstrange baryons and experimentally found baryon resonances with $3 \leq \ell \leq 8$. All masses are in GeV.

where (i_1,s_1) are the isospin and spin of the diquark. For each ℓ the state $N_A(1/2)$ has the lower mass, while the B states, $N_B(1/2)$, $N(3/2)$, $\Delta(1/2)$ and $\Delta(3/2)$ are degenerate at a higher mass. The predicted masses
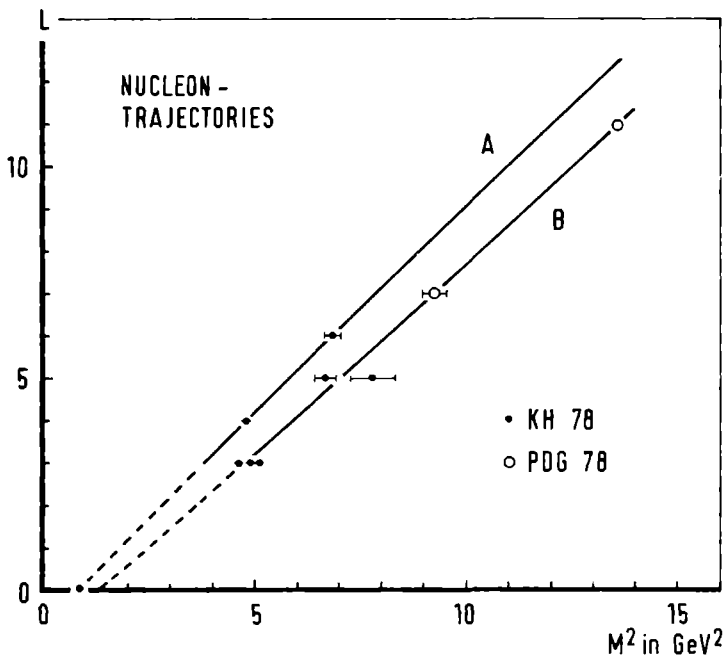
*Fig. 3.2: The A and B nucleon trajectories. For the Karlsruhe-Helsinki
(KH 78) points [Höh 78] the spin and parity are known and
the best guess for ℓ has been made. For the two plotted
Particle Data Group points [PDG 78] no J^P is known. We just
made the best choice for ℓ.*

and possible candidates up to ℓ = 8 are given in table 3.10. The

predicted trajectories for nucleon and delta resonances have been

plotted together with the experimentally established resonances in

figs 3.2 and 3.3. The trajectories directly follow from our assump-

tions; no free parameters had to be fitted. The agreement with the

experimental data is fairly good, although still many of the predicted
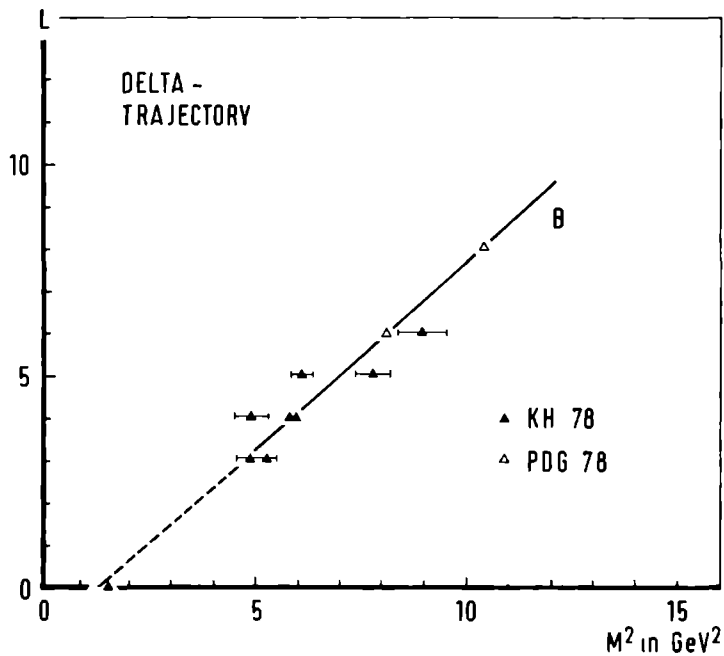
Fig. 3.3: The delta trajectory. See caption of fig. 3.2.

resonances have to be found.

For the interpretation of the baryon resonances the coupling to baryon-meson channels is often useful and sometimes even necessary. An example is the (D15) 5/2 $^-$ resonance found at 1.92 GeV in the reaction $\pi^- p \rightarrow K^0 \Lambda^0$ [Sax 80]. As the B states decouple from the ΛK channel (see section 3.6.6) it must be the A state predicted at 1.95 GeV and the (D15) 5/2 $^-$ state at 2.23 GeV [Hoh 78] probably is a B state.

3.3. The mass spectrum of strange baryons

In this section we calculate the mass spectra of orbitally and

radially excited strange Q^2-Q baryons, Λ, Σ, $\equiv$, and Ω resonances. We

restrict ourselves to the Λ and Σ resonances when we discuss the

experimental mass spectra and the possibility of $Q^4\bar{Q}$ states showing up.

These resonances are labeled by their J^P values or by the $\overline{KN}$-waves,

L I 2J, to which they couple.

3.3.1. Q^2-Q baryon resonances

We use the mass formula in eq. 3.9 for orbitally excited strange

baryons. The parameters ΔM, M_1 and m_{12} are assumed to be flavor-inde-

pendent. The results from sections 3.2.1, 3.2.3 and 3.2.4 are used to

calculate the masses for strange baryon resonances with $\ell^P = 1^-$, 2^+

and 0^{*+} (radial excitations). The multiplet mass for radial excitations

states (spin)	mass [GeV]	eigenstates				
$\ell^P = 1^-$ states						
$\Lambda(1/2)$	1.582	$\begin{bmatrix} 0.086 \\ -0.295 \\ 0.952 \end{bmatrix}$	$\begin{matrix} 0.974 \\ 0.225 \\ -0.018 \end{matrix}$	$\begin{matrix} -0.209 \\ 0.929 \\ 0.307 \end{matrix}$	$\begin{bmatrix} 56,\underline{8} \\ 70,\underline{1} \\ 70,\underline{8} \end{bmatrix}$	
	1.639					
	1.944					
$\Lambda(3/2)$	1.796				$70,\underline{8}$	
$\Sigma(1/2)$	1.653	$\begin{bmatrix} -0.290 \\ -0.026 \\ 0.957 \end{bmatrix}$	$\begin{matrix} 0.957 \\ 0.014 \\ 0.290 \end{matrix}$	$\begin{matrix} -0.021 \\ 1.000 \\ 0.021 \end{matrix}$	$\begin{bmatrix} 56,\underline{8} \\ 70,\underline{8} \\ 70,\underline{10} \end{bmatrix}$	
	1.759					
	1.954					
$\Sigma(3/2)$	1.802	$\begin{bmatrix} -0.019 \\ 1.000 \end{bmatrix}$	$\begin{matrix} 1.000 \\ 0.019 \end{matrix}$		$\begin{bmatrix} 56,\underline{10} \\ 70,\underline{8} \end{bmatrix}$	
	2.049					
$\Xi(1/2)$	1.779	$\begin{bmatrix} -0.274 \\ -0.021 \\ 0.961 \end{bmatrix}$	$\begin{matrix} 0.962 \\ 0.013 \\ 0.274 \end{matrix}$	$\begin{matrix} -0.018 \\ 1.000 \\ 0.018 \end{matrix}$	$\begin{bmatrix} 56,\underline{8} \\ 70,\underline{8} \\ 70,\underline{10} \end{bmatrix}$	
	1.881					
	2.073					
$\Xi(3/2)$	1.919	$\begin{bmatrix} -0.015 \\ 1.000 \end{bmatrix}$	$\begin{matrix} 1.000 \\ 0.015 \end{matrix}$		$\begin{bmatrix} 56,\underline{10} \\ 70,\underline{8} \end{bmatrix}$	
	2.171					
$\Omega(1/2)$	2.049				$70,\underline{10}$	
$\Omega(3/2)$	2.299				$56,\underline{10}$	

(table 3.11)

$\ell^P = 2^+$ states

$\Lambda(1/2)$	1.788	$\begin{bmatrix} 0.882 & 0.164 & -0.442 \\ -0.169 & 0.985 & 0.028 \\ 0.440 & 0.050 & 0.897 \end{bmatrix}$			$\begin{bmatrix} 56,\underline{8} \\ 70,\underline{1} \\ 70,\underline{8} \end{bmatrix}$	
	1.871					
	1.959					
$\Lambda(3/2)$	2.102				$70,\underline{8}$	
$\Sigma(1/2)$	1.809	$\begin{bmatrix} 0.907 & -0.421 & -0.008 \\ 0.415 & 0.898 & -0.146 \\ 0.069 & 0.129 & 0.989 \end{bmatrix}$			$\begin{bmatrix} 56,\underline{8} \\ 70,\underline{8} \\ 70,\underline{10} \end{bmatrix}$	
	1.966					
	1.997					
$\Sigma(3/2)$	2.003	$\begin{bmatrix} 0.999 & -0.044 \\ 0.044 & 0.999 \end{bmatrix}$			$\begin{bmatrix} 56,\underline{10} \\ 70,\underline{8} \end{bmatrix}$	
	2.109					
$\Xi(1/2)$	1.916	$\begin{bmatrix} 0.918 & -0.397 & -0.007 \\ 0.395 & 0.913 & -0.103 \\ 0.048 & 0.091 & 0.995 \end{bmatrix}$			$\begin{bmatrix} 56,\underline{8} \\ 70,\underline{8} \\ 70,\underline{10} \end{bmatrix}$	
	2.065					
	2.100					
$\Xi(3/2)$	2.106	$\begin{bmatrix} 0.999 & -0.038 \\ 0.038 & 0.999 \end{bmatrix}$			$\begin{bmatrix} 56,\underline{10} \\ 70,\underline{8} \end{bmatrix}$	
	2.206					
$\Omega(1/2)$	3.319				$70,\underline{10}$	
$\Omega(3/2)$	2.217				$56,\underline{10}$	

(table 3.11)

is calculated the same as for nonstrange baryons. Using the spherical bag approximation with one quark in a (2s) state (q^*) one finds $M(nn\text{-}n^*) = 1.684$ GeV, $M(nn\text{-}s^*) = 1.754$ GeV and $M(ns\text{-}n^*) = 1.849$ GeV. As for nonstrange baryons we use $M_{0*} = M(qq\text{-}q^*) + \Lambda M_{0*}$ with $\Delta M_{0*} = -74$ MeV (flavor-independent). The masses and eigenstates are given in table 3.11.

The comparison of the predicted states with the experimentally established resonances [Lan 76, PDG 78, Oza 78, Als 78, Cam 78] is shown in fig. 3.4. Owing to the abundance of predicted resonances, assignments are often difficult and only a few general conclusions can be drawn. The first conclusion is that the calculated masses of the

$\ell^P = 0^{*+}$ states

$\Lambda(1/2)$	1.491	$\begin{bmatrix} 0.774 & 0.357 & -0.523 \\ -0.326 & 0.933 & 0.153 \\ 0.542 & 0.052 & 0.839 \end{bmatrix}$	$\begin{bmatrix} 56,\underline{8} \\ 70,\underline{1} \\ 70,\underline{8} \end{bmatrix}$
	1.663		
	1.880		
$\Lambda(3/2)$	1.837		$70,\underline{8}$
$\Sigma(1/2)$	1.586	$\begin{bmatrix} 0.895 & 0.445 & -0.039 \\ 0.399 & 0.836 & 0.378 \\ -0.201 & -0.322 & 0.925 \end{bmatrix}$	$\begin{bmatrix} 56,\underline{8} \\ 70,\underline{8} \\ 70,\underline{10} \end{bmatrix}$
	1.816		
	1.925		
$\Sigma(3/2)$	1.651	$\begin{bmatrix} 0.955 & 0.296 \\ -0.296 & 0.955 \end{bmatrix}$	$\begin{bmatrix} 56,\underline{10} \\ 70,\underline{8} \end{bmatrix}$
	1.793		
$\Xi(1/2)$	1.665	$\begin{bmatrix} 0.845 & -0.535 & 0.024 \\ 0.424 & 0.696 & 0.580 \\ -0.327 & -0.479 & 0.815 \end{bmatrix}$	$\begin{bmatrix} 56,\underline{8} \\ 70,\underline{8} \\ 70,\underline{10} \end{bmatrix}$
	1.980		
	2.065		
$\Xi(3/2)$	1.782	$\begin{bmatrix} 0.976 & 0.218 \\ -0.218 & 0.976 \end{bmatrix}$	$\begin{bmatrix} 56,\underline{10} \\ 70,\underline{8} \end{bmatrix}$
	1.975		
$\Omega(1/2)$	2.064		$70,\underline{10}$
$\Omega(3/2)$	1.919		$56,\underline{10}$

Table 3.11: The masses and eigenstates of strange baryon resonances from eqs 3.9 and 3.11.

$\ell = 1$ states in the region 1650 – 1900 MeV reasonably explain the resonance structure in this region, although some resonances are still missing. Below 1650 MeV and above 1900 MeV the situation is less clear.

The lowest negative parity resonances are the $\Lambda(1405)$, $J^P = 1/2^-$, and the $\Lambda(1520)$, $J^P = 3/2^-$, resonances. The lowest $\Lambda(1/2)$ state is calculated at 1580 MeV. The assignment of this state is not only troublesome because of the discrepancy between the predicted and experimental masses, especially the $\Lambda(1405)$, but it also asks for an explanation of the large spin-orbit splitting between the $J^P = 1/2^-$
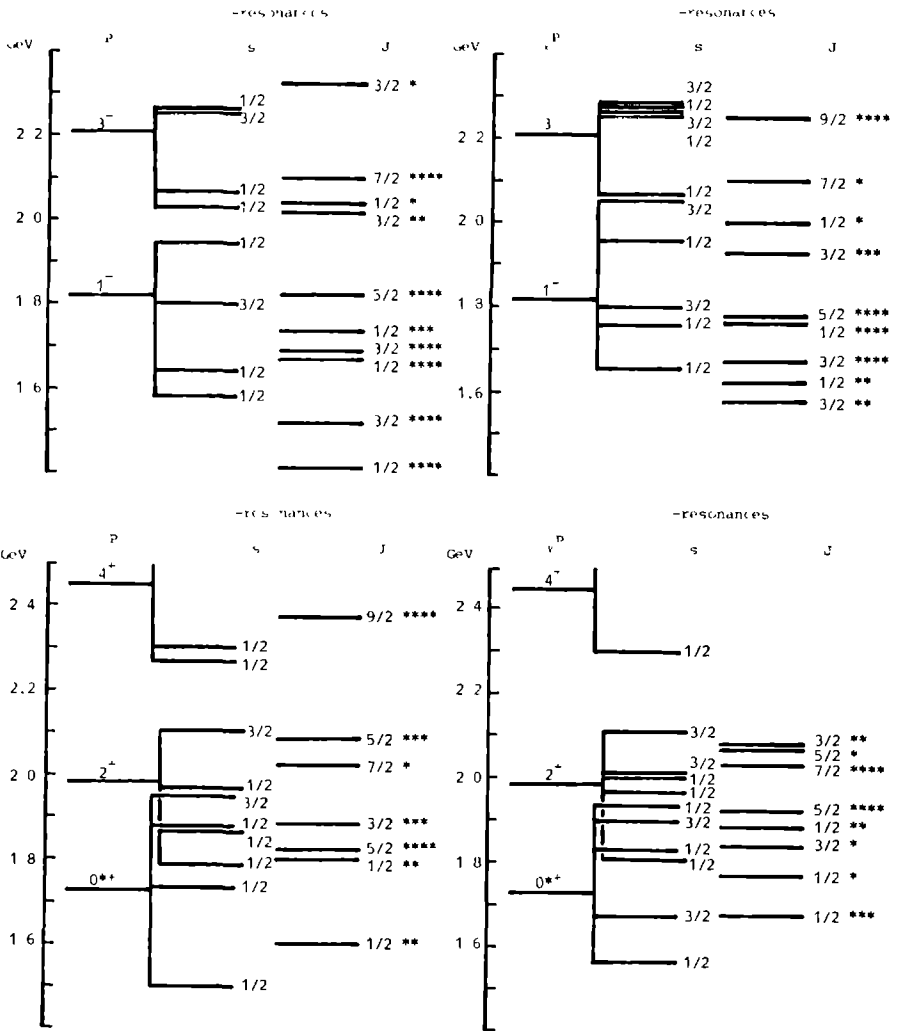
Fig. 3.4: The comparison of the predicted Λ and Σ baryons and the experimental resonances. Each predicted level stands for a multiplet with J^P values $J = |l-s|$, $|l-s|+1,..,|l+s|$ and $P = (-)^l$. As no spin-orbit term is included these levels are predicted degenerate.

and 3/2 ⁻ resonances. This might be due to a spin-orbit interaction which is large for the strange baryons and small for the nonstrange baryons [Rei 78]. A solution can be also found from the $Q^4\bar{Q}$ mass spectrum.

3.3.2. s-wave $Q^4\bar{Q}$ states

In the region below 1.55 GeV there are no Q^3 states with $y = 0$ predicted. There, however, are predicted two $Q^4\bar{Q}$ states, namely degenerate (S01) 1/2 ⁻ and (S11) 1/2 ⁻ resonances with a strong attractive color-magnetic energy contribution ($\Delta = -9.045$). Their mass is $M = 1.46$ GeV using our approximations (sections 2.1 and 2.2). Using the "exact" spherical bag approximation (sections 1.6 and 1.7) these states are also degenerate and have a mass $M = 1.416$ GeV [Jaf 76]. This $Q^4\bar{Q}$ state lies close to the $\bar{K}N$ and $\pi\Sigma$ thresholds and therefore might be assigned to the $\Lambda(1405)$ which is a $\bar{K}N$ bound state decaying into $\pi\Sigma$. This assignment does explain the low mass of the $\Lambda(1405)$ with respect to other Λ resonances, but it does not explain another problem with the $\Lambda(1405)$, namely the discrepancy between the theoretical and experimental values for the ratio $R = |g_{\bar{K}N}/g_{\pi\Sigma}|$. The experimental value is $R \simeq 2.1$. For the lowest $Q^4\bar{Q}$, $J^P = 1/2^-$, state the calculated value is $R = \sqrt{2/3}$ which is identical to the theoretical value for a $(f,s) = (\underline{1},1/2)$ state in the $[70,1^-]$ multiplet. For the lowest $\ell^P = 1^-$ Q^2-Q baryon (table 3.11) which is a mixture of flavor-spin basis states we find $R = 1.22$. A candidate for the $Q^4\bar{Q}$ Σ-state is the $\Sigma(1480)$ [PDG 78, Eng 79].

3.4. The mass spectrum of (exotic) $Y = 2$ baryons

A possibility to study the influence of $Q^4\bar{Q}$ states without being

(wave) J^P	mass	(wave) J^P	mass
Z_0^* resonances		Z_1^* resonances	
(S01) 1/2 $^-$	1.71	(D13) 3/2 $^-$	1.80
(D03) 3/2 $^-$	1.99	(S11) 1/2 $^-$	1.89
Z_2^* resonances		(S11) 1/2 $^-$	2.13
3/2 $^-$	2.16	(D13) 3/2 $^-$	2.16
1/2 $^-$	2.40	(D15) 5/2 $^-$	2.16

Table 3.12: The predicted $Y = 2$ $Q^4\bar{Q}$ states. All masses are in GeV.

hinderd by the presence of Q^3 states is offered in the $Y = 2$ baryon region (Z^* resonances). The resonances are labeled by their J^P values or by the KN-waves, L I 2J, to which they couple. Multiquark baryons with $Y = 2$ must contain four nonstrange quarks and one strange antiquark. The predicted mass spectrum of the s-wave $Q^4\bar{Q}$ states is given in table 3.12.

The $J^P = 1/2$ $^-$ resonances strongly couple to the KN S-wave. They probably will not show up as clear resonances but will give an attractive phase shift in the S01-wave ($M = 1.71$ GeV, $k_R = 0.45$ GeV, $k_R b \simeq 2.7 < \pi$) and a repulsive phase shift in the S11-wave ($M = 1.89$ GeV, $k_R = 0.60$ GeV, $k_R b \simeq 3.6 > \pi$).

The coupling of $J^P = 3/2$ $^-$ and 5/2 $^-$ resonances to the KN-waves is suppressed. They couple strongly to K*N, KΔ or K*Δ waves. The lowest of these resonances are the D13 (1.80) and D03 (1.99). Experimentally indications exist for a D03 (1.865) resonance [PDG 78, Oza 78].

Orbitally excited $Q^4\bar{Q}$ states might be responsible for positive parity Z^* resonances. In the $I = 0$ channel the lowest $Q^2\bar{Q}$-Q^2 excitation

consists of an $n^2\bar{s}$ cluster with $\Delta = -5.42$ and $(\imath,s) = (0,1/2)$ and a

nonstrange T_0-diquark. This gives a KN P01 (1.72) resonance. Experimen-

tal indications for such a resonance, P01 (1.78) exist [PDG 78]. In

the I = 1 channel the lowest $Q^2\bar{Q}-Q^2$ excitation consists of an $n^2\bar{s}$

cluster with $\Delta = -2.42$ and $(\imath,s) = (1,1/2)$ and a nonstrange T_0-diquark.

This gives a KN P11 (1.91) resonance. Slightly higher, the combination

of the $n^2\bar{s}$ cluster with $\Delta = -5.42$ and a nonstrange T_1-diquark gives a

P13 (1.94) resonance for which indications exist around 1.90 GeV

[PDG 78].

3.5. The coupling to baryon-meson channels

The decay of an excited baryon into a baryon and a meson proceeds

via quark-antiquark creation. The vertex for this decay is given in

fig. 3.5. In the Quark-Pair-Creation model (or $^3P_0$ model) it is

described by

$$H_{QPC} \; |Q^3> \; = \; \varepsilon \; \left| (Q^3)\,(Q\bar{Q})_{0^+} \right>$$ (3.13)

The created quark-antiquark pair has vacuum quantum numbers

$J^{PC} = 0^{++}$, $I^G = 0^+$, color singlet. All other quarks are assumed to

have the same quantum numbers in initial and final states. This

assumption determines that the dependence on isospin, spin and total

spin (J) quantum numbers is contained in recoupling factors for iso-

spin, spin and angular momenta. The quark pair creation still depends

on the flavor of the created pair ($n\bar{n}$ or $s\bar{s}$), the center of mass

momentum k in the final state and the spatial wave functions, i.e. the

orbital angular momenta ℓ and L in initial and final state.

The transition matrix element for the decay $B^* \to BM$ is
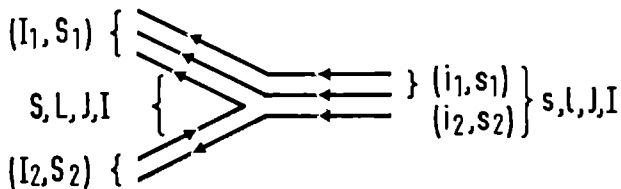
Fig. 3.5: The vertex for the decay of baryon resonances to baryon-meson channels.

$$<BM|H_{QPC}(q\bar{q})|B^*> = <B(((\iota_1,s_1)(\iota_q,s_q)I_1,S_1)M(I_2,S_2),I,S)L,J|$$

$$H_{QPC}|B^*((\iota_1,s_1)(\iota_2,s_2)I,s)\ell,J> \quad . \qquad (3.14)$$

Here the initial and final state baryons are diquark-quark basis states. The physical initial and final state baryons generally are a linear combination of diquark-quark states. The initial states are excited baryons and the eigenstates have been given in tables 3.3, 3.6, 3.7 and 3.9. The final states belong to the $[56,0^+]$ ground state multiplet and the recoupling to diquark-quark states has been given in table 3.2. The meson is an s-wave $Q\bar{Q}$ state. The transition matrix element for the diquark-quark baryons is [Jaf 78]

$$<BM|H_{QPC}(q\bar{q})|B^*> = \varepsilon \ (k,\ell,L,q\bar{q})\cdot g_I(q\bar{q})\cdot g_S\cdot g_J \qquad , \qquad (3.15)$$

where the coefficients g_I, g_S and g_J are the recoupling of isospins, spins and angular momenta. The coefficients g are proportional to a 9j-symbol [LB 68];

$$g = \begin{bmatrix} \ell_1 & s_1 & J_1 \\ \ell_2 & s_2 & J_2 \\ \ell_3 & s_3 & J_3 \end{bmatrix} = [(2\ell_3+1)(2s_3+1)(2J_1+1)(2J_2+1)]^{1/2}\cdot \begin{Bmatrix} \ell_1 & s_1 & J_1 \\ \ell_2 & s_2 & J_2 \\ \ell_3 & s_3 & J_3 \end{Bmatrix}$$

and

$$g_S = \begin{bmatrix} s_1 & 1/2 & S_1 \\ s_2 & 1/2 & S_2 \\ S & 1 & S \end{bmatrix} \qquad , \qquad g_J = \begin{bmatrix} s & \ell & J \\ 1 & 1 & 0 \\ S & L & J \end{bmatrix} \qquad , \qquad (3.16)$$

$$g_I(n\bar{n}) = \sqrt{2/3} \begin{bmatrix} \imath_1 & 1/2 & I_1 \\ \imath_2 & 1/2 & I_2 \\ I & 0 & I \end{bmatrix} \quad , \quad g_I(s\bar{s}) = \sqrt{1/3} \begin{bmatrix} \imath_1 & 0 & I_1 \\ \imath_2 & 0 & I_2 \\ I & 0 & I \end{bmatrix} = \sqrt{1/3} .$$

The square root factors in the expressions for g_I are introduced such that if ε $(k,\ell,L,n\bar{n}) = \varepsilon$ $(k,\ell,L,s\bar{s})$ the created $Q\bar{Q}$ pair is an SU(3) flavor singlet and flavor SU(3) is not broken. Both the initial and final states are color singlets; the color recoupling factor for states with a color structure $\underline{3}$-$\underline{3}^*$ is

$$g_C = \begin{bmatrix} \underline{c}_1 & \underline{3} & \underline{c}_1 \\ \underline{c}_2 & \underline{3}^* & \underline{c}_2 \\ \underline{c} & \underline{1} & \underline{c} \end{bmatrix} = \begin{bmatrix} \underline{3}^* & \underline{3} & \underline{1} \\ \underline{3} & \underline{3}^* & \underline{1} \\ \underline{1} & \underline{1} & \underline{1} \end{bmatrix} = 1 \quad . \qquad (3.17)$$

The orbital angular momentum L in the final state is $L = \ell \pm 1$, as parity conservation forbids $L = \ell$. The quantity

$$g - <BM|H_{QPC}|B^*>/\varepsilon \qquad (3.18)$$

is called the coupling constant in the decay $B^* \to BM$. The isospin, spin and angular momentum recoupling coefficients are given in tables 3.13, 3.14 and 3.15. Instead of g_I the coefficients $\tilde{g}_I$ are given in table 3.13. These coefficients describe the isospin recoupling of a baryon resonance to a baryon and a meson, where the final state baryon is a member of the flavor-spin irrep {56} and therefore a linear combination of diquark-quark states.

In order to compare the widths of baryon resonances we take into account certain phase space factors. We use the quantity

$$\tilde{\Gamma} = g^2 \frac{k}{\sqrt{s}} B_L(kR) \qquad , \qquad (3.19)$$

with $R = 3$ GeV^{-1} in the barrier factor $B_L(x)$ for which we use [Bla 52]

$$B_L^{-1}(x) = x^2 \, (j_L^2(x) + n_L^2(x))$$

$$= (2x)^{-2L} \sum_{\ell=0}^{L} \frac{(2L-\ell)! \, (2L-2\ell)!}{\ell! \, [(L-\ell)!]^2} (2x)^{2\ell} \qquad . \qquad (3.20)$$

$\tilde{g}_I^2(n\bar{n})$	$N\pi$	$N\eta_n$	$\Delta\pi$	$\Delta\eta_n$				
	No	Nω	$\Delta\rho$	$\Delta\omega$				
A(nn)(n)N	1/4	1/12	–	–				
B(nn)(n)N	–1/36	1/12	4/9	–				
B(nn)(n)Δ	–1/9	–	5/18	1/6				
$\tilde{g}_I^2(n\bar{n})$	$N\bar{K}$	$\Lambda\bar{K}$	$\Lambda\pi$	$\Sigma\pi$	$\Sigma^*\pi$	$\Lambda\eta_n$	$\Sigma\eta_n$	$\Sigma^*\eta_n$
	$N\bar{K}^*$	$\Delta\bar{K}^*$	$\Lambda\rho$	$\Sigma\rho$	$\Sigma^*\rho$	$\Lambda\omega$	$\Sigma\omega$	$\Sigma^*\omega$
A(nn)(s)Λ	1/3	–	–	–	–	–	–	–
A(ns)(n)Λ	–	–	–	1/4	–	–1/36	–	–
B(ns)(n)Λ	–	–	–	–1/12	1/3	–1/12	–	–
A(ns)(n)Σ	–	–	1/36	1/6	–	–	1/12	–
B(nn)(s)Σ	–1/9	4/9	–	–	–	–	–	–
B(ns)(n)Σ	–	–	1/12	–1/18	2/9	–	–1/36	1/9
$\tilde{g}_I^2(n\bar{n})$	$\Lambda\bar{K}$	$\Sigma\bar{K}$	$\Sigma^*\bar{K}$	$\Xi\pi$	$\Xi^*\pi$	$\Xi\eta_n$	$\Xi^*\eta_n$	
	$\Lambda\bar{K}^*$	$\Sigma\bar{K}^*$	$\Sigma^*\bar{K}^*$	$\Xi\rho$	$\Xi^*\rho$	$\Xi\omega$	$\Xi^*\omega$	
A(ns)(s)Ξ	1/36	1/4	–	–	–	–	–	
B(ns)(s)Ξ	1/12	–1/12	1/3	–	–	–	–	
B(ss)(n)Ξ	–	–	–	–1/6	1/6	–1/18	1/18	

(table 3.13)

$\tilde{g}_I^2(n\bar{n})$	$\Xi\bar{K}$ $\Xi\bar{K}^*$	$\Xi^*\bar{K}$ $\Xi^*\bar{K}^*$
B(ss)(s)Ω	-2/9	2/9

$\tilde{g}_I^2(s\bar{s})$	ΛK ΛK*	ΣK ΣK*	Σ*K Σ*K*
A(nn)(n)N	1/9	-	-
B(nn)(n)N	-	1/9	1/9
B(nn)(n)Δ	-	1/9	1/9

$\tilde{g}_I^2(s\bar{s})$	$\Lambda\eta_s$ $\Lambda\phi$	$\Sigma\eta_s$ $\Sigma\phi$	$\Sigma^*\eta_s$ $\Sigma^*\phi$	ΞK ΞK*	Ξ*K Ξ*K*
A(nn)(s)Λ	1/9	-	-	-	-
A(ns)(n)Λ	-	-	-	1/6	-
B(ns)(n)Λ	-	-	-	1/18	2/9
A(ns)(n)Σ	-	-	-	1/6	-
B(nn)(s)Σ	-	1/9	1/9	-	-
B(ns)(n)Σ	-	-	-	1/18	2/9

$\tilde{g}_I^2(s\bar{s})$	$\Xi\eta_s$ $\Xi\phi$	$\Xi^*\eta_s$ $\Xi^*\phi$	ΩK ΩK*
A(ns)(s)Ξ	1/6	-	-
B(ns)(s)Ξ	1/18	2/9	-
B(ss)(n)Ξ	-	-	1/3

(table 3.13)

96

$\tilde{g}^2_I(s\bar{s})$	$\Omega\eta_s$
	$\Omega\phi$
$B(ss)(s)\Omega$	$1/3$

Table 3.13: The isospin recoupling coefficients $\tilde{g}_I$ (see text). The squared coefficients $\tilde{g}^2_I$ have been given but the signs of $\tilde{g}_I$ have been preserved. η_n, ω, η_s and ϕ are ideally mixed states, i.e. $n\bar{n}$ and $s\bar{s}$.

g^2_S		BP	DP	BV	BV	DV	DV	DV
	S =	1/2	3/2	1/2	3/2	1/2	3/2	5/2
A, s = 1/2		3/4	−	−1/4	1	−	−	−
B, s = 1/2		−1/12	−1/3	25/36	1/9	2/9	5/9	−
B, s = 3/2		2/3	5/12	2/9	5/9	−1/9	1/36	1

Table 3.14: The spin recoupling coefficients. g^2_S has been given, but the sign of g_S has been preserved. $B = 1/2^+$ baryon, $D = 3/2^+$ baryon, $P = 0^-$ meson, and $V = 1^-$ meson.

S	s	J	L	g^2_J
1/2	1/2	$\ell - 1/2$	$\ell - 1$	$\dfrac{2}{9} \times \dfrac{2\ell - 1}{2\ell}$
		$\ell + 1/2$	$\ell + 1$	$-\dfrac{2}{9} \times \dfrac{2\ell + 3}{2\ell + 2}$
	3/2	$\ell - 3/2$	$\ell - 1$	$\dfrac{1}{6}$
		$\ell - 1/2$	$\ell - 1$	$\dfrac{1}{18} \times \dfrac{\ell + 1}{\ell}$
		$\ell + 1/2$	$\ell + 1$	$\dfrac{1}{18} \times \dfrac{\ell}{\ell + 1}$
		$\ell + 3/2$	$\ell + 1$	$\dfrac{1}{6}$

(table 3.15)

S	s	J	L	g_J^2
3/2	1/2	$\ell - 1/2$	$\ell - 1$	$\dfrac{1}{9} \times \dfrac{(\ell - 1)(2\ell - 1)}{\ell(2\ell + 1)}$
			$\ell + 1$	$\dfrac{1}{3} \times \dfrac{2\ell + 3}{2\ell + 1}$
		$\ell + 1/2$	$\ell - 1$	$\dfrac{1}{3} \times \dfrac{2\ell - 1}{2\ell + 1}$
			$\ell + 1$	$\dfrac{1}{9} \times \dfrac{(2\ell + 3)(\ell + 2)}{(2\ell + 1)(\ell + 1)}$
	3/2	$\ell - 3/2$	$\ell - 1$	$\dfrac{2}{15} \times \dfrac{2\ell - 3}{2\ell}$
		$\ell - 1/2$	$\ell - 1$	$\dfrac{8}{45} \times \dfrac{(\ell - 1)(2\ell + 2)}{\ell(2\ell + 1)}$
			$\ell + 1$	$-\dfrac{2}{15} \times \dfrac{(2\ell - 1)(2\ell + 3)}{(2\ell + 1)(2\ell + 2)}$
		$\ell + 1/2$	$\ell - 1$	$\dfrac{2}{15} \times \dfrac{(2\ell - 1)(2\ell + 3)}{2\ell(2\ell + 1)}$
			$\ell + 1$	$-\dfrac{8}{45} \times \dfrac{2\ell(\ell + 2)}{(2\ell + 1)(\ell + 1)}$
		$\ell + 3/2$	$\ell + 1$	$-\dfrac{2}{15} \times \dfrac{2\ell + 5}{2\ell + 2}$
5/2	3/2	$\ell - 3/2$	$\ell - 1$	$\dfrac{1}{30} \times \dfrac{(\ell - 2)(2\ell - 3)}{\ell(2\ell + 1)}$
			$\ell + 1$	$\dfrac{1}{3} \times \dfrac{2\ell + 3}{2\ell + 1}$
		$\ell - 1/2$	$\ell - 1$	$\dfrac{1}{10} \times \dfrac{(2\ell - 3)(\ell - 1)}{\ell(2\ell + 1)}$
			$\ell + 1$	$\dfrac{1}{5} \times \dfrac{(2\ell + 3)(\ell + 2)}{(2\ell + 1)(\ell + 1)}$
		$\ell + 1/2$	$\ell - 1$	$\dfrac{1}{5} \times \dfrac{(\ell - 1)(2\ell - 1)}{\ell(2\ell + 1)}$
			$\ell + 1$	$\dfrac{1}{10} \times \dfrac{(\ell + 2)(2\ell + 5)}{(2\ell + 1)(\ell + 1)}$
		$\ell + 3/2$	$\ell - 1$	$\dfrac{1}{3} \times \dfrac{2\ell - 1}{2\ell + 1}$
			$\ell + 1$	$\dfrac{1}{30} \times \dfrac{(2\ell + 5)(\ell + 3)}{(2\ell + 1)(\ell + 1)}$

Table 3.15: The recoupling coefficient for angular momenta. g_J^2 has been given, but the sign of g_J has been preserved. The numerical factor in front of the × sign is the limit for $\ell \to \infty$.

3.6. Decay of nonstrange baryon resonances

3.6.1. The (S11) 1/2⁻ nucleon resonances ($\ell = 1$)

The mass spectrum for the (S11) $1/2^-$ nucleon resonances has been given in section 3.2.1. The resonances are listed in table 3.16 to-gether with their coupling to the $N\pi$, $\Delta\tau$, $N\eta$, ΛK and ΣK channels (the η is a linear combination of η_n and η_s, namely $\eta = 0.511 \, \eta_n - 0.860 \, \eta_s$).

(S11) 1/2⁻ resonances							$N\pi$	$\Delta\tau$	$N\eta$	ΛK	ΣK
$\begin{bmatrix} N_1(1509) \\ N_2(1684) \\ N_3(1829) \end{bmatrix}$	=	$\begin{bmatrix} -0.901 & 0.433 & 0. \\ 0. & 0. & 1. \\ 0.433 & 0.901 & 0. \end{bmatrix}$			$\begin{bmatrix} N_A(1/2) \\ N_B(1/2) \\ N(3/2) \end{bmatrix}$		$-.123$ $-.045$ $.077$	$-.124$ $-.101$ $-.259$	$-.044$ $.040$ $.006$	$-.087$ $.0$ $.042$	$-.014$ $.091$ $-.029$

Table 3.16: The (S11) $1/2^-$ Q^3 resonances and their couplings to the lowest BM channels.

Experimentally the lowest three (S11) $1/2^-$ resonances have the follow-ing branching ratios [PDG 78]:

(i) N(1530) has a large branching ratio to $N\eta$ (65 %) and a branching ratio of 30 % to $N\pi$;

(ii) N(1670) has branching ratios of 55 % to $N\pi$, 30 % to $N\pi\pi$ (Nρ and $\Delta\tau$) and 10 % to ΛK;

(iii) N(1880) has a branching ratio of 5 - 10 % to $N\pi$.

The couplings in table 3.15 cannot explain the experimental branching ratios. The usual solution [Hey 75] is introducing a mixing between the lowest two (S11) resonances. The mixing angle is about 30°;

$$\begin{bmatrix} N_1' \\ N_2' \end{bmatrix} \simeq \begin{bmatrix} \sqrt{3/4} & -1/2 \\ 1/2 & \sqrt{3/4} \end{bmatrix} \begin{bmatrix} N_1 \\ N_2 \end{bmatrix} \qquad (3.21)$$

The couplings of these mixed states N_1' and N_2' are given in table 3.17.

(S11) 1/2⁻ resonances				Nπ	Δπ	Nη	ΛK	ΣK

$$\begin{bmatrix} N'_1 \\ N'_2 \end{bmatrix} = \begin{bmatrix} -0.780 & 0.375 & -0.500 \\ -0.451 & 0.217 & 0.866 \end{bmatrix} \begin{bmatrix} N_A(1/2) \\ N_B(1/2) \\ N(3/2) \end{bmatrix}$$

	Nπ	Δπ	Nη	ΛK	ΣK
	-.084	-.057	-.058	-.075	-.058
	-.100	-.150	.013	-.044	.072

Table 3.17: The couplings of the mixed states N'_1, N'_2 to the lowest BM channels.

The mixing explains the coupling of the N(1670) to ΛK, but the large coupling of the N(1530) to Nη still has not been explained.

We think that there is no considerable mixing between the N_1(1509) and N_2(1684). First there is no term in the mass operator which explains such a mixing. Secondly the small mass differences between the two N_1(1/2) states ($J^P = 1/2^-$ and $3/2^-$) and between the three N(3/2) states ($J^P = 1/2^-$, $3/2^-$ and $5/2^-$) indicate that only a small mixing is allowed, except if one wants to believe accidental degeneracies. We propose another solution. The coupling of excited baryons (Q^2-Q) to BM channels, derived in section 3.5, can be expanded in the following way:

$$< |H_{QPC}| > = <(Q^3)(Q\bar{Q})| |Q^2\text{-}Q>$$

$$= \sum_1 <(Q^3)(Q\bar{Q})|| (Q^4\bar{Q})_1 >< (Q^4\bar{Q})_1 || Q^2\text{-}Q> \quad . \quad (3.22)$$

If all $(Q^4\bar{Q})$ states are degenerate there would be no difference between the decay in fig. 3.5 and the decay where the $Q^4\bar{Q}$ states really act as (on mass shell) intermediate particles. However, the $Q^4\bar{Q}$ states are not degenerate, but rather are split by the color-magnetic interactions. The nearby levels therefore give a larger contribution than the

100

levels which lie far away. From table 3.5 we see that there are $Q^4\bar{Q}$ states with $J^P = 1/2^-$ which almost coincide with the positions of the $\ell = 1$ Q^3 resonances. For the (D13) $3/2^-$ Q^3 resonances there are no really close-lying $Q^4\bar{Q}$ states present. This can explain why there exists a large influence of the $Q^4\bar{Q}$ states on the (S11) $1/2^-$ Q^3 resonances, and only a small influence on the (D13) $3/2^-$ resonances (see section 3.6.2). The coupling to BM channels for the lowest three $(Q^4\bar{Q})$ $1/2^-$ states is given in table 3.18 [Som 78, Str 79]. The normalization of the couplings is such that the sum over the couplings

state	$N\pi$	$\Delta\pi$	$N\eta$	ΛK	ΣK
$N_1^*(1.51)$	−0.750	0.	0.221	0.	0.
$N_2^*(1.68)$	0.	0.	−0.525	−0.249	0.748
$N_3^*(1.71)$	0.349	0.	0.309	0.	0.

Table 3.18: Coupling of the lowest $Q^4\bar{Q}$ states with $J^P = 1/2^-$ to the lowest BM channels.

squared gives 1. To incorporate the larger influence, which is expected from $N_1^*(1.51)$ in the decay of $N_1(1509)$ and from $N_2^*(1.67)$ and $N_3^*(1.71)$ in the decay of $N_2(1684)$ we consider the states

$$N_1'' = 0.993\ N_1 - 0.125\ N_1^* \qquad ,$$
$$N_2'' = 0.99\ N_2 + 0.10\ N_2^* + 0.02\ N_3^* \qquad .$$

(3.23)

The coupling to BM channels is given in table 3.19. The quantities $\tilde{\Gamma}$, calculated for N_1'' and N_2'' from the couplings in table 3.19 and for N_3 from the couplings in table 3.16, are proportional to the widths Γ if the matrix element is the same for the decay of all $\ell = 1$ baryons.

101

state	$N\pi$	$\Delta\tau$	$N\eta$	ΛK	ΣK
N_1''	-0.028	-0.123	-0.072	-0.086	-0.014
N_2''	-0.038	-0.100	-0.007	-0.025	0.165

Table 3.19: Coupling of the mixed states N_1'', N_2'' to the lowest BM channels.

Phase space factors and barrier factors have been included in $\overset{\sim}{\Gamma}$ (eq. 3.1). The results are given in table 3.20. The combinations N_1'' and N_2'' have been chosen such that the quantities $\overset{\sim}{\Gamma}$ explain the ratios between the experimental branching ratios. Of course this choice is

resonance	channel	$\overset{\sim}{\Gamma}$	theoretical $\sqrt{xx'}$	theoretical fraction (%)	experimental fraction (%)
$N_1''(1509)$	$N\pi$	2.33×10^{-4}	0.34	34	30
	$\Delta\pi$	0.38	0.14	6	~ 1
	$N\eta$	4.15	0.45	60	65
$N_2''(1684)$	$N\pi$	4.88	0.59	59	55
	$\Delta\pi$	2.40	0.42	29	4 - 15
	$N\eta$	0.11	0.09	1	
	ΛK	0.84	0.25	10	10
$N_3 (1829)$	$N\pi$	21.52	0.25	25	~ 9
	$\Delta\pi$	40.10	-0.34	47	
	$N\rho(^2S)$	10.26	-0.17	12	
	others	14.02		16	

Table 3.20: The quantity $\overset{\sim}{\Gamma}$, the predicted amplitude at resonance and branching ratio, and the comparison with the experimental branching ratio for the (S11) $1/2^-$ nucleon resonances.

rather arbitrary as it is not based on any calculation; it only indicates the possible influence when a complete analysis of the decays of negative parity baryon resonances including the $Q^4\bar{Q}$ states is performed.

3.6.2. The (D13) 3/2⁻ nucleon resonances ($\ell = 1$)

The eigenstates have been listed in table 3.3. We can calculate the couplings to the baryon-meson channels and compare them with the experimental branching ratios via the quantity $\tilde{\Gamma}$. The results are given in table 3.21. For the (D13) 3/2⁻ states there is reasonable agreement

resonance	channel	g	$\tilde{\Gamma}$	$\sqrt{xx'}$	theoretical fraction (%)	experimental fraction (%)
N_1 (1509)	$N\pi$	0.194	20.65×10^{-4}	0.82	82	55
	$\Delta\pi$ (^4S)	-0.155	4.36	-0.38	17 $\big\}$	23
	$\Delta\pi$ (^4D)	-0.088	0.19	-0.08	1	
	$N\eta$	0.070	0.01	0.02	0	< 1
N_2 (1684)	$N\pi$	-0.023	0.58	0.01	1	10
	$\Delta\pi$ (^4S)	0.143	45.19	-0.01	70 $\big\}$	15 - 40
	$\Delta\pi$ (^4D)	-0.181	7.87	0.01	29	
	$N\eta$	0.020	0.11	-0.00	3	
	ΛK	0.	0.		0	$\sim$ 1
N_3 (1829)	$N\pi$	-0.122	23.21	0.23	23	$\sim$ 6
	$\Delta\pi$ (^4S)	-0.115	35.05	0.28	34	
	$\Delta\pi$ (^4D)	-0.182	19.80	0.21	19	
	others		24.48		24	

Table 3.21: The coupling g, the quantity $\tilde{\Gamma}$, the predicted amplitude at resonance and branching ratio, and the comparison with the experimental branching ratios for the $\ell = 1$ Q^3 (D13) 3/2⁻ nucleon resonances.

with the experimental results, like in the older flavor-spin analyses
[Hey 75]. There is no need for a strong mixing. In this case the
presence of $Q^4\bar{Q}$ resonances does not strongly influence the decay modes.
The $Q^4\bar{Q}$ state with $J^P = 3/2^-$ at 1.616 GeV lies neither close to the
$N_1(1509)$ nor close to the $N_2(1684)$.

3.6.3. The (D15) 5/2⁻ nucleon resonance ($\ell = 1$)

The results for the N(1684) are given in table 3.22. There is a
reasonable agreement with the experimental results. This resonance does
not mix with other (D15) 5/2⁻ resonances. There are no other $\ell = 1$
(D15) resonances; the $\ell = 3$ resonances and the $Q^4\bar{Q}$ states lie above
1.9 GeV.

We want to note that the $Q^4\bar{Q}$ state with $J^P = 5/2^-$ and a mass
M = 2.01 GeV has only the $\Delta\rho$ system as two-color-singlet component. The
$\Delta\rho$ threshold coincides with the mass. Therefore this state may be
interesting experimentally, but as both the widths of Δ and ρ are large
there still may be no rapid increase of the phase shift. The
coupling to other BM channels, e.g. $N\pi$, is suppressed, because a spin-
flip is required for the decay of an s-wave $Q^4\bar{Q}$ in D-waves. We mention

resonance	channel	g	$\overset{\curlyvee}{\Gamma}$	theoretical		experimental
				$\sqrt{xx'}$	fraction (%)	fraction (%)
N(1684)	$N\pi$	-0.056	3.43×10^{-4}	0.24	24	45
	$\Delta\pi(^4D)$	-0.208	10.39	0.41	72	47
	$N\eta$	0.049	0.64	-0.10	4	< 0.5

*Table 3.22: The coupling g, the quantity $\overset{\curlyvee}{\Gamma}$, the predicted amplitude at
resonance and branching ratio, and the comparison with the
experimental branching ratio for the $\ell = 1$ Q^3 (D15) 5/2⁻
nucleon resonance.*

resonance	channel	g	$\tilde{\Gamma}$	$\sqrt{xx'}$	theoretical fraction (%)	experimental fraction (%)
(S31) 1/2⁻ resonances						
Δ(1644)	Nπ	0.032	3.38×10^{-4}	0.28	28	32
	Δπ(^{4}D)	-0.227	8.60	-0.45	72	50
Δ(1934)	Nπ	-0.091	31.30	0.35	35	~ 8
	Δπ(^{4}D)	0.188	32.55	-0.35	36	
	ΣK	0.091	18.80	-0.27	21	
	others		7.88		9	
(D33) 3/2⁻ resonances						
Δ(1644)	Nπ	-0.050	2.42	0.09	9	15
	Δπ(^{4}S)	-0.102	21.43	0.26	76 ⎫	45 - 60
	Δπ(^{4}D)	-0.160	4.27	0.11	15 ⎭	
	ΣK	0.050	0.	-0.		
Δ(1934)	Nπ	-0.045	3.80	0.04	4	~ 5
	Δπ(^{4}S)	0.113	37.16	-0.13	41	
	Δπ(^{4}D)	-0.143	18.83	0.09	21	
	Nρ(^{4}S)	-0.083	15.84	0.09	17	
	others		15.40		17	
(D35) 5/2⁻ resonances						
Δ(1934)	Nπ	-0.111	23.14	0.38	38	4 - 12
	Δπ	-0.164	24.77	0.39	40	
	others		13.45		22	

Table 3.23: The coupling g, the quantity $\tilde{\Gamma}$, the predicted amplitude at resonance and branching ratio, and the comparison with the experimental branching ratio for the $\ell = 1$ Q^3 delta resonance.

this state because the $Q^4\bar{Q}$ states for which the decay to BM channels is suppressed might be the only ones which are stable enough to be

detectable.

3.6.4. The $\ell = 1$ delta resonances

The results for delta resonances, given in table 3.23, agree reasonably well with the experimental results. No strong admixtures of $Q^4\bar{Q}$ states or mixtures between different resonances with the same quantum numbers are needed.

3.6.5. Nucleon and delta resonances coupling to $N\pi$

All of the predicted nucleon and delta states couple to $N\pi$. The spectroscopic notation used for these baryons gives the $N\pi$ wave. There are large differences in the coupling strength. The strength for the coupling to $N\pi$ is given in table 3.24. The resonances with the strongest coupling to $N\pi$ are both $N_A(1/2)$ baryons ($J = \ell \pm 1/2$) and the two $\Delta(3/2)$ baryons with $J = \ell \pm 3/2$. Not all these resonances have been

resonance	$g^2_{N\pi}$	resonance	$g^2_{N\pi}$
$N_A(1/2)$ $J = \ell-1/2$	$.0417 \times \dfrac{\ell-1/2}{\ell}$		
$N_A(1/2)$ $J = \ell+1/2$	$.0417 \times \dfrac{\ell+3/2}{\ell+1}$		
$N(3/2)$ $J = \ell-3/2$	$.0031$	$\Delta(3/2)$ $J = \ell-3/2$	$.0123$
$N_B(1/2)$ $J = \ell-1/2$	$.0005 \times \dfrac{\ell-1/2}{\ell}$	$\Delta(1/2)$ $J = \ell-1/2$	$.0021 \times \dfrac{\ell-1/2}{\ell}$
$N(3/2)$ $J = \ell-1/2$	$.0010 \times \dfrac{\ell+1}{\ell}$	$\Delta(3/2)$ $J = \ell-1/2$	$.0041 \times \dfrac{\ell+1}{\ell}$
$N_B(1/2)$ $J = \ell+1/2$	$.0005 \times \dfrac{\ell+3/2}{\ell+1}$	$\Delta(1/2)$ $J = \ell+1/2$	$.0021 \times \dfrac{\ell+3/2}{\ell+1}$
$N(3/2)$ $J = \ell+1/2$	$.0010 \times \dfrac{\ell}{\ell+1}$	$\Delta(3/2)$ $J = \ell+1/2$	$.0041 \times \dfrac{\ell}{\ell+1}$
$N(3/2)$ $J = \ell+3/2$	$.0031$	$\Delta(3/2)$ $J = \ell+3/2$	$.0123$

Table 3.24: Coupling of nonstrange baryon resonances to $N\pi$.

	predicted	experimental
Nucleon resonances:		
S11	: 1.51 , 1.68 , 1.83	1.53*, 1.67*, 1.88*
D13	: 1.51 , 1.68 , 1.83 , 2.18	1.52*, 1.70*, 1.83*, 2.08
D15	: 1.68 , 1.95 , 2.18(2x)	1.68*, 1.92(?), 2.23
G17	: 1.95 , 2.18(2x), 2.64	2.14
G19	: 2.18 , 2.42 , 2.64(2x)	2.27 , 2.79
I1,11:	2.42 , 2.64(2x), 3.04	2.58
I1,13:	2.64 , 2.81 , 3.04(2x)	
L1,15:	2.81 , 3.04(2x), 3.39	
L1,17:	3.04 , 3.16 , 3.39(2x)	3.03(?)
N1,19:	3.16 , 3.39(2x), 3.70	
P11	: 2.01	(1.42), (1.72), 2.05*
P13	: 1.68 , 1.87 , 2.01	1.71*
F15	: 1.68 , 1.87 , 2.01 , 2.42	1.68*, 1.88*
F17	: 2.01 , 2.20 , 2.42(2x)	2.01*
H19	: 2.20 , 2.42(2x), 2.85	2.21
H1,11:	2.42 , 2.62 , 2.85(2x)	
K1,13:	2.62 , 2.85(2x), 3.22	2.61
K1,15:	2.85 , 2.99 , 3.22(2x)	
M1,17:	2.99 , 3.22(2x), 3.56	
Delta resonances:		
S31	: 1.64 , 1.93	1.62*, 1.88*, (2.15)
D33	: 1.64 , 1.93 , 2.18	1.71*, 2.01*
D35	: 1.93 , 2.18(2x)	1.91*, 2.31
G37	: 2.18(2x), 2.64	2.22
G39	: 2.18 , 2.64(2x)	2.17 , 2.47
I3,11:	2.64(2x), 3.04	
I3,13:	2.64 , 3.04(2x)	2.79
L3,15:	3.04(2x), 3.39	
L3,17:	3.04 , 3.39(2x)	
P31	: 1.91	1.90*
P33	: 1.90 , 1.91	(1.56), 1.88*
F35	: 1.90 , 1.91 , 2.42	1.91*
F37	: 1.91 , 2.42(2x)	1.92*, 2.43
H39	: 2.42(2x), 2.85	2.22
H3,11:	2.42 , 2.85(2x)	2.42
K3,13:	2.85(2x), 3.22	
K3,15:	2.85 , 3.22(2x)	2.99
M3,17:	3.22(2x), 3.56	
M3.19:	3.22 , 3.56(2x)	3.23(?)

* candidates for $\ell = 1$ and $\ell = 2$ states
( ) candidates for radial excitations

Table 5.25: Comparison of predicted and experimentally found $N\pi$

resonances for each wave.

seen experimentally, while weaker resonances have been seen. For a more
clear overview we have constructed table 3.25. For each channel the
resonances which are predicted and those for which experimental
evidence exist, have been given. The underlined predicted states are
those which have the largest coupling to Nπ. For most of them candi-
dates exist when they are the lowest resonance predicted in one of the
Nπ channels. Besides this we can only note that many of the predicted
resonances are absent.

Nπ		predicted		experimental [Sax 80]	
wave	M[GeV]	$(g^2_{\Lambda K}/g^2_{N\pi})$	$(\Gamma_{\Lambda K}/\Gamma_{N\pi})$	M[GeV]	$(X_{\Lambda K}/X_{N\pi})$
S11	1.684	0.44	0.17	1.68	0.13
D13	1.684	0.	0.	1.65	0.03
D15	1.684	0.	0.	1.67	0.003
P11	radial excitation			1.73	0.51
P13	1.672	0.44	0.06	1.69	0.4
F15	1.672	0.44	0.0007		
S11	1.829	0.30	0.18		
D13	1.829	0.30	0.06	1.90	0.3
D15	1.949	0.44	0.16	1.92	0.4
G17	1.949	0.44	0.03	2.18	0.02
D15	2.176	0.	0.		
G17	2.176	0.	0.		
F17	2.195	0.44	0.18		
H19	2.195	0.44	0.06		

*Table 3.26: Comparison of predictions and experimental results for the
ratio between coupling to ΛK and N .*

3.6.6. Nucleon resonances coupling to ΛK

Only states on the A-trajectory couple to ΛK. Resonances coupling to ΛK therefore are identified as resonances belonging to the A-trajectory or they indicate the presence of admixtures of A-states. For the (S11) resonances we discussed such mixing in section 3.6.1. The predicted ratio between the coupling constants for the coupling to ΛK and Nπ is given in table 3.26. This is compared with the experimental ratio of the branching ratios using the quantity $\tilde{\Gamma}$. We prefer the assignments of A-trajectory nucleons to the D15 and G17 resonances in ref. [Sax 80].

Although during the last twenty years several candidates for dibaryon resonances have been found, they have not been considered very seriously until recently. One tried to explain nonstrange dinucleon resonances as strong $N\Delta$ or $\Delta\Delta$ interactions [Arn 68, Kam 77.2] or in three-body treatments as $NN\pi$ resonances [Ued 78, Klo 77]. Calculations of s-wave Q^6 states [Jaf 77.1, Aer 78.1, Mat 77, Høg 79] and their orbital excitations [Mul 78.1, Aer 78.2, Mul 78.3, Lic 78] show that one may expect some low-lying six-quark states.

We will denote experimentally observed dibaryon resonances as $B^2(Y, I, J^P;$ mass) and the predicted six-quark states as $D(Y, I, J^P;$ mass), where Y, I, J, and P are the hypercharge, isospin, spin, and parity of these resonances. In the section 4.3, 4.4 and 4.5 where we discuss the $Y = 2$, 1, and 0 channels respectively Y is omitted. The mass is quoted in GeV.

Except for the deuteron, $B^2(2, 0, 1^+; 1.875)$, which is a bound state in the $^3S_1 + ^3D_1$ NN wave, the longest known dibaryon resonance is the $B^2(2, 1, 2^+; 2.17)$ which first showed up as an enhancement at the $N\Delta$ threshold in the cross section of the photodisintegration of the deuteron [Kec 56]. Later some more NN resonances with masses above 2.6 GeV were found in the reactions $pp \rightarrow \tau^+ x^+$ [Lam 66], $pp \rightarrow \pi^+ d$ [Coc 63, And 68], $K^- d \rightarrow K^- \pi^+ \pi^- d$ [Den 71], and $dp \rightarrow ppn$ [Ala 76]. Recent measurements [Kam 77.1, Ike 79] of the proton polarization in $\gamma d \rightarrow pn$ revealed a structure around 2.38 GeV, that can be interpreted as a dibaryon resonance $B^2(2, 0, 3^+; 2.38)$. Further recent evidence for dibaryon resonances comes from the Argonne experiments [Aue 77, Boe 75,

Bie 78, Hid 77] with polarized beams and targets. These experiments
indicate several resonances in the energy region below 2.5 GeV, the
clearest one being $B^2(2, 1, 3^-; 2.26)$, a $^3F_3$ NN resonance [Hos 78,
Kro 78, Gre 78]. Also the already mentioned resonance $B^2(2, 1, 2^+;$
2.17) is seen in these experiments [Hos 79]. In a recent πd elastic
scattering experiment [Kan 79] the resonances in the $^3F_3$ and probably
also the $^1S_0$ wave have been seen. These resonances are naturally
explained as six-quark states.

The experimental information for the strange dibaryon resonances
mainly comes from invariant mass plots for the different channels. The
best established resonance is the $B^2(1, \frac{1}{2}, 1^+; 2.129)$ which has been
seen in many different experiments. The spin and parity of this state
comes from models [Swa 79.1] where this state is satisfactory
explained as the companion of the deuteron in the flavor SU(3)
irreducible representation 10*. A long standing difficulty has
been the shoulder [Tan 69] in the Λp invariant mass spectrum around
2.14 GeV. In this chapter a quite natural explanation of this shoulder
as a $J^P = 1^-$ six-quark state will be given. In recent experiments
[Sha 79]   Shahbazian has clearly seen a Λp resonance at 2.256 GeV and
found evidence for more strange dibaryon resonances.

If the explanation for the dibaryon resonances as six-quark states
is correct, then it is quite easy to understand why the lowest *strange*
dibaryon resonances are much closer to the corresponding two body
thresholds than the lowest dinucleon resonances. The color-magnetic
interactions split dibaryons which have different flavor and spin
structure. The more antisymmetric flavor irreps (with lower values
for the flavor SU(3) quadratic Casimir operator) have a lower energy.

112

These flavor irreps, e.g. $\underline{f} = \underline{8}$, or $\underline{f} = \underline{1}$ only contain members with at least one or two strange quarks, they do not contain members with only nonstrange quarks. As a consequence we expect the study of these dibaryon resonances to be easier in ΛN final-state interactions, despite the fact that the statistics and variety in pp scattering experiments is of course much larger.

4.1. The masses of dibaryon resonances

In order to calculate the masses of the Q^6 states we use the mass formula explained in chapter 2. Because only a few candidates exist we cannot include the phenomenological contributions to the mass. Moreover, we think they are here less important as the masses are above 2 GeV (see section 2.6.1). The masses of the s-wave $(Q^6)_1$ states are found from

$$M = M_0 + m \Delta \qquad (4.1)$$

The relevant values of M_0, m, and Λ can be found in tables 2.3, 2.4, and 2.7. For orbitally excited dibaryons we have the following possibilities:

$$(Q^5)_{3*} - (Q)_3 \; ; \; (Q^4)_3 - (Q^2)_{3*} \; ; \; (Q^4)_{6*} - (Q^2)_6 \; ; \; (Q^3)_8 - (Q^3)_8 \quad .$$

The masses are found from

$$M = [M_0^2 + (1/\alpha')\ell]^{1/2} + m_1\Delta_1 + m_2\Delta_2 \qquad (4.2)$$

The relevant values of M_0, m_1, m_2, Δ_1 and Δ_2 can be found in tables 2.3, 2.4, and 2.12 - 2.17.

This prescription enables us to compute the masses of the six-quark states (only one cluster present) and their orbital excitations (two clusters present). Several effects which can influence the actual value of the masses have been omitted. First of all, we have neglected the influence of decay channels and final-state interactions. Secondly, we did not include splittings arising from the spin-orbit and tensor forces, which presumably are rather small. Apart from these contributions, small mass-shifts may arise from mixing, but they are neglected. We mention the color-magnetic interactions between the two clusters and the exchange contributions, due to the overlap of the quark wave

114

functions. They cause mixing between $\underline{3}$-$\underline{3}^*$ and $\underline{6}^*$-$\underline{6}$ Q^4-Q^2 states and also between $\underline{8}$-$\underline{8}$ and $\underline{1}$-$\underline{1}$ Q^3-Q^3 configurations (see also section 4.2). We also want to mention the effect of tunneling of a quark from one end of the bag to the other end. For baryons this causes an exchange-like contribution to the mass, as the tunneling of a quark is equivalent to the exchange of the other two quarks. The Q^2-Q structure is preserved. For dibaryons, tunneling causes transitions between the various structures

$$Q^5\text{-}Q \leftrightarrow Q^4\text{-}Q^2 \leftrightarrow Q^3\text{-}Q^3$$

In chapter 3 the tunneling effects turned out to be at most 100 MeV for $\ell = 1$ and to disappear rapidly for higher ℓ-values. The mixing due to tunneling is strongest between those dibaryons which have approximately the same masses, e.g. for $\ell = 1$ between the $(Q^5)_{3*}$-$(Q)_3$ and $(Q^4)_3$-$(Q^2)_{3*}$ or between the $(Q^4)_{6*}$-$(Q^2)_6$ and $(Q^3)_8$-$(Q^3)_8$ states. Tunneling also may lead to the decay mode $(Q^4)_3$-$(Q^2)_{3*}$ $\rightarrow$ $(Q^3)_1$-$(Q^3)_1$, which will be considered in section 4.2.

In order to illustrate the mass formula we consider two examples. We calculate the spectrum of the nonstrange $(Q^6)_1$ and $(Q^4)_3$-$(Q^2)_{3*}$ dibaryons. For the $(Q^6)_1$ dibaryons the color-magnetic contribution, calculated using tables 2.4 and 2.7, is added to the multiplet mass M_0, which is found in table 2.3. This is illustrated for dinucleons in fig. 4.1. For the $(Q^4)_3$-$(Q^2)_{3*}$ dibaryons the color-magnetic interactions contain two contributions, one from the Q^2 system and the other from the Q^4 system. In the final spectrum this leads to degenerate levels, as illustrated for dinucleons in fig. 4.2. In this figure the masses for the $\ell = 1$ levels have been given. The other orbitally
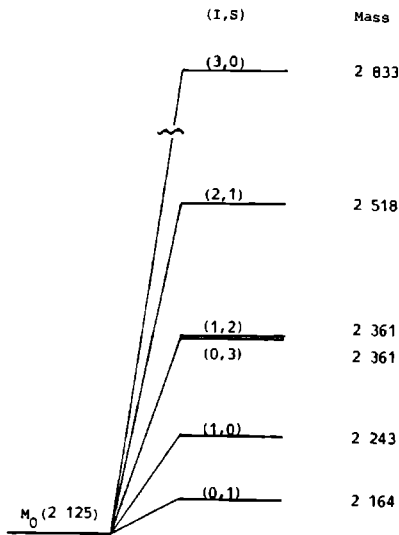
Fig. 4.1: The color-magnetic splitting for the $\ell = 0$ Q^6 dibaryons. All masses are in GeV.

excited $(Q^4)_3 - (Q^2)_{3*}$ levels show the same color-magnetic splitting, only the multiplet mass is different: e.g., for $\ell = 2$, $M_2 = 2.591$ GeV.

4.2. Stability and decay of dibaryons

One of the main decay modes of the s-wave Q^6 states is fission. If it is energetically favorable a Q^6 state will decay into two colorless baryons. The change in energy, neglecting the color-magnetic interaction,

$$\delta M_0 = M_0(Q^6) - 2\,M_0(Q^3) \qquad , \qquad (4.3)$$

is not very large ($\delta M_0 \simeq -50$ MeV). To determine whether fission into two colorless parts is energetically favorable, one has to look at the change in the color-magnetic interaction energy,
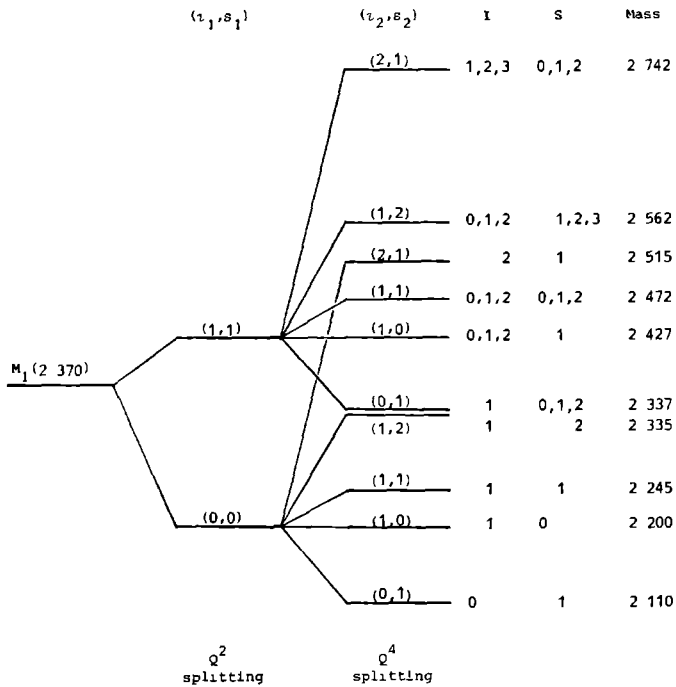
$$\delta M_m = M_m(Q^6) - 2\,M_m(Q^3) \qquad . \qquad (4.4)$$

116

(ι_1, s_1)	(ι_2, s_2)	I	S	Mass
	(2,1)	1,2,3	0,1,2	2 742
(1,1)	(1,2)	0,1,2	1,2,3	2 562
	(2,1)	2	1	2 515
	(1,1)	0,1,2	0,1,2	2 472
	(1,0)	0,1,2	1	2 427
	(0,1)	1	0,1,2	2 337
	(1,2)	1	2	2 335
(0,0)	(1,1)	1	1	2 245
	(1,0)	1	0	2 200
	(0,1)	0	1	2 110

$M_1(2\ 370)$

Q^2 splitting Q^4 splitting

Fig. 4.2: *The color-magnetic splitting for the $\iota = 1$ color-triplet Q^4-Q^2 dibaryons. All masses are in GeV.*

We will approximate this by

$$\delta M \simeq m\, \Delta_{12}(Q^6) \qquad , \qquad (4.5)$$

with

$$\Delta_{12}(Q^6) = \Delta(Q^6) - \Delta_1(Q^3) - \Delta_2(Q^3) \qquad . \qquad (4.6)$$

Δ_{12} is a measure for the color-magnetic attraction in the Q^6 cluster between the two $(Q^3)_1$ subsets. The stability increases when Δ_{12} decreases. We will assume that the color-magnetic interaction energy determines also the stability of clusters other than $(Q^6)_1$. For example a $(Q^4)_3$ cluster can fission into a colorless baryon and a quark,

$$(Q^4)_3 \rightarrow (Q^3)_1 (Q)_3 \qquad . \qquad (4.7)$$

The stability of this cluster is then measured by

$$\Delta_{12}(Q^4) = \Delta(Q^4) - \Delta(Q^3) \qquad . \qquad (4.8)$$

In the following we will briefly discuss the various possibilities for the decay of dibaryon resonances.

The first possibility is the fission of an s-wave Q^6 dibaryon into two baryons (BB). Because of parity conservation the final-state baryons are in an even L-wave. The decay in S-waves is expected to have a very large width. The decay in D- or higher waves is suppressed due to the angular momentum barrier and due to the spin-flip of the quarks that is required in order to conserve the total angular momentum. The vectorial change of the angular momenta, such that $\Delta J^P = 0^+$, is given by $\Delta L = \Delta S = 0$ for the decay in S-waves and by $\Delta L = \Delta S = 2$ for the decay in D-waves.

Fission is also possible for orbitally excited dibaryons but it will not be important because other decay modes will dominate. The reason is that the orbitally excited baryon $(Q - Q^2)$ which is formed in the decay

$$((Q^4)_3 - (Q^2)_{3*}) \longrightarrow ((Q^3)_1 (Q)_3 - (Q^2)_{3*}) \longrightarrow (Q^3)_1 (Q-Q^2)_1 \qquad (4.9)$$

is usually quite heavy.

Very important for the coupling of excited dibaryons to the BB channels is the tunneling mode. In excited multiquark states the quarks reside at the ends of the rotating stringlike bag. Nevertheless it is possible that a quark tunnels from one end of the bag through the angular momentum barrier to the other end. This gives the

recoupling

$$((Q^4)_3 \xrightarrow{\ell} (Q^2)_3) \rightarrow ((Q^3)_1 \xrightarrow{L} (Q^3)_1) \quad . \qquad (4.10)$$

This tunneling will be easy when the tunneling quark is not "bound" to the Q^4 cluster $(\Delta_{12}(Q^4) > 0)$ and when $L = \ell$. This coupling to the BB channel will not be so strong when $\ell \neq L$, because then the process has to be accompanied by a spin-flip in order to conserve the total angular momentum.

The final decay mode which we want to discuss proceeds via quark-antiquark creation. The s-wave and excited color-triplet dibaryons will decay via $Q\bar{Q}$ creation into BBM channels,

$$Q^6 \rightarrow Q^7\bar{Q} \rightarrow (Q^3)(Q^3)(Q\bar{Q}) \qquad ; \qquad (4.11)$$

$$(Q^4\text{-}Q^2) \rightarrow (Q^4(\bar{Q}Q)Q^2) \rightarrow (Q^3)(Q\bar{Q})(Q^3) \qquad ; \qquad (4.12)$$

$$(Q^5\text{-}Q) \rightarrow (Q^5(Q\bar{Q})Q) \rightarrow (Q^3)(Q^3)(\bar{Q}Q) \qquad . \qquad (4.13)$$

In order to conserve angular momentum and parity, $\Delta J^P = 0^+$, the $Q\bar{Q}$ pair is created in a $^3P_0$ wave; i.e. $\Delta L = \Delta S = 1$ for this decay. The total orbital angular momentum in the final state is $L = \ell + 1$.

Color-sextet and color-octet orbital excitations with $\ell = 1$ can also decay easily via $Q\bar{Q}$ creation. The reason is that the pair creation can take away one unit of orbital angular momentum. This can then leave all quarks in relative s-waves and the color is easily annihilated by recoupling, e.g.

$$((Q^4)_{6*}\text{-}(Q^2)_6) \rightarrow ((Q^4)_{6*}(Q)_3(\bar{Q})_{3*}(Q^2)_6) \rightarrow (Q^3)_1(Q^3)_1(Q\bar{Q})_1 . \quad (4.14)$$

4.3. Nonstrange $(Y = 2)$ dibaryon resonances

In this section we discuss the nonstrange dibaryon resonances. The

mass (GeV)	width (MeV) elasticity	I	J^P (NN wave)	remarks	refs
1.875	–	0	1^+ $(^3S_1 + {}^3D_1)$	deuteron	
2.17	$\Gamma \approx 35-100$ $x \simeq 0.1$	1	2^+ $(^1D_2)$	$\gamma d \to pn$	Kec 56
				$K^- d \to K^- \pi^- \pi^+ d$	Den 71
				$dp \to ppn$	Ala 76
				$pp \to pp$ (PWA)	Hos 79
2.2–2.3	$\Gamma \approx 100-300$ $x \simeq 0.2$	1	3^- $(^3F_3)$	$pp \to pp$ (PWA,DA,P,LCM)	Hos 78 Kro 78 Gre 78
				$\pi d \to \pi d$	Kan 79
2.38		0?	3^+? $(^3D_3 + {}^3G_3)$	$\gamma d \to pn$ (P)	Kam 77 Ike 79
2.4–2.5	$\bar\Gamma \approx 100-200$	1	0^+ or 4^+? $(^1S_0$ or $^1G_4)$	$pp \to pp$ (PWA,DA)	Hos 78 Kro 79 Gre 78
				$\pi d \to \pi d$	Kan 79
~ 2.6				$pp \to \pi^+ x^+$	Lam 66
~ 2.9				$pp \to \pi^+ x^+$	Lam 66
				$pp \to \pi^+ d$	Coc 63 And 68
~ 3.6				$pp \to \pi^+ d$	And 68
				$pp \to \pi^+ x^+$	Lam 66
~ 3.9				$pp \to \pi^+ x^+$	Lam 66

Table 4.1: Candidates for nonstrange (Y = 2) dibaryon resonances.
PWA = partial wave analysis, DA = dispersion analysis,
LCM = legendre coefficient method, P = polarization.

predicted mass spectrum will be compared with the experimentally known

resonances, which have been listed in table 4.1. The lowest

experimentally observed resonances are good candidates for six-quark states. They are $B^2(1, 2^+; 2.17)$, $B^2(1, 3^-; 2.2 - 2.3)$, $B^2(0, 3^+; 2.38)$ and $B^2(1, 0^+$ or $4^+; 2.4 - 2.5)$, although the (I, J^P) assignments of the higher two are less definite.

The flavor and spin structure of the $Y = 2$ dibaryons is given in table 4.2. This structure determines the magnitude of the color-magnetic energy M_m. It also determines to which baryon-baryon (BB) channels the dibaryon can couple. For the $(Q^6)_1$ states, which fission into two colorless baryons in S-waves, and for the $(Q^4)_3-(Q^2)_{3*}$ states, which decay via quark-tunneling into two colorless baryons in L-waves with $L = \ell$, the BB-channels have been given in table 4.2. The flavor and spin structure is independent of the orbital angular momentum ℓ of the quark-bag. The mass of every dibaryon resonance is found by adding the color-magnetic interaction energy M_m to the multiplet-mass M_ℓ. For the $(Q^3)_8-(Q^3)_8$ dibaryons we have to take into account the fact that we are combining two identical fermion-systems.

The predicted masses are listed with greater accuracy than warranted by the model in order to distinguish between the resonances. We start the discussion with the s-wave Q^6 states, which can fission into baryon-baryon channels in even L-waves.

4.3.1. The s-wave Q^6 states

$D(0, 1^+; 2.16)$ and $D(1, 0^+; 2.24)$ are the lowest predicted $(Q^6)_1$ nonstrange dibaryons. They fission into S-waves, the $^3S_1$ and $^1S_0$ NN waves, respectively. These dibaryons are very unstable. The change in color-magnetic energy, measured by Δ_{12}, is very large; $\Delta_{12} = 14/3$ and 6, respectively. Such states probably do not show up as pronounced resonances in a BB-channel; rather they only give a background

$(Q^6)_1$ Y = 2

f(y,ı)s	NN(1.88)	NΔ(2.17)	ΛΛ(2.46)	M_m	M_0
10*(2,0)1	x		x	39	2164
27 (2,1)0	x		x	118	2243
27 (2,1)2		x	x	236	2361
10*(2,0)3			x	236	2361
35 (2,2)1		x	x	393	2518
28 (2,3)0			x	708	2833

$(Q^4)_3 - (Q^2)_{3*}$ Y = 2

f(y,ı)s	f(y,ı)s	s	ı	NN(1.88)	ΔN(2.17)	ΔΛ(2.46)	M_m	M_1	M_2	M_3
6*(4/3,0)1	3*(2/3,0)0	1	0	x			−260	2110	2331	2536
15 (4/3,1)0	"	0	1	x			−170	2200	2421	2626
15 (4/3,1)1	"	1	1	x	x		−125	2245	2466	2671
15 (4/3,1)2	"	2	1		x		− 35	2335	2556	2761
6*(4/3,0)1	6 (2/3,1)1	0,1,2	1	x	x		− 33	2337	2558	
15 (4/3,1)0	"	1	0,1,2	x	x		57	2427	2648	
15 (4/3,1)1	"	0,1,2	0,1,2	x	x	x	102	2472	2693	
15$_s$(4/3,2)1	3*(2/3,0)0	1	2		x	x	145	2515	2736	
15 (4/3,1)2	6 (2/3,1)1	1,2,3	0,1,2		x	x	192	2562	2783	
15$_s$(4/3,2)1	6 (2/3,1)1	0,1,2	1,2,3		x	x	372	2742	2963	

$(Q^5)_{3*} - (Q)_3$ Y = 2

f(y,ı)s	f(y,ı)s	s	ı	M_m	M_1	M_2
15*(5/3,1/2)1/2	3(1/3,1/2)1/2	0,1	0,1	0	2370	2591
15*(5/3,1/2)3/2	"	1,2	0,1	63	2433	2654
15*(5/3,1/2)5/2	"	2,3	0,1	167	2537	2758
24 (5/3,3/2)1/2	"	0,1	1,2	188	2558	2779
24 (5/3,3/2)3/2	"	1,2	1,2	251	2621	2842
21 (5/3,5/2)1/2	"	0,1	2,3	502	2872	3093

(table 4.2)

$(Q^4)_{6*} - (Q^2)_6$	$Y = 2$				
f(y,1)s	f(y,1)s	s	1	M_m	M_1
6*(4/3,0)0	3*(2/3,0)1	1	0	-96	2405
6*(4/3,0)0	6 (2/3,1)0	0	1	18	2519
6*(4/3,0)2	3*(2/3,0)1	1,2,3	0	39	2540
15 (4/3,1)1	3*(2/3,0)1	0,1,2	1	84	2585
6*(4/3,0)2	6 (2/3,1)0	2	1	153	2654
15 (4/3,1)1	6 (2/3,1)0	1	0,1,2	198	2699
15_s(4/3,2)0	3*(2/3,0)1	1	2	310	2811
15_s(4/3,2)0	6 (2/3,1)0	0	1,2,3	423	2924

$(Q^3)_8 - (Q^3)_8$	$Y = 2$					
f(y,1)s	f(y,1)s	s	1		M_m	M_1
8(1,1/2)1/2	8(1,1/2)1/2	0,1	0,1	*	-74	2409
8(1,1/2)3/2	8(1,1/2)1/2	1,2	0,1		0	2483
8(1,1/2)3/2	8(1,1/2)3/2	0,1,2,3	0,1	*	74	2557
10(1,3/2)1/2	8(1,1/2)1/2	0,1	1,2		149	2632
10(1,3/2)1/2	8(1,1/2)3/2	1,2	1,2		223	2706
10(1,3/2)1/2	10(1,3/2)1/2	0,1	0,1,2,3	*	372	2859

```
    *   i even,  s even,  ℓ odd
                 s odd,   ℓ even
        ı odd,   s even,  ℓ even
                 s odd,   ℓ odd
```

Table 4.2: Y = 2 dibaryon resonances. The flavor and spin structure of each cluster and of the combination is given. M_m is the color-magnetic contribution. $M_m = m \Delta$ for $(Q^6)_1$ or $M_m = m_1\Delta_1 + m_2\Delta_2$ for the other dibaryons. M_ℓ is the sum of the multiplet mass and the color-magnetic contribution (eqs 4.1 and 4.2). It indicates a multiplet of resonances with $J = |\ell-s|, \ldots, |\ell+s|$ and $P = (-)^\ell$. All masses are in GeV.

contribution. This can be compared with the $\varepsilon(760) \rightarrow \pi\pi$, which can be interpreted as the fission of a $Q^2\bar{Q}^2$ bag into two mesons [Jaf 77.2, Jaf 79.1]. The momenta in the NN channel are $k_R = 0.54$ GeV for the $D(0, 1^+; 2.16)$ and $k_R = 0.61$ GeV for the $D(1, 0^+; 2.24)$. The behavior of the phase shift expected from a P-matrix analysis, however, is obscured by the attractive one-boson-exchange (O.B.E.) potential. This leads to a bound state in the $^3S_1 + {}^3D_1$ wave and a strong attraction in the $^1S_0$ wave. A possible way to link the NN-potential [Nag 78] and the six-quark bag states via deformed bags is discussed by DeTar [DeT 78, DeT 79].

D(0, 3^+; 2.36) cannot fission in S-waves. It couples to the $^7S_3$ $\Delta\Delta$-wave, but its mass is below the $\Delta\Delta$ threshold at 2.47 GeV. It can, however, fission into BB-channels in an (even) L-wave with $L \neq 0$, accompanied by a spin-flip, or it can decay into BBM-channels through quark-pair creation. Fission into a $^3D_3$ NN-wave is possible. As the coupling to NN is suppressed due to the angular momentum barrier and the necessary spin-flip, a reasonable width may emerge. We think that this state is responsible for the experimental resonance-structure found around 2.38 GeV in deuteron photodisintegration [Kam 77.1]. Therefore we prefer to make the identification $B^2(2.38) = D(2, 0, 3^+; 2.36)$.

D(1, 2^+; 2.36) is an intermediate case. It couples to the $^1D_2$ NN-wave through fission in a D-wave, but it can also couple to the $^5S_2$ NΔ-wave through fission in S-waves. While for the latter decay possibility the coupling is larger (S-wave vs D-wave fission), for the former more phase space is available. Experimentally an $(I, J^P) = (1, 2^+)$ state shows up in the $^1D_2$ NN-wave and in NNπ just at the NΔ threshold

124

(table 4.1). We therefore prefer to make the identification $B^2(2, 1, 2^+; 2.17) - D(2, 1, 2^+; 2.36)$. This situation can be understood in a potential model [Gon 79] where the bag is coupled to a $^1D_2$ NN and a $^5S_2$ NΔ channel. In this model the pole positions are followed in the complex energy plane. When the bag is weakly coupled to the NN and NΔ channels tne $D(1, 2^+; 2.36)$ is represented by one set of conjugate poles on the third Riemann sheet (Im $k_{NN} < 0$, Im $k_{N\Delta} < 0$), connected with the physical sheet above the NΔ threshold and another set of conjugate poles on the fourth sheet (Im $k_{NN} > 0$, Im $k_{N\Delta} < 0$), connected with the second sheet above the NΔ threshold. The second sheet (Im $k_{NN} < 0$, Im $k_{N\Delta} > 0$) is reached from the physical sheet by passing the unitarity cut between the NN and NΔ thresholds, the poles all lie near $E \simeq 2.36$ GeV. When the coupling of the bag and the NN and NΔ channels is increased the poles move. The poles on the third sheet move away from the unitarity cut and the resonance structure around $E = 2.36$ GeV weakens. Increasing the coupling strength the poles on the fourth sheet move towards the NΔ threshold. Still above the threshold they cross the unitarity cut into the second sheet and finally show up as poles in the second sheet quite close to the NΔ threshold. This means a NN resonance near the NΛ threshold. An analogous case is the coupled $\pi\pi$ and $K\bar{K}$ system. Here the $S^*(0.98$ GeV) is predicted in the bag model as a $Q^2\bar{Q}^2$ state at 1.20 GeV and shows up as a $\pi\pi$ resonance near the $K\bar{K}$ threshold [Jaf 79.1, Som 80].

The higher $(Q^6)_1$ dibaryons $D(2, 1^+; 2.52)$ and $D(3, 0^+; 2.83)$ do not couple to NN, but only to NΔ and $\Delta\Delta$.

4.3.2. Orbitally excited Q^6 states

Other dibaryons which we expect to couple strongly to BB-channels

are the $(Q^4)_3-(Q^2)_{3*}$ states. Through tunneling they decay into BB-channels. The stability depends on the color-magnetic energy gained when the Q^4 cluster fissions into a baryon and a quark. This is measured by $\Delta_{12}(Q^4)$. Of all nonstrange Q^4 clusters the cluster with $(\underline{f}, s; \Delta) = (\underline{15}, 2; 2)$ has the smallest value Λ_{12}, namely $\Lambda_{12} = 0$. The cluster with $(\underline{f}, s; \Lambda) = (\underline{6}, 1; -4/3)$ has $\Lambda_{12} = 2/3$; the others have $\Delta_{12} \geq 2$.

The clusters with $\Delta_{12} > 0$ are unstable. They easily fission and the quark recombines after tunneling with the other diquark to a baryon or the diquark and quark recouple after quark–antiquark creation to a baryon and meson. If a large enough phase space is available, those $(Q^4)_3-(Q^2)_{3*}$ states decay easily into NN, NΛ and NNτ. Probably their widths still are large ($\Gamma \gtrsim 300$ MeV) and their elasticity is small $(x < 0.3)$.

The $(Q^4)_3$ cluster with $(\underline{f}, s; \Delta) = (\underline{15}, 2; 2)$ is different. It cannot easily fission in a Λ and a quark, because $\Delta_{12} = 0$, and also the fission into a nucleon and a quark is suppressed because it cannot happen in S-waves and has to be accompanied by a spin-flip. This cluster therefore is less unstable and the width of the $(Q^4)_3-(Q^2)_{3*}$, built from this cluster, might not be too large; the elasticity will still be small. The resonances with the highest total angular momentum $(j = \ell + s)$, which are most easy to detect, are the resonances in the $^3F_3$, $^1G_4$, $^3H_5$, ... waves. Therefore we think that it is the $(Q^4)_3-(Q^2)_{3*}$ states, containing the $s = 2$ (Q^4) cluster, that have been observed experimentally.

$D(0, J^P; 2.110)$ with $J^P = 0^-$, 1^- and 2^- are the lowest nonstrange dibaryon resonances. The $D(0, 1^-; 2.11)$ can decay in the $^1P_1$ NN-wave.

It has a strong coupling to NN and cannot decay into NNπ in S-waves, and therefore should have a large elasticity. This $^1P_1$ resonance, predicted at $T_{lab} \simeq .5$ GeV is an important test for the validity of this model for orbitally excited Q^4-Q^2 dibaryon resonances. In the neighborhood of this $D(0, 1^-; 2.11)$ resonance no other $I = 0$ dibaryon resonances are predicted. Because its mass is so low it will probably give a clear signal in the $^1P_1$ NN-wave. We would like to urge the experimentalists to look for this resonance in np-scattering experiments in the mass range $2.06 < M < 2.16$ GeV, that is the laboratory momentum range 0.94 GeV/c $< P_{lab} < 1.23$ GeV/c, or the laboratory kinetic energy range 390 MeV $< T_{lab} < 610$ MeV. The presence of this resonance in the lower part of this range is perhaps already excluded by present day experiments.

The states with $J^P = 0^-$ and 2^- are extraneous states [Mul 78.1]. The quantum numbers $(I, J^P) = (0, 0^-)$ and $(0, 2^-)$ are forbidden for the NN system. Thus these extraneous states cannot decay into NN; however, they can decay into NNπ. They can be produced in the reaction

$$pp \rightarrow \pi^+ \; X^+ \qquad\qquad (4.15)$$
$$\qquad\quad \rule[0.5ex]{0pt}{0pt}\!\!\sqsubset\!\!\longrightarrow NN^- \qquad .$$

The $D(0, 2^-; 2.11)$ is experimentally likely to be rather narrow as it cannot decay into NNπ in S-waves.

$D(1, 1^-; 2.200)$ couples to the $^3P_1$ NN-wave and to NNπ in S-waves. $D(1, J^P; 2.245)$ with $J^P = 0^-$, 1^-, and 2^- couples to the ^3P NN-waves, to NΔ and to NNπ. All these resonances are probably rather unstable and have small elasticities.

$D(1, J^P; 2.335)$ with $J^P = 1^-$, 2^- and 3^- contains the relatively stable (Q^4) cluster with spin s = 2. They yield $^3P_1$, $^3P_2 + ^3F_2$ and $^3F_3$

NN resonances whose widths are not too large, however, with a small

elasticity. Experimentally structure is seen in the ^3P and ^3F waves

($J \leq 3$) in the region 2.2 - 2.3 GeV [Hos 78, Kro 78]. Clear evidence

exists for a resonance in the $^3F_3$ NN-wave [Hos 78] with a small

elasticity ($x \simeq 0.2$). The dispersion analysis [Gre 78] shows that the

structure comes mainly from the triplet uncoupled waves $^3P_1$ and $^3F_3$.

We think that the complete structure in this region is rather complex,

due to the presence of many dibaryons. Including the $D(1, J^P, 2.337)$

as well, there are predicted in the region 2.2 - 2.35 GeV two $^3P_0$,

six $^3P_1$, four $^3P_2 + ^3F_2$ and two $^3F_3$ NN resonances. As $J = 3$ is the

highest spin and one of the $^3F_3$ resonances is somewhat stable, it is

understandable why this resonance is most clearly seen. The great

number of $^3P_1$ resonances might explain the effect in the triplet

uncoupled channels.

D(0, J^P; 2.331) with $J^P = 1^+$, 2^+, and 3^+ is the lowest $\ell = 2$

dibaryon. It couples to NN and NNπ through tunneling and quark-anti-

quark creation respectively. It probably is a rather inelastic,

unstable resonance.

D(1, J^P; 2.556) with $J^P = 0^+$, 1^+, 2^+, 3^+, and 4^+ is the $\ell = 2$

$(Q^4)_3 - (Q^2)_{3*}$ dibaryon which contains the $s = 2$ (Q^4) cluster. The

D(1, 1^+) and D(1, 3^+) are extraneous in NN. While many dibaryons (most

of them unstable) with $J^P = 2^+$ ($^1D_2$ NN-wave) appear in this region,

the D(1, 0^+) and D(1, 4^+) resonances are more isolated. Therefore

resonances in the $^1S_0$ and $^1G_4$ NN-waves will show the most clear

resonant behavior, and they are candidates for the experimentally

observed structure in the region 2.4 - 2.5 GeV.

The higher recurrences of the D(1, J^P; 2.335) and D(1, J^P; 2.556)

lie at 2.76, 2.95, and 3.13 GeV for $\ell = 3$, 4, and 5.

We think that the splittings due to the color-magnetic interaction are reliable in so far as we may neglect the final-state interactions. It appears that for the nonstrange dibaryon resonances $(Q^4)_3 - (Q^2)_{3*}$ the observed masses are about 50 - 100 MeV lower than the predicted ones, but this of course strongly depends on the assignments. Moreover, it is difficult to determine an experimental mass. This depends on the method of analysis, e.g. for the $^3F_3$ in refs [Hos 78] and [Gre 78].

The importance of dibaryon resonances, other than Q^6 or $(Q^4)_3 - (Q^2)_{3*}$, is at present not clear to us. The Q^5-Q resonances probably do not couple strongly to BB-channels. The nonstrange $(Q^3)_8 - (Q^3)_8$ dibaryons are probably very unstable. Through gluon exchange (electric) they easily couple to BB-channels.

4.4. The Y = 1 dibaryon resonances

Experimental evidence exists for several Y = 1 dibaryon resonances B^2(I, mass). The evidence for the I = 1/2 resonances comes from Λp invariant mass plots. A collection of such plots is given in fig. 4.3.

The most pronounced enhancement, $B(\frac{1}{2}$, 2.13), lies near the ΣN threshold with a mass M = 2.129 GeV and a width $\Gamma \simeq 6$ MeV. This certainly is not a candidate for a six-quark state, rather, just like the deuteron it is explained very well in potential theory [Swa 62, Dos 78] as being a ΣN "bound" state showing up as a ΛN resonance. This enhancement is accompanied by a shoulder [Tan 69] which can be fit by a Breit-Wigner resonance $B^2(\frac{1}{2}$, 2.14) with M = 2.139 GeV and $\Gamma = 9$ MeV.
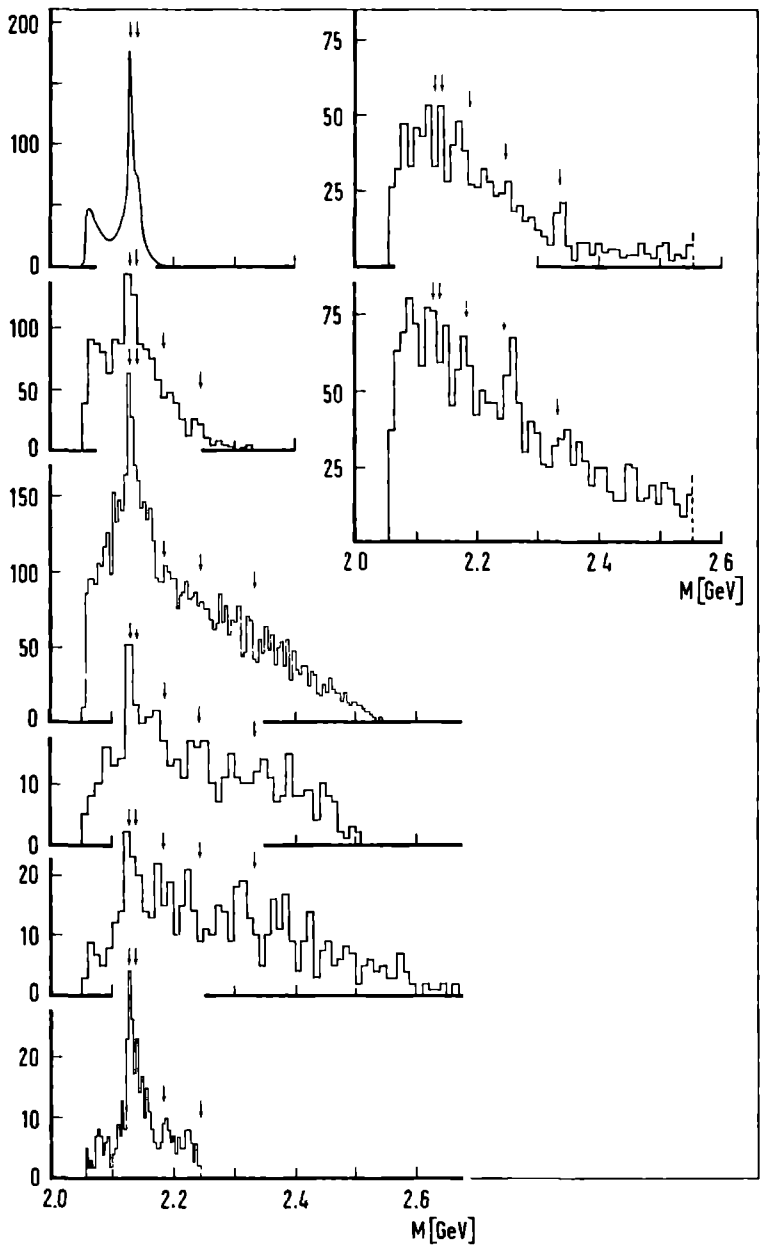
Recently B.A. Shahbazian and coworkers at Dubna [Sha 79] determined Λp invariant mass spectra in the reactions n $C^{12} \to \Lambda$(mp)X and $\pi^- C^{12} \to \Lambda$(mp)X. They found evidence for two more enhancements: $B^2(\frac{1}{2}$, 2.18) and $B^2(\frac{1}{2}$, 2.25). They try to explain the $B^2(\frac{1}{2}$, 2.18) enhancement as an effect due to $\Sigma N \to \Lambda$p conversion at large relative momenta. They want to explain the $B^2(\frac{1}{2}$, 2.14) resonance in the same way. We prefer to retain the resonance explanation for the $B^2(\frac{1}{2}$, 2.18) enhancement. We note that it is also recognizable (although of course not statistically significant) in most of the other analyses of fig. 4.3.

The resonance $B^2(\frac{1}{2}$, 2.25) with mass M = 2.256 GeV and width $_1 \sim$ 15 MeV is a 5 to 6 standard-deviation effect in the Dubna experiments. This state also shows up weakly in most of the other analyses. Shahbazian [Sha 79] gives arguments why the $B^2(\frac{1}{2}$, 2.25) state is clearly visible in their n C^{12} and $\tau^- C^{12}$ experiments, while it is not clearly visible in the K^-d experiments. Around 2.34 GeV an enhancement $B^2(\frac{1}{2}$, 2.34) shows up in several analyses [Bei 76, Sha 73, Kad 71]. Beillière et al. [Bei 76] calculate a 2.8 standard-deviation significance, but conclude for no evidence for a resonance at this position.

Fig. 4.3: Λp invariant-mass plots in the reaction $K^-d \to \Lambda p \pi^-$ (left) or K^--Nucleus interactions (right). On the left from top to bottom taken from [Tan 69, Cli 68, Bra 77, Sim 71, Ale 69, Eas 71]. On the right from [Bei 76, Sha 79]. The plots are ordered by their (increasing) K^- incident momentum. We have drawn arrows at 2.13, 2.14, 2.18, 2.24 and 2.34 GeV to guide the eye.

In the $\Lambda p r^+$ invariant mass plots Shahbazian et al. [Sha 79] found evidence for $I = \frac{3}{2}$ resonances around 2.5 GeV and 2.99 GeV. A state at 2.5 GeV also shows up in the $\Lambda p \pi^-$ invariant mass plots.

In table 4.3 we have listed the predicted $Y = 1$ dibaryon resonances. What strikes us is the enormous number of predicted resonances. In order to show up in the experimental data a resonance must have strong enough coupling to the 'N and/or 'N channels and its width may not be unreasonably large.

The Q^6-states with $J^P = 0^+$ in the flavor irreps $\underline{8}$ and $\underline{27}$, and with $J^P = 1^+$ in the irreps $\underline{8}$, $\underline{10}$ and $\underline{10}^*$, can decay spontaneously in the s-wave ΛN or ΣN channels. As in the NN case we expect these states to have a very large width and therefore not be visible in invariant-mass plots.

$(Q^6)_1$ $Y = 1$ f(y,i)s	$\Lambda N(2.05)$	$\Sigma N(2.13)$	$\Sigma^*N(2.32)$	$\Lambda\Delta(2.35)$	$\Sigma\Delta(2.42)$	$\Sigma^*\Lambda(2.62)$	M_m	M_0
$\underline{8}$ (1,1/2)1	x	x	x		x		-126	2169
$\underline{8}$ (1,1/2)2			x		x		-54	2241
$\underline{10}$ (1,3/2)1		x	x	x	x		36	2331
$\underline{10}^*$(1,1/2)1	x	x				x	36	2331
$\underline{27}$ (1,1/2)0	x	x				x	108	2403
$\underline{27}$ (1,3/2)0		x				x	108	2403
$\underline{27}$ (1,1/2)2			x		x	x	216	2511
$\underline{27}$ (1,3/2)2			x	x	x	x	216	2511
$\underline{10}^*$(1,1/2)3						x	216	2511
$\underline{35}$ (1,3/2)1			x	x	x	x	361	2656
$\underline{35}$ (1,5/2)1					x	x	361	2656
$\underline{28}$ (1,5/2)0						x	649	2944

(table 4.3)

$(Q^4)_3 - (Q^2)_{3*}$ $Y = 1$				$\Lambda N(2.05)$	$\Sigma N(2.13)$	$\Gamma^*N(2.32)$	$\Lambda\Delta(2.35)$	$\Sigma\Delta(2.42)$	$\Gamma^*\Delta(2.62)$			
f(y,l)s	f(y,l)s	s	l							M_m	M_1	M_2
3 (1/3,1/2)0	3*(2/3,0)0	0	1/2	x	x					-411	2112	2322
3 (1/3,1/2)1	3*(2/3,0)0	1	1/2	x	x					-371	2152	2362
6*(1/3,1/2)1	3*(2/3,0)0	1	1/2	x	x					-250	2273	2483
6*(4/3,0)1	3*(-1/3,1/2)0	1	1/2	x	x					-231	2292	2502
3 (1/3,1/2)0	6 (2/3,1)1	1	1/2,3/2	x	x	x	x	x		-184	2339	2549
15 (1/3,1/2)0	3*(2/3,0)0	0	1/2	x	x					-170	2353	2563
15 (1/3,3/2)0	3*(2/3,0)0	0	3/2		x					-170	2353	2563
3 (1/3,1/2)1	6 (2/3,1)1	0,1,2	1/2,3/2	x	x	x	x	x		-144	2379	2589
15 (4/3,1)0	3*(-1/3,1/2)0	0	1/2,3/2	x	x					-140	2383	2593
15 (1/3,1/2)1	3*(2/3,0)0	1	1/2	x	x	x				-130	2393	2603
15 (1/3,3/2)1	3*(2/3,0)0	1	3/2		x	x	x			-130	2393	2603
15 (4/3,1)1	3*(-1/3,1/2)0	1	1/2,3/2	x	x		x	x		-95	2428	2638
15 (1/3,1/2)2	3*(2/3,0)0	2	1/2			x				-50	2473	2683
15 (1/3,3/2)2	3*(2/3,0)0	2	3/2		x	x				-50	2473	2683
6*(4/3,0)1	6 (-1/3,1/2)1	0,1,2	1/2	x	x	x				-43	2480	2690
6*(1/3,1/2)1	6 (2/3,1)1	0,1,2	1/2,3/2	x	x	x	x	x		-23	2500	2710
15 (4/3,1)2	3*(-1/3,1/2)0	2	1/2,3/2				x	x		-5	2518	2728
15 (4/3,1)0	6 (-1/3,1/2)1	1	1/2,3/2	x	x	x				47	2570	
15 (1/3,1/2)0	6 (2/3,1)1	1	1/2,3/2	x	x	x	x	x		57	2580	
15 (1/3,3/2)0	6 (2/3,1)1	1	1/2,3/2,5/2		x			x		57	2580	
15 (4/3,1)1	6 (-1/3,1/2)1	0,1,2	1/2,3/2	x	x	x	x	x	x	92	2615	
15 (1/3,1/2)1	6 (2/3,1)1	0,1,2	1/2,3/2	x	x	x	x	x	x	97	2620	
15 (1/3,3/2)1	6 (2/3,1)1	0,1,2	1/2,3/2,5/2		x	x		x	x	97	2620	
15ₛ(1/3,3/2)1	3*(2/3,0)0	1	3/2		x					110	2633	
15ₛ(4/3,2)1	3*(-1/3,1/2)0	1	3/2,5/2				x	x		175	2698	
15 (1/3,1/2)2	6 (2/3,1)1	1,2,3	1/2,3/2		x				x	177	2700	
15 (1/3,3/2)2	6 (2/3,1)1	1,2,3	1/2,3/2,5/2		x			x	x	177	2700	
15 (4/3,1)2	6 (-1/3,1/2)1	1,2,3	1/2,3/2				x	x	x	182	2705	
15ₛ(1/3,3/2)1	6 (2/3,1)1	0,1,2	1/2,3/2,5/2		x			x	x	337	2860	
15ₛ(4/3,2)1	6 (-1/3,1/2)1	0,1,2	3/2,5/2				x	x	x	362	2885	

(table 4.3)

$(Q^5)_{3*} - (Q)_3 \qquad Y = 1$

f(y,ı)s	f(y,ı)s	s	ı	M_m	M_1	M_2
3*(2/3,0)1/2	3(1/3,1/2)1/2	0,1	1/2	-227	2296	2506
3*(2/3,0)3/2	3(1/3,1/2)1/2	1,2	1/2	-170	2353	2563
6 (2/3,1)1/2	3(1/3,1/2)1/2	0,1	1/2,3/2	-114	2409	2619
6 (2/3,1)3/2	3(1/7,1/2)1/2	1,2	1/2,3/2	-57	2466	2676
15*(2/3,0)1/2	3(1/3,1/2)1/2	0,1	1/2	0	2523	2733
15*(2/3,1)1/2	3(1/3,1/2)1/2	0,1	1/2,3/2	0	2523	2733
15*(5/3,1/2)1/2	3(-2/3,0)1/2	0,1	1/2	0	2523	2733
15*(2/3,0)3/2	3(1/3,1/2)1/2	1,2	1/2	57	2580	
15*(2/3,1)3/2	3(1/3,1/2)1/2	1,2	1/2,3/2	57	2580	
15*(5/3,1/2)3/2	3(-2/3,0)1/2	1,2	1/2	63	2586	
15*(2/3,0)5/2	3(1/3,1/2)1/2	2,3	1/2	152	2675	
15*(2/3,1)5/2	3(1/3,1/2)1/2	2,3	1/2,3/2	152	2675	
15*(5/3,1/2)5/2	3(-2/3,0)1/2	2,3	1/2	167	2690	
24 (2/3,1)1/2	3(1/3,1/2)1/2	0,1	1/2,3/2	170	2693	
24 (2/3,2)1/2	3(1/3,1/2)1/2	0,1	3/2,5/2	170	2693	
24 (5/3,3/2)1/2	3(-2/3,0)1/2	0,1	3/2	188	2711	
24 (2/3,1)3/2	3(1/3,1/2)1/2	1,2	1/2,3/2	227	2750	
24 (2/3,2)3/2	3(1/3,1/2)1/2	1,2	3/2,5/2	227	2750	
24 (5/3,3/2)3/2	3(-2/3,0)1/2	1,2	3/2	251	2774	
21 (2/3,2)1/2	3(1/3,1/2)1/2	0,1	3/2,5/2	454	2977	
21 (5/3,5/2)1/2	3(-2/3,0)1/2	C,1	5/2	502	3025	

(table 4.3)

134

$Q^1_{6*} - Q^2_6$ Y = 1					
f(y,ı)s	f(y,ı)s	s	ı	M_m	M_1
3 (1/3,1/2)1	3*(2/3,0)1	0,1,2	1/2	~169	2478
6*(4/3,0)0	3*(-1/3,1/2)1	1	1/2	-91	2556
6*(1/3,1/2)0	3*(2/3,0)1	1	1/2	-89	2558
3 (1/3,1/2)1	6 (2/3,1)0	1	1/2,3/2	-55	2592
6*(4/3,0)0	6 (-1/3,1/2)0	0	1/2	3	2650
6*(1/3,1/2)0	6 (2/3,1)0	0	1/2,3/2	25	2672
6*(1/3,1/2)2	3*(2/3,0)1	1,2,3	1/2	32	2679
6*(4/3,0)2	3*(-ı/3,1/2)1	1,2,3	1/2	44	2691
15 (1/3,1/2)1	3*(2/3,0)1	0,1,2	1/2	72	2719
1/3,3/2)1	3*(2/3,0)1	0,1,2	3/2	72	2719
15 (4/3,1)1	3*(-1/3,1/2)1	0,1,2	/2,3/2	89	2736
6*(4/3,0)2	6 (-1/3,1/2)0	2	1/2	138	2785
6*(1/3,1/2)2	6 (2/3,1)0	2	1/2,3/2	145	2792
15 (4/3,1)1	6 (-1/3,1/2)0	1	1/2,3/2	183	2830
15 (1/3,1/2)1	6 (2/3,1)0	1	1/2,3/2	185	2832
15 ı1/3,3/2)1	6 (2/3,1)0	1	1/2,3/2,5/2	185	2832
15_s(1/3,3/2)0	3*(2/3,0)1	1	3/2	272	2919
15_s(4/3,2)0	3*(-1/3,1/2)1	1	3/2,5/2	315	2962
15_s(1/3,3/2)0	6 (2/3,1)0	0	1/2,3/2,5/2	386	3033
15_s(4/3,2)0	6 (-1/3,1/2)0	0	3/2,5/2	408	3055

(table 4.3)

4.4.1. The s-wave Q^6 states

D($\frac{1}{2}$, 2^+; 2.24) is the lowest Q^6 state which could be visible. It belongs to an octet and couples to the $^1D_2$ and $^3D_2$ ΛN and ΣN channels. As can be seen in table 4.3 it also couples to the S-wave $\Sigma^*(1385)$N and ΔΣ channels, but its mass is below the corresponding thresholds. We would like to make the assignment D($\frac{1}{2}$, 2^+; 2.24) ≡ B^2($\frac{1}{2}$; 2.25). Because this state is above the ΛNπ threshold (E_{th} ≈ 2.19 GeV) this state could also decay via $Q\bar{Q}$ pair creation. The final-state must then

$(Q^3)_8 - (Q^3)_8$	$Y = 1$				
$f(y,\imath)s$	$f(y,\imath)s$	s	$\imath$	M_m	M_1
$\underline{1}(0,0)\,1/2$	$\underline{8}(1,1/2)\,1/2$	$0,1$	$1/2$	-262	2368
$\underline{1}(0,0)\,1/2$	$\underline{8}(1,1/2)\,3/2$	$1,2$	$1/2$	-188	2442
$\underline{8}(0,0)\,1/2$	$\underline{8}(1,1/2)\,1/2$	$0,1$	$1/2$	-69	2561
$\underline{8}(0,1)\,1/2$	$\underline{8}(1,1/2)\,1/2$	$0,1$	$1/2,3/2$	-69	2561
$\underline{1}(0,0)\,1/2$	$\underline{10}(1,3/2)\,1/2$	$0,1$	$3/2$	-39	2591
$\underline{8}(0,0)\,3/2$	$\underline{8}(1,1/2)\,1/2$	$1,2$	$1/2$	-5	2625
$\underline{8}(0,1)\,3/2$	$\underline{8}(1,1/2)\,1/2$	$1,2$	$1/2,3/2$	-5	2625
$\underline{8}(0,0)\,1/2$	$\underline{8}(1,1/2)\,3/2$	$1,2$	$1/2$	5	2635
$\underline{8}(0,1)\,1/2$	$\underline{8}(1,1/2)\,3/2$	$1,2$	$1/2,3/2$	5	2635
$\underline{8}(0,0)\,3/2$	$\underline{8}(1,1/2)\,3/2$	$0,1,2,3$	$1/2$	69	2699
$\underline{8}(0,1)\,3/2$	$\underline{8}(1,1/2)\,3/2$	$0,1,2,3$	$1/2,3/2$	69	2699
$\underline{10}(0,1)\,1/2$	$\underline{8}(1,1/2)\,1/2$	$0,1$	$1/2,3/2$	124	2754
$\underline{8}(0,0)\,1/2$	$\underline{10}(1,3/2)\,1/2$	$0,1$	$3/2$	154	2784
$\underline{8}(0,1)\,1/2$	$\underline{10}(1,3/2)\,1/2$	$0,1$	$1/2,3/2,5/2$	154	2784
$\underline{10}(0,1)\,1/2$	$\underline{8}(1,1/2)\,3/2$	$1,2$	$1/2,3/2$	198	2828
$\underline{8}(0,0)\,3/2$	$\underline{10}(1,3/2)\,1/2$	$1,2$	$3/2$	218	2848
$\underline{8}(0,1)\,3/2$	$\underline{10}(1,3/2)\,1/2$	$1,2$	$1/2,3/2,5/2$	218	2848
$\underline{10}(0,1)\,1/2$	$\underline{10}(1,3/2)\,1/2$	$0,1$	$1/2,3/2,5/2$	347	2977

Table 4.3: The masses (in GeV) of $Y = 1$ dibaryon resonances. Each mass
M_ℓ *indicates a multiplet of resonances with*
$J = |\ell-s|, \ldots, |\ell+s|$ *and* $P = (-)^\ell$.

also contain an angular momentum barrier. The observed small width is
perhaps not in contradiction with this assignment.

D($\frac{1}{2}$, 2^+; 2.51) and D($\frac{3}{2}$, 2^+; 2.51) are companions of the
D(2, 1, 2^+; 2.36) dinucleon resonance in the irrep $\underline{27}$. They couple not
only to the $^1D_2$ ΛN and I = 1/2 ΣN channel and to the $^1D_2$ I = 3/2 ΣN
channel, but also to the $^5S_2$ Σ^*N and $\Sigma\Delta$ channels. Because their mass
is above the thresholds for these latter channels we expect, as
observed in the NN case, the resonance poles to shift (due to the
final-state interactions) to the neighborhood of these thresholds.

On these grounds one could expect for these states an experimental mass of about 2.32 GeV.

$D(\frac{1}{2}, 3^+; 2.51)$ is a companion of the $^3D_3$ NN resonance $D(2, 0, 3^+; 2.36)$ in the irrep $\underline{10}^*$. It couples to the $^3D_3$ ΛN and ΣN channels and to the $^7S_3$ $\Sigma^*\Delta$ channel. It is below the threshold for the latter channel. It is also coupled to ΛNπ via $Q\bar{Q}$ pair creation. We expect therefore a width for this state of the order of 100 MeV.

4.4.2. Orbitally excited Q^6 states

Having discussed the relevant Q^6 states we will turn now our attention to the orbitally excited states. Of these we will discuss only the states with the lowest masses.

$D(\frac{1}{2}, 1^-; 2.11)$ belongs to a nonet in the configuration $(Q^4)_3 - (Q^2)_3$ with $s = 0$, $\ell^P = 1^-$ and therefore $J^P = 1^-$. We would like to assign this state to the shoulder $B^2(\frac{1}{2}; 2.14)$. This state is then coupled to the $^1P_1$ and $^3P_1$ ΛN and ΣN channels. This state decays via the tunneling of a nonstrange quark into ΛN or ΣN or via the tunneling of a strange quark into ΛN. No change of orbital angular momentum and therefore no spin-flip is required in this tunneling. The observed small width, $\Gamma \approx 9$ MeV, does not seem unreasonable.

$D(\frac{1}{2}, J^P; 2.15)$ belongs again to a nonet in the configuration $(Q^4)_3 - (Q^2)_{3*}$ but now with $s = 1$, $\ell^P = 1^-$ and therefore $J^P = 0^-$, 1^- and 2^-. These states are coupled to the $^3P_0$, $^1P_1 + ^3P_1$, and the $^3P_2 + ^3F_2$ waves of the ΛN and ΣN channels. We would like to assign these states to the $B^2(\frac{1}{2}; 2.18)$ enhancement. The decay via tunneling goes exactly the same way as for the $D(\frac{1}{2}, 1^-; 2.11)$ state. The assignments of $D(2.11)$ and $D(2.15)$ to the states $B^2(2.14)$ and $B^2(2.18)$ is supported by the fact that their mass difference is only 40 MeV. This mass

difference is of color-magnetic origin. We believe that the mass

differences between states are much more accurately known in this

model (neglecting final-state interactions) than their total mass. It

is even surprising that the total masses seem to be only 30 MeV off.

It is noteworthy that extraneous states can also occur in the

$Y = 1$ channel. For baryons with spin $s = 1/2$, belonging to the flavor

octet B_8 the flavor representation in the baryon-baryon system B_8B_8

is given by

$$\underline{8} \otimes \underline{8} = (\underline{1} \oplus \underline{8}_S \oplus \underline{27}) \oplus (\underline{8}_A \oplus \underline{10} \oplus \underline{10}^*) \quad .$$

The flavor part of the wave function is symmetric for the flavor

irreps $\underline{1}$, $\underline{8}_S$, and $\underline{27}$, while it is antisymmetric for the irreps $\underline{8}_A$, $\underline{10}$

and $\underline{10}^*$. According to the generalized Pauli principle, the symmetric

flavor wave functions are allowed only in the ${}^1S$, ${}^3P$, ${}^1D$, ${}^3F$, etc.

waves and the antisymmetric flavor wave functions are allowed only in

the ${}^3S$, ${}^1P$, ${}^3D$, ${}^1F$, etc. waves of the B_8B_8 system. Dibaryon resonances

belonging to the flavor irreps $\underline{1}$ or $\underline{27}$ with $J^P = 1^+$, 3^+, 5^+, etc. and

belonging to the irreps $\underline{10}$ and $\underline{10}^*$ with $J^P = 0^+$; 0^-, 2^-, 4^-, etc.

therefore cannot decay into B_8B_8 and are called extraneous to B_8B_8 (see

table 4.4). As an example consider the $D(\frac{3}{2}$, $(0^-,\ 1^-,\ 2^-)$; 2.339)

states. The flavor representation $\underline{f}$ is found from table 4.3;

$\underline{f} = \underline{3} \otimes \underline{6} = \underline{8} \oplus \underline{10}$. As $(Y,\ I) = (1,\ 3/2)$ these states belong to the

irrep $\underline{10}$. The states $D(\frac{3}{2}$, 0^-; 2.339) and $D(\frac{3}{2}$, 2^-; 2.339) are thus

extraneous. Therefore the decay $D(1, \frac{3}{2}$, $(0^-,\ 2^-)$; 2.339) $\to \Sigma N$ is

forbidden. The $I = 1/2$ analogues of these states, $D(1, \frac{1}{2}$, $(0^-,\ 1^-,$

$2^-)$; 2.339), are not extraneous. As $(Y,\ I) = (1,\ 1/2)$ these states

belong to the irrep $\underline{8}$. This irrep, however, generally couples to both

the symmetric and antisymmetric octet in the B_8B_8 system. Another

138

baryon x baryon	flavor (isospin)	allowed BB waves	extraneous dibaryon states
$B_8 B_8$ (NN)	$\underline{1} + \underline{8}_D + \underline{27}$ (I = 1)	${}^1S_0 \qquad {}^1D_2$ ${}^3P_{0,1,2}$ $\cdots$	$1^+,\ 3^+,\ 5^+,\ \ldots$
	$\underline{8}_F + \underline{10} + \underline{10}^*$ (I = 0)	${}^3S_1 \quad {}^3D_{1,2,3}$ ${}^1P_1$ $\qquad \cdots$	0^+ $0^-,\ 2^-,\ 4^-,\ \ldots$
$B_{10} B_{10}$ (ΔΔ)	$\underline{27} + \underline{28}$ (I = 1, 3)	${}^1S, {}^5S \qquad {}^1D, {}^5D$ ${}^3P, {}^7P$ $\quad \cdots$	
	$\underline{35} + \underline{10}^*$ (I = 0, 2)	${}^3S, {}^7S \qquad {}^3D, {}^7D$ ${}^1P, {}^5P$ $\quad \cdots$	0^+ 0^-

Table 4.4: Extraneous dibaryon states (see text).

instructive example is formed by the Q^4-Q^2 states $D(1, \frac{3}{2}, (0^-, 1^-, 2^-); 2.393)$ and $D(1, \frac{3}{2}, (0^-, 1^-, 2^-); 2.428)$. The flavor representation is $\underline{15} \otimes \underline{3} = \underline{8} \oplus \underline{10} \oplus \underline{27}$. As the flavor symmetry is broken, the states with $(Y, I) = (1, 3/2)$ do not belong to either the irrep $\underline{10}$ or $\underline{27}$, but rather are mixtures. The 0^- and 2^- states then decay via the $\underline{27}$ component, which does couple to the $B_8 B_8$ system. The states at 2.393 GeV have the structure $(n^3 s)_3 - (n^2)_{3^*}$ and the states at 2.428 GeV the structure $(n^4)_3 - (ns)_{3^*}$. The energy difference is due to the different color-magnetic interactions of the nonstrange quarks n and strange quarks s.

The lowest ΛN resonances are predicted much closer to the ΛN threshold than the lowest NN resonances to the NN threshold. Therefore these ΛN resonances are more pronounced than the NN resonances and it is advisable to plan high statistics experiments to reconfirm these ΛN

resonances. We think here of $K^-d \rightarrow \Lambda\pi^-$ or $K^{-4}He \rightarrow (\Lambda N)X$ at
sufficiently high incident K^- momenta.

4.5. The Y = 0 dibaryon resonances

The calculated masses for the $Y = 0$ states are presented in
table 4.5. In the $I = 0$ channel the lowest state is $D(0, 0^+; 2.164)$,
which is a $\Lambda\Lambda$ bound state [Jaf 77.1]. Only via weak interactions can
it decay into ΛN. It has not yet been found [Car 78]. The states
$D(0, 1^-; 2.295)$ and $D(0, 1^-; 2.297)$ are predicted not far above the
thresholds of the $\Lambda\Lambda$ and ΞN thresholds to which they couple strongly
after tunneling. A probably narrow state is $D(0, 2^+; 2.414)$, which
requires a spin-flip to decay into ΞN and $\Lambda\Lambda$.

$(Q^6)_1$ Y = 0 $f(y,i)s$	$\Lambda\Lambda$ (2.23)	$N\Xi$ (2.25)	$\Lambda\Xi$ (2.31)	$\Sigma\Lambda$ (2.38)	$N\Xi^*$ (2.47)	$\Lambda\Sigma^*$ (2.50)	$\Delta\Xi$ (2.55)	$\Sigma\Sigma^*$ (2.58)	$\Delta\Xi^*$ (2.76)	$\Sigma^*\Gamma^*$ (2.77)	M_m	M_0
1 (0,0)0	x	x		x							-297	2164
8 (0,0)1	x	x		x	x			x			-115	2349
8 (0,1)1		x	x	x	x	x	x	x			-115	2349
8 (0,0)2					x			x			-50	2414
8 (0,1)2					x	x	x	x			-50	2414
10 (0,1)1		x	x	x	x	x	x	x			33	2497
10*(0,1)1		x	x	x					x	x	33	2497
27 (0,0)0	x	x		x						x	99	2563
27 (0,1)0		x	x	x					x	x	99	2563
27 (0,2)0				x					x	x	99	2563
27 (0,0)2					x			x		x	198	2662
27 (0,1)2					x	x	x	x	x	x	198	2662
27 (0,2)2							x	x	x	x	198	2662
10*(0,1)3									x	x	198	2662
35 (0,1)1					x	x	x	x	x	x	330	2794
35 (0,2)1							x	x	x	x	330	2794
28 (0,2)0									x	x	594	3058

(table 4.5)

$(Q^4)_3 - (Q^2)_{3^*}$ $Y = 0$				$\Lambda\Lambda$ (2.23)	$\bar N$ (2.25)	$\Lambda\Sigma$ (2.31)	$\Sigma\Sigma$ (2.38)	$\bar N^*$ (2.47)	$\Lambda\Sigma^*$ (2.50)	$\Delta\Xi$ (2.55)	$\Sigma\Sigma^*$ (2.58)	$\Lambda\Xi^*$ (2.76)	$\Sigma^*\Sigma^*$ (2.77)		
$f(y,i)s$	$f(y,i)s$	s	i											M_m	M_1
3 (−2/3,0)0	3* (2/3,0)0	0	0	×	×									−383	2295
3 (1/3,1/2)0	3* (−1/3,1/2)0	0	0,1	×	×	×	×							−381	2297
3 (−2/3,0)1	3* (2/3,0)0	1	0	×	×									−348	2330
3 (1/3,1/2)1	3* (−1/3,1/2)0	0	0,1	×	×	×	×							−341	2337
6* (−2/3,1)1	3* (2/3,0)0	1	1		×	×								−241	2437
6* (1/3,1/2)1	3* (−1/3,1/2)0	1	0,1	×	×	×	×							−221	2457
3 (1/3,1/2)0	6 (−1/3,1/2)1	1	0,1	×	×	×	×	×	×		×			−194	2484
15 (−2/3,0)0	3* (2/3,0)0	0	0	×	×									−170	2508
15 (−2/3,1)0	3* (2/3,0)0	0	1		×	×								−170	2508
3 (−2/3,0)0	6 (2/3,1)1	1	1		×	×			×	×				−157	2521
3 (1/3,1/2)1	6 (−1/3,1/2)1	0,1,2	0,1	×	×	×	×	×	×		×			−154	2524
15 (1/3,1/2)0	3* (−1/3,1/2)0	0	0,1	×	×	×	×							−140	2538
15 (1/3,3/2)0	3* (−1/3,1/2)0	0	1,2		×	×								−140	2538
15 (−2/3,0)1	3* (2/3,0)0	1	0	×	×			×						−135	2543
15 (−2/3,1)1	3* (2/3,0)0	1	1		×	×			×	×				−135	2543
3 (−2/3,0)1	6 (2/3,1)1	0,1,2	1		×	×			×	×				−121	2557
15 (1/3,1/2)1	3* (−1/3,1/2)0	1	0,1	×	×	×	×		×		×			−100	2578
15 (1/3,3/2)1	3* (−1/3,1/2)0	1	1,2		×	×			×	×	×			−100	2578
15 (−2/3,0)2	3* (2/3,0)0	2	0					×						−64	2614
15 (−2/3,1)2	3* (2/3,0)0	2	1					×	×					−64	2614
6* (4/3,0)1	6 (−4/3,0)1	0,1,2	0		×			×						−52	2626
6* (1/3,1/2)1	6 (−1/3,1/2)1	0,1,2	0,1	×	×	×	×	×	×		×			−33	2645
15 (1/3,1/2)2	3* (−1/3,1/2)0	2	0,1						×		×			−20	2658
15 (1/3,3/2)2	3* (−1/3,1/2)0	2	1,2						×	×	×			−20	2658
6* (−2/3,1)1	6 (2/3,1)1	0,1,2	0,1,2		×		×			×	×			−14	2664
15 (4/3,1)0	6 (−4/3,0)1	1	1		×			×						38	2716
15 (1/3,1/2)0	6 (−1/3,1/2)1	1	0,1	×	×	×	×	×	×		×			47	2725
15 (1/3,3/2)0	6 (−1/3,1/2)1	1	1,2		×	×					×			47	2725
15 (−2/3,0)0	6 (2/3,1)1	1	1		×	×			×	×				57	2735
15 (−2/3,1)0	6 (2/3,1)1	1	0,1,2		×			×		×	×			57	2735
15_s (−2/3,1)1	3* (2/3,0)0	1	1						×	×				79	2757
15 (4/3,1)1	6 (−4/3,0)1	0,1,2	1		×			×		×		×		83	2761
15 (1/3,1/2)1	6 (−1/3,1/2)1	0,1,2	0,1	×	×	×	×	×	×		×		×	87	2765
15 (1/3,3/2)1	6 (−1/3,1/2)1	0,1,2	1,2		×	×			×	×	×	×	×	87	2765
15 (−2/3,0)1	6 (2/3,1)1	0,1,2	1		×	×			×	×	×	×		92	2770
15 (−2/3,1)1	6 (2/3,1)1	0,1,2	0,1,2		×			×	×	×	×	×	×	92	2770
15_s (1/3,3/2)1	3* (−1/3,1/2)0	1	1,2						×	×	×			140	2818

(table 4.5)

141

$(Q^4)_3 - (Q^2)_{3*}$ Y = 0				(2.23) $\Lambda\Lambda$	(2.25) $\bar{N}$	(2.31) $\Lambda\Xi$	(2.38) $\Gamma\Xi$	(2.47) $N\bar{\Xi}^*$	(2.50) $\Lambda\bar{\Sigma}$	(2.55) Δ^-	(2.58) $\Sigma\bar{\Xi}^*$	(2.76) Δ^-	(2.77) $\Sigma\bar{\Sigma}^*$	M_m	M_1
f(y,ı)s	f(y,ı)s	s	ı												
<u>15</u> (-2/3,0)2	<u>6</u> (2/3,1)1	1,2,3	1					x			x			164	2842
<u>15</u> (-2/3,1)2	<u>6</u> (2/3,1)1	1,2,3	0,1,2					x		x	x	x		164	2842
<u>15</u> (1/3,1/2)2	<u>6</u> (-1/3,1/2)1	1,2,3	0,1						x		x		x	167	2845
<u>15</u> (1/3,3/2)2	<u>6</u> (-1/3,1/2)1	1,2,3	1,2						x	x	x	x	x	167	2845
<u>15</u> (4/3,1)2	<u>6</u> (-4/3,0)1	1,2,3	1							x		x		174	2852
<u>15</u>$_s$ (-2/3,1)1	<u>6</u> (2/3,1)1	0,1,2	0,1,2					x		x	x	x		306	2984
<u>15</u>$_s$ (1/3,3/2)1	<u>6</u> (-1/3,1/2)1	0,1,2	1,2						x	x	x	x	x	327	3005
<u>15</u>$_s$ (4/3,2)1	<u>6</u> (-4/3,0)1	0,1,2	2							x		x		354	3032

Table 4.5: The masses (in GeV) of Y = 0 dibaryon resonances. Each mass
M_ℓ indicates a multiplet of resonances with
$J = |\ell-s|,\ldots,|\ell+s|$ and $P = (-)^\ell$.

Experimental evidence for an I = 0 dibaryon resonance is seen ın
the enhancement in the $\Lambda\Lambda$ invarıant mass plots at 2.365 MeV wıth
$\Gamma \simeq 50$ MeV [Bei 72, Sha 78]. This ıs a candıdate for the D(0, 2^+;
2.414).

In the I = 1 channel the lowest state ıs D(1, 1^-; 2.297), decaying
into ΞN. D(1, 2^+; 2.414) and D(1, 3^+; 2.662) are narrow $(Q^6)_1$ states
decaying into $\Sigma\Lambda$ and ΞN after a spin-flıp.

In the I = 2 channel we mention D(2, 1^-; 2.538) decaying into $\Sigma\Sigma$,
and D(2, $(1^-, 2^-, 3^-)$; 2.658) decaying ınto $\Delta\Xi$ and $\Sigma\Sigma^*$. In both cases
these states are the lowest above the thresholds of the channels
mentioned.

Appendix A. Conventions and Notations

A.1. Metric tensor

$$g_{00} = -1 \quad , \quad g_{kk} = 1 \quad k \in \{1,2,3\} \quad , \quad g_{\mu\nu} = 0 \text{ when } \mu \neq \nu \quad .$$

A.2. γ-Matrices

The γ-matrices satisfy

$$\{\gamma_\mu, \gamma_\nu\} = 2 \, g_{\mu\nu} \qquad . \qquad (A.1)$$

We use the Pauli-Dirac representation. The matrices can be written as the direct product of 2×2 (hermitean) matrices (the matrix $\mathbf{1}$ and the Pauli matrices ρ_k or σ_k, $k \in \{1,2,3\}$). Explicitly the matrices are

$$\gamma_0 = i \, \rho_3 \qquad = \begin{pmatrix} i\mathbf{1} & 0 \\ 0 & -i\mathbf{1} \end{pmatrix}$$

$$\gamma_k = \rho_2 \, \sigma_k \qquad = \begin{pmatrix} 0 & -i\sigma_k \\ i\sigma_k & 0 \end{pmatrix}$$

$$\gamma_4 = -i \, \gamma_0 = \rho_3 = \begin{pmatrix} \mathbf{1} & 0 \\ 0 & -\mathbf{1} \end{pmatrix}$$

$$\gamma_5 = i \, \gamma_0\gamma_1\gamma_2\gamma_3$$
$$= \gamma_1\gamma_2\gamma_3\gamma_4 = -\rho_1 = \begin{pmatrix} 0 & -\mathbf{1} \\ -\mathbf{1} & 0 \end{pmatrix} \qquad (A.2)$$

Some of the γ-matrices are not hermitean; they all satisfy

$$\gamma_\mu^+ = \gamma_0\gamma_\mu\gamma_0 = -\gamma_4\gamma_\mu\gamma_4 \qquad . \qquad (A.3)$$

The contraction of a four-vector, e.g. p^μ and the matrices γ_μ is denoted

$$\not{p} = p^\mu \, \gamma_\mu \qquad . \qquad (A.4)$$

A.3. Fermion fields

The Lagrangian for massive free fermion fields is

$$\mathcal{L} = - \bar{\psi} \ (\not{\partial} + m) \ \psi \qquad , \qquad\qquad (A.5)$$

with

$$\bar{\psi} = \psi^+ \ \gamma_4 \qquad\qquad . \qquad\qquad (A.6)$$

The left-handed component of the Dirac spinor, which in momentum space is given by

$$\psi = \sqrt{E + m} \quad \begin{pmatrix} \chi \\ \dfrac{\vec{\sigma} \cdot \vec{p}}{E+m} \chi \end{pmatrix} \qquad\qquad (A.7)$$

is denoted by ψ_L and is projected out in the following way,

$$\psi_L = \begin{pmatrix} \dfrac{1 + \gamma_5}{2} \end{pmatrix} \psi \qquad\qquad . \qquad\qquad (A.8)$$

A.4. Units

We use units such that $\hbar = c = 1$. Then e.g. $1 \ \mathrm{GeV}^{-1} = .1973 \ \mathrm{fm}$, $1 \ \mathrm{GeV}^{-2} = .389 \ \mathrm{mb}$, $1 \ \mathrm{GeV}^{-1} = 6.582 \times 10^{-25} \ \mathrm{sec}$.

Appendix B. SU(n) groups

B.1. Irreducible representations of SU(n)

There is a one-to-one correspondence between irreducible represen-
tations (irreps) of the special unitary group SU(n) and the irreps of
the permutation groups SU(N), which are uniquely determined by Young
diagrams. A Young diagram for SU(n) has no more than n-1 rows and is
denoted by the number of blocks in each row (f_i) or equivalently by the
number of columns with i blocks.
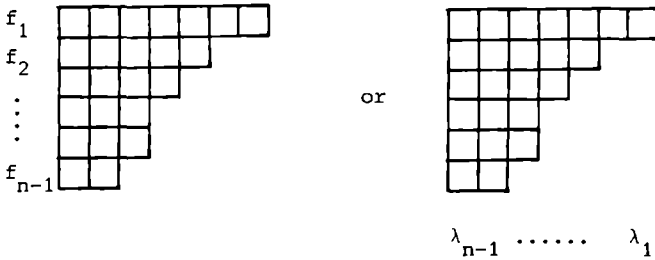
$$[f_1,f_2,\ldots,f_{n-1}] \qquad \text{or} \qquad (\lambda_1,\lambda_2,\ldots,\lambda_{n-1}) \qquad \text{(B.1)}$$

Using $q_i = \lambda_i + 1$ the dimensions of an irrep of SU(n) is given by

$$d(\lambda_i) = \{(q_1)(q_1+q_2)\ldots\ldots\ldots\ldots\ldots(q_1+q_2+\ldots+q_{n-1})/1!\}$$
$$\times \{(q_2)\ldots\ldots\ldots\ldots\ldots(q_2+\ldots+q_{n-1})/2!\}$$
$$\times \ldots$$
$$\times \{(q_{n-1})/(n-1)!\} \qquad \text{(B.2)}$$

For a more detailed discussion of Young diagrams and useful formulae
we refer to text books on group theory [Wyb 74, Lit 59] and the review
on Young tableaux [Itz 66].

B.2. SU(2)

Relevant SU(2) groups are the isospin and spin SU(2) groups,
denoted by SU(2,I) and SU(2,S).

B.2.1. Generators of SU(2)

The three generators of SU(2), when denoted by S_k, $k \in \{1,2,3\}$, satisfy the commutation relations

$$[S_k, S_\ell] = i \, \varepsilon_{k\ell m} \, S_m \qquad . \tag{B.3}$$

In the two-dimensional (self-conjugate) defining representation the generators are represented by the 2×2 matrices $S_k = \sigma_k/2$, where σ_k are the Pauli matrices,

$$\sigma_1 = \begin{pmatrix} 0 & 1 \\ 1 & 0 \end{pmatrix}, \quad \sigma_2 = \begin{pmatrix} 0 & -i \\ i & 0 \end{pmatrix}, \quad \sigma_3 = \begin{pmatrix} 1 & 0 \\ 0 & -1 \end{pmatrix}. \tag{B.4}$$

For isospin we use the notation I_k for the generators and τ_k for the Pauli matrices.

B.2.2. Irreps of SU(2), labeling, dimension and quadratic Casimir operators

The SU(2) quadratic Casimir operator for an N-particle system (particles labeled i,j) is

$$S^2 = \sum_{i,j} S_i \cdot S_j \qquad , \tag{B.5}$$

where the dot means summation over the group indices $k \in \{1,2,3\}$. The eigenvalue of this operator is $S(S + 1)$ where S has half-integer or integer values and is used to label the irreps, whose dimension is $2S + 1$.

B.2.3. Two-particle operators and permutation operators

The two-particle operator $\sigma_i \cdot \sigma_j$ can be expressed using the quadratic Casimir operator S^2 for the two-particle irrep;

$$\sigma_i \cdot \sigma_j = 2 \, S^2 - 3 \tag{B.6}$$

The value in the symmetric and antisymmetric two-particle irreps is:

Young diagram	S	$\sigma_1 \cdot \sigma_j$
⊟	0	-3
⊞	1	1

The two-particle permutation operator for SU(2) is given by

$$P_{ij} = \frac{1}{2}\,(1 + \sigma_1 \cdot \sigma_j) \qquad . \qquad\qquad (B.7)$$

B.3. SU(3) [Swa 66]

The important SU(3) groups are flavor SU(3) and color SU(3), denoted by SU(3,F) and SU(3,C).

B.3.1. Generators of SU(3)

The eight generators of SU(3) are denoted by F^a, $a \in \{1,\ldots,8\}$ and provided with a subscript c or f, if confusion about color and flavor may arise. In the three-dimensional defining representation (quarks) the generators are represented by the 3×3 matrices $F^a = \lambda^a/2$, where λ^a are the eight Gell-Mann matrices,

$$\lambda^1 = \begin{pmatrix} \cdot & 1 & \cdot \\ 1 & \cdot & \cdot \\ \cdot & \cdot & \cdot \end{pmatrix} \quad \lambda^2 = \begin{pmatrix} \cdot & -1 & \cdot \\ 1 & \cdot & \cdot \\ \cdot & \cdot & \cdot \end{pmatrix} \quad \lambda^3 = \begin{pmatrix} 1 & \cdot & \cdot \\ \cdot & -1 & \cdot \\ \cdot & \cdot & \cdot \end{pmatrix}$$

$$\lambda^4 = \begin{pmatrix} \cdot & \cdot & 1 \\ \cdot & \cdot & \cdot \\ 1 & \cdot & \cdot \end{pmatrix} \quad \lambda^5 = \begin{pmatrix} \cdot & \cdot & -1 \\ \cdot & \cdot & \cdot \\ 1 & \cdot & \cdot \end{pmatrix} \quad \lambda^6 = \begin{pmatrix} \cdot & \cdot & \cdot \\ \cdot & \cdot & 1 \\ \cdot & 1 & \cdot \end{pmatrix}$$

$$\lambda^7 = \begin{pmatrix} \cdot & \cdot & \cdot \\ \cdot & \cdot & -1 \\ \cdot & 1 & 0 \end{pmatrix} \quad \lambda^8 = \frac{1}{\sqrt{3}} \begin{pmatrix} 1 & \cdot & \cdot \\ \cdot & 1 & \cdot \\ \cdot & \cdot & -2 \end{pmatrix} \qquad , \qquad (B.8)$$

normalized to $\mathrm{Tr}\,\lambda^a \lambda^b = 2\,\delta_{ab}$. The matrices in the conjugate representation (antiquarks) are $F^a = -\lambda^{a*}/2$.

B.3.2. Irreps of SU(3), labeling, dimension and quadratic Casimir operators

The most common notations for SU(3) irreps are

$$(\lambda,\mu) \qquad \text{or} \qquad D(\lambda,\mu) \qquad \text{or} \qquad \underline{d} \qquad , \qquad (B.9)$$

where (λ,μ) is the notation from eq. (B.1) and $\underline{d}$ is the labeling with the dimension of the irrep,

$$d = (1 + \lambda)(1 + \mu)(1 + \frac{\lambda + \mu}{2}) \qquad (B.10)$$

As the classification of the irreps by their dimension is sometimes not unique subscripts have to be used in this case. The eigenvalue of the quadratic Casimir operator,

$$F^2 = \sum_{i,j} F_i \cdot F_j \qquad , \qquad (B.11)$$

in the irrep $D(\lambda,\mu)$ is given by

$$f^2 = \frac{1}{3}(\lambda^2 + \lambda\mu + \mu^2) + \lambda + \mu \qquad . \qquad (B.12)$$

For some relevant irreps we have listed the dimension and the eigenvalue of the quadratic Casimir operator.

Young diagram	(λ,μ)	$\underline{d}$	f^2
	(0,0)	$\underline{1}$	0
	(1,0)	$\underline{3}$	4/3
	(0,1)	$\underline{3}*$	4/3
	(2,0)	$\underline{6}$	10/3
	(1,1)	$\underline{8}$	3
	(3,0)	$\underline{10}$	6
	(0,2)	$\underline{6}*$	10/3
	(2,1)	$\underline{15}$	16/3
	(4,0)	$\underline{15}_s$	28/3
	(1,2)	$\underline{15}*$	16/3
	(3,1)	$\underline{24}$	25/3

Young diagram	(λ,μ)	$\underline{d}$	f^2
⊞⊞⊞⊞⊞	(5,0)	$\underline{21}$	40/3
⊞⊞	(0,3)	$\underline{10}^*$	6
⊞⊞⊞	(2,2)	$\underline{27}$	8
⊞⊞⊞⊞	(4,1)	$\underline{35}$	12
⊞⊞⊞⊞⊞⊞	(6,0)	$\underline{28}$	18

B.3.3. Decomposition $SU(3) \supset SU(2) \otimes U(1)$

Within the $SU(3)$ irreps $D(\lambda,\mu)$ the states can be distinguished by the $SU(2)$ quantum numbers I and I_3, and the hypercharge Y. The decomposition $SU(3) \supset SU(2) \otimes U(1)$ is given for some relevant irreps.

$SU(3)$ irrep		$SU(2) \otimes U(1)$ content $\sum(I,Y)$
$\underline{1}$	$\supset$	(0,0)
$\underline{3}$	$\supset$	(1/2,1/3) + (0,-2/3)
$\underline{6}$	$\supset$	(1,2/3) + (1/2,-1/3) + (0,-4/3)
$\underline{8}$	$\supset$	(1/2,1) + (0,0) + (1,0) + (1/2,-1)
$\underline{10}$	$\supset$	(3/2,1) + (1,0) + (1/2,-1) + (0,-2)
$\underline{15}$	$\supset$	(1,4/3) + (1/2,1/3) + (3/2,1/3) + (0,-2/3) + (1,-2/3)
		+ (1/2,-5/3)
$\underline{15}_s$	$\supset$	(2,4/3) + (3/2,1/3) + (1,-2/3) + (1/2,-5/3) + (0,-8/3)
$\underline{24}$	$\supset$	(3/2,5/3) + (1,2/3) + (2,2/3) + (1/2,-1/3) + (3/2,-1/3)
		+ (0,-4/3) + (1,-4/3) + (1/2,-7/3)
$\underline{21}$	$\supset$	(5/2,5/3) + (2,2/3) + (3/2,-1/3) + (1,-4/3)
		+ (1/2,-7/3) + (0,-10/3)
$\underline{27}$	$\supset$	(1,2) + (1/2,1) + (3/2,1) + (0,0) + (1,0) + (2,0)
		+ (1/2,-1) + (3/2,-1) + (1,-2)
$\underline{35}$	$\supset$	(2,2) + (3/2,1) + (5/2,1) + (1,0) + (2,0) + (1/2,-1)
		+ (3/2,-1) + (0,-2) + (1,-2) + (1/2,-3)
$\underline{28}$	$\supset$	(3,2) + (5/2,1) + (2,0) + (3/2,-1) + (1,-2) + (1/2,-3)
		+ (0,-4)

B.3.4. Two-particle operators and permutation operators

Using the quadratic Casimir operator the two-particle operator $F_i \cdot F_j$ is

$$F_i \cdot F_j = \frac{1}{2} F^2 - 4/3 \qquad , \qquad (B.13)$$

and its value in the symmetric and antisymmetric two-particle irreps is

Young diagram	$\underline{d}$	$F_i \cdot F_j$
	$\underline{3}^*$	$-2/3$
	$\underline{6}$	$1/3$

The two-particle permutation operator is

$$P_{ij} = 2 \ (\frac{1}{6} + F_i \cdot F_j) \qquad . \qquad (B.14)$$

B.4. SU(6)

The relevant SU(6) groups are the flavor-spin and color-spin groups, denoted by SU(6,FS) and SU(6,CS).

B.4.1. Generators of SU(6)

One way of writing down the generators of SU(6) is using the direct product of generators of SU(3) and SU(2). For the six-dimensional defining representation the 35 generators then are

$$\begin{array}{l} \frac{1}{\sqrt{6}} \ \sigma_k \\[4pt] F^a \\[4pt] \sigma_k \otimes F^a \end{array} \qquad k \in \{1,2,3\}, \ a \in \{1,\ldots,8\} \qquad (B.15)$$

These generators $A^\alpha, \alpha \in \{1,\ldots,35\}$, are normalized such that $\text{Tr} \ A^\alpha A^\beta = \delta_{\alpha\beta}$.

B.4.2. Irreps of SU(6), dimension and quadratic Casimir operators

The irreps of SU(6) are denoted by $[f]$, (λ) or $\{d\}$. $[f]$ and (λ)

are the notations introduced in eq. (B.1). {d} is the classification
with the dimension, which, if not unique, is provided with a subscript.
[f] is the most convenient notation, when one wants to reconstruct the
Young diagram, (λ) is most convenient to calculate the dimension (see
eq. (B.2)) or the eigenvalue a^2 of the quadratic Casimir operator A^2;

$$A^2 = \sum_{i,j} A_i \cdot A_j \quad ,$$

$$\begin{aligned}
a^2 = \frac{2}{3} [& 5 \lambda_1^2 + 8 \lambda_2^2 + 9 \lambda_3^2 + 8 \lambda_4^2 + 5 \lambda_5^2 \\
& + 30 \lambda_1 + 48 \lambda_2 + 54 \lambda_3 + 48 \lambda_4 + 30 \lambda_5 \\
& + 8 \lambda_1\lambda_2 + 6 \lambda_1\lambda_3 + 4 \lambda_1\lambda_4 + 2 \lambda_1\lambda_5 \\
& + 12 \lambda_2\lambda_3 + 8 \lambda_2\lambda_4 + 4 \lambda_2\lambda_5 + 12 \lambda_3\lambda_4 \\
& + 6 \lambda_3\lambda_5 + 8 \lambda_4\lambda_5]
\end{aligned} \qquad (B.16)$$

For some relevant irreps we have listed the dimension and the eigen-
value of the quadratic Casimir operator

[f]	{d}	a^2	[f]	{d}	a^2
[1]	{6}	35/6	$[2,1^3]$	{84}	95/6
$[1^2]$	{15}	28/3	$[2^2,1]$	$\{210_2\}$	131/6
[2]	{21}	40/3	$[3,1^2]$	{336}	155/6
$[1^3]$	{20}	21/2	[3,2]	{420}	179/6
[2,1]	{70}	33/2	$[1^6]$	{1}	0
[3]	{56}	45/2	$[2,1^4]$	{35}	12
$[1^4]$	{15*}	28/3	$[2^2,1^2]$	{189}	20
$[2,1^2]$	$\{105_1\}$	52/3	$[3,1^3]$	{280}	24
$[2^2]$	$\{105_2\}$	64/3	$[2^3]$	{175}	24
[3,1]	$\{210_1\}$	76/3	[3,2,1]	{896}	30
$[1^5]$	{6*}	35/6	$[3^2]$	{490}	36

B.4.3. Decomposition SU(6) $\supset$ SU(3) $\otimes$ SU(2)

As SU(6) is important because it is the direct product of an SU(3) and an SU(2) group, e.g. color and spin, which govern the color interactions, we are often interested in the decomposition in SU(3) and SU(2) irreps.

SU(6) irrep		SU(3) $\otimes$ SU(2) content $\quad \sum (\underline{d}, S)$
$\{1\}$	$\supset$	$(\underline{1}, 0)$
$\{6\}$	$\supset$	$(\underline{3}, 1/2)$
$\{15\}$	$\supset$	$(\underline{3}^*, 1) \oplus (\underline{6}, 0)$
$\{21\}$	$\supset$	$(\underline{3}^*, 0) \oplus (\underline{6}, 1)$
$\{20\}$	$\supset$	$(\underline{1}, 3/2) \oplus (\underline{8}, 1/2)$
$\{70\}$	$\supset$	$(\underline{1}, 1/2) \oplus (\underline{8}, 1/2) \oplus (\underline{8}, 3/2) \oplus (\underline{10}, 1/2)$
$\{56\}$	$\supset$	$(\underline{8}, 1/2) \oplus (\underline{10}, 3/2)$
$\{105_1\}$	$\supset$	$(\underline{3}, 0) \oplus (\underline{3}, 1) \oplus (\underline{3}, 2) \oplus (\underline{6}^*, 1) \oplus (\underline{15}, 0) \oplus (\underline{15}, 1)$
$\{105_2\}$	$\supset$	$(\underline{3}, 1) \oplus (\underline{6}^*, 0) \oplus (\underline{6}^*, 2) \oplus (\underline{15}, 1) \oplus (\underline{15}_s, 0)$
$\{210_1\}$	$\supset$	$(\underline{3}, 0) \oplus (\underline{3}, 1) \oplus (\underline{6}^*, 1) \oplus (\underline{15}, 0) \oplus (\underline{15}, 1) \oplus (\underline{15}, 2)$ $\oplus (\underline{15}_s, 1)$
$\{84\}$	$\supset$	$(\underline{3}^*, 1/2) \oplus (\underline{3}^*, 3/2) \oplus (\underline{6}, 1/2) \oplus (\underline{6}, 3/2) \oplus (\underline{15}^*, 1/2)$
$\{210_2\}$	$\supset$	$(\underline{3}^*, 1/2) \oplus (\underline{3}^*, 3/2) \oplus (\underline{3}^*, 5/2) \oplus (\underline{6}, 1/2) \oplus (\underline{6}, 3/2)$ $\oplus (\underline{15}^*, 1/2) \oplus (\underline{15}^*, 3/2) \oplus (\underline{24}, 1/2)$
$\{336\}$	$\supset$	$(\underline{3}^*, 1/2) \oplus (\underline{3}^*, 3/2) \oplus 2(\underline{6}, 1/2) \oplus (\underline{6}, 3/2) \oplus (\underline{6}, 5/2)$ $\oplus (\underline{15}^*, 1/2) \oplus (\underline{15}^*, 3/2) \oplus (\underline{24}, 1/2) \oplus (\underline{24}, 3/2)$
$\{420\}$	$\supset$	$(\underline{3}^*, 1/2) \oplus (\underline{3}^*, 3/2) \oplus (\underline{6}, 1/2) \oplus (\underline{6}, 3/2) \oplus (\underline{15}^*, 1/2)$ $\oplus (\underline{15}^*, 3/2) \oplus (\underline{15}^*, 5/2) \oplus (\underline{24}, 1/2) \oplus (\underline{24}, 3/2) \oplus (\underline{21}, 1/2)$
$\{35\}$	$\supset$	$(\underline{1}, 1) \oplus (\underline{8}, 0) \oplus (\underline{8}, 1)$
$\{175\}$	$\supset$	$(\underline{1}, 1) \oplus (\underline{1}, 3) \oplus (\underline{8}, 1) \oplus (\underline{8}, 2) \oplus (\underline{10}, 0) \oplus (\underline{10}^*, 0)$ $\oplus (\underline{27}, 1)$

$\{189\}$ ⊃ $(\underline{1},0)$ ⊕ $(\underline{1},2)$ ⊕ $(\underline{8},0)$ ⊕ $2(\underline{8},1)$ ⊕ $(\underline{8},2)$ ⊕ $(\underline{10},1)$

⊕ $(\underline{10}^*,1)$ ⊕ $(\underline{27},0)$

$\{280\}$ ⊃ $(\underline{1},1)$ ⊕ $(\underline{8},0)$ ⊕ $2(\underline{8},1)$ ⊕ $(\underline{8},2)$ ⊕ $(\underline{10},0)$ ⊕ $(\underline{10},1)$

⊕ $(\underline{10},2)$ ⊕ $(\underline{10}^*,0)$ ⊕ $(\underline{27},1)$

$\{896\}$ ⊃ $(\underline{1},1)$ ⊕ $(\underline{1},2)$ ⊕ $2(\underline{8},0)$ ⊕ $3(\underline{8},1)$ ⊕ $2(\underline{8},2)$ ⊕ $(\underline{8},3)$

⊕ $(\underline{10},0)$ ⊕ $2(\underline{10},1)$ ⊕ $(\underline{10},2)$ ⊕ $(\underline{10}^*,1)$ ⊕ $(\underline{10}^*,2)$

⊕ $(\underline{27},0)$ ⊕ $2(\underline{27},1)$ ⊕ $(\underline{27},2)$ ⊕ $(\underline{35},0)$ ⊕ $(\underline{35},1)$

$\{490\}$ ⊃ $(\underline{1},0)$ ⊕ $(\underline{8},1)$ ⊕ $(\underline{8},2)$ ⊕ $(\underline{10},1)$ ⊕ $(\underline{10}^*,1)$ ⊕ $(\underline{10}^*,3)$

⊕ $(\underline{27},0)$ ⊕ $(\underline{27},2)$ ⊕ $(\underline{28},0)$ ⊕ $(\underline{35},1)$

B.4.4. Two-particle operators and permutation operators

Using the quadratic Casimir operator of SU(6) the two-particle
operator $A_i \cdot A_j$ is

$$A_i \cdot A_j = \frac{1}{2} C_6 - 35/6 \qquad\qquad (B.17)$$

and its value in the symmetric and antisymmetric two-particle irreps is

Young diagram	$\{d\}$	$A_i \cdot A_j$
⊟	$\{15\}$	$-7/6$
⊞	$\{21\}$	$5/6$

The two-particle permutation operator is

$$P_{ij} = \frac{1}{6} + A_i \cdot A_j \qquad\qquad . \qquad\qquad (B.18)$$

References

Abe 73   E.S. Abers and B.W. Lee, Phys.Rep. 9C, 1 (1973)

Aer 78.1 A.T. Aerts, P.J. Mulders and J.J. de Swart, Phys.Rev. D 17, 260 (1978)

Aer 78.2 A.T. Aerts, P.J. Mulders and J.J. de Swart, in *Proceedings of the 8. International Conference in Graz, Few Body Systems and Nuclear Forces*, Graz, 1978, edited by H. Zingl, M. Haftel and H. Zankel (Springer-Verlag, New York, 1978), vol. I, p. 78

Aer 79.1 A.T. Aerts, *The MIT bag model and some spectroscopic applications*, thesis University of Nijmegen, June 1979

Aer 79.2 A.T. Aerts, P.J. Mulders and J.J. de Swart, University of Nijmegen report no THEF-NYM-79.18, to be published in Phys. Rev. D

Ala 76   B.S. Aladashvili et al., Nucl.Phys. A274, 486 (1976)

Ale 69   G. Alexander et al., Phys.Rev.Lett. 22, 483 (1969)

Als 78   M. Alston-Garnjost et al., Phys.Rev. D 18, 182 (1978)

And 68   H.L. Anderson et al., Phys.Rev.Lett. 21, 853 (1968)

Arn 68   R.A. Arndt, Phys.Rev. 165, 1834 (1968)

Aue 77   I.P. Auer et al., Phys.Lett. 67B, 113 (1977) and 70B, 475 (1977); Phys.Rev.Lett. 41, 354 (1978)

Aye 76   R. Ayed, thesis Saclay, 1976 (CEA-N-192)

Bei 72   P. Beillière et al., Phys.Lett. 39B, 671 (1972); G.A. Wilquet et al., Phys.Lett. 57B, 97 (1975)

Bei 76   P. Beillière et al., University of Brussels (ULB-VUB) report no IIHE-76.9 (1976)

Ben 76   C.M. Bender and P. Hays, Phys.Rev. D 14, 2622 (1976)

Bie 78   E.K. Biegert et al., Phys.Lett. <u>73B</u>, 235 (1978)

Bla 52   J.M. Blatt and V.F. Weisskopf, *Theoretical nuclear physics*,
          Wiley, New York (1952)

Boe 75   W. de Boer et al., Phys.Rev.Lett. <u>34</u>, 558 (1975)

Bow 77   K.C. Bowler and A.J.G. Hey, Phys.Lett. <u>69B</u>, 469 (1977)

Bow 79   K.C. Bowler and P.J. Walters, Phys.Rev. <u>D 19</u>, 3330 (1979)

Bra 77   O. Braun et al., Nucl.Phys. <u>B124</u>, 45 (1977)

Bro 79   G.E. Brown and M. Rho, Phys.Lett. <u>82B</u>, 177 (1979)

Cam 78   W. Cameron et al., Nucl.Phys. <u>B146</u>, 327 (1978)

Car 78   A.S. Carroll et al., Phys.Rev.Lett. <u>41</u>, 777 (1978)

Cha 77   Chan Hong-Mo and H. Høgaasen, Phys.Lett. <u>72B</u>, 121 (1977) and
          <u>72B</u>, 400 (1978)

Cha 78   Chan Hong-Mo and H. Høgaasen, Nucl.Phys. <u>B136</u>, 401 (1978)

Cho 74   A. Chodos, R.L. Jaffe, K. Johnson, C.B. Thorn and V.F.
          Weisskopf, Phys.Rev. <u>D 9</u>, 3471 (1974)

Cho 74   A. Chodos and C.B. Thorn, Phys.Rev. <u>D 12</u>, 2733 (1975)

Cli 68   D. Cline, R. Laumann and J. Mapp, Phys.Rev.Lett. <u>20</u>, 1452
          (1968)

Coc 63   G. Cocconi et al., Phys.Lett. <u>7</u>, 222 (1963)

Cut 77   R.E. Cutkosky and R.E. Hendrick, Phys.Rev. <u>D 16</u>, 2902 (1977)

Cut 79   R.E. Cutkosky, C.P. Forsyth, R.E. Hendrick and R.L. Kelly,
          Phys.Rev. <u>D 20</u>, 2839 (1979); R.E. Cutkosky et al., Phys.
          Rev. <u>D 20</u>, 2804 (1979)

Dal 79   R.H. Dalitz and L.J. Reinders, Oxford University report 1979
          (unpublished)

Dau 79   C. Daum et al. (ACCMOR Collaboration), CERN report no EP/
          79-110 (1979), submitted to Phys.Lett. <u>B</u>

DeG 75   T. DeGrand, R.L. Jaffe, K. Johnson and J. Kiskis, Phys.Rev.
          D 12, 2060 (1975)

DeG 76   T.A. DeGrand and R.L. Jaffe, Ann.Phys. (NY) 100, 425 (1976)
          and 101, 496 (1976)

DeG 78   T. DeGrand and C. Rebbi, Phys.Rev. D 17, 2358 (1978)

Den 71   D. Denegri et al., Nucl.Phys. B28, 13 (1971)

DeT 78   C. DeTar, Phys.Rev. D 17, 302 (1978) and D 17, 323 (1978)

DeT 79   C. DeTar, Phys.Rev. D 19, 1451 (1979)

Don 79   J.F. Donoghue and K. Johnson, MIT report no CTP-802 (1979)

Dos 78   H.G. Dosch and V. Hepp, Phys.Rev. D 18, 4071 (1978)

Eas 71   D. Eastwood et al., Phys.Rev. D 3, 2603 (1971)

Eng 79   J.J. Engelen, *Multichannel analysis of high statistics data
          on the reaction $K^-p \to \bar{K}^0 \pi^- p$ at 4.2 GeV/c*, thesis University
          of Nijmegen, February 1979

Fag 79   P.S. Fage, *The three-body problem and baryon spectroscopy*,
          thesis Oxford University, 1979

Fri 71   H. Fritzsch and M. Gell-Mann in *Proceedings of the Interna-
          tional Conference on duality and symmetry in hadron physics*
          (Weizmann Science Press, Jerusalem, 1971)

Fuk 78   M. Fukugita, K. Konishi and T.H. Hansson, Rutherford
          Laboratory report no RL-78-007/A

Gel 61   M. Gell-Mann, California Institute of Technology Synchroton
          Laboratory report no CTSL-20 (1961)

Gel 62   M. Gell-Mann, Phys.Rev. 125, 1067 (1962)

Gel 64   M. Gell-Mann, Phys.Lett. 8, 214 (1964)

Gla 61   S.L. Glashow, Nucl.Phys. 22, 579 (1961)

Gla 65   S.L. Glashow, Phys.Rev.Lett. 14, 35 (1965)

Gon 79 S. Gonggrijp, *Coupled channel approach to N-scattering involving inelasticity and bags. A study of the $^{1}D_{2}$ partial wave*, scriptie University of Nijmegen, 1979

Gre 64 O.W. Greenberg, Phys.Rev.Lett. <u>13</u>, 598 (1964)

Gre 78 W. Grein and P. Kroll, Nucl.Phys. <u>B137</u>, 173 (1978)

Gro 73 D. Gross and F. Wilczek, Phys.Rev.Lett. <u>30</u>, 1343 (1973)

Hau 77 J.M. Hauptmann, J.A. Kadijk and G.H. Trilling, Nucl.Phys. <u>B125</u>, 29 (1977)

Hey 75 A.J.G. Hey, P.J. Litchfield and R.J. Cashmore, Nucl.Phys. <u>B95</u>, 516 (1975)

Hid 77 K. Hidaka et al., Phys.Lett. <u>70B</u>, 479 (1977)

Hig 64 P.W. Higgs, Phys.Rev.Lett. <u>12</u>, 132 (1964) and <u>13</u>, 508 (1964)

Hir 79 T. Hirose et al., Nuov.Cim. <u>50A</u>, 120 (1979) and Tokyo Metropolitan University report no TMU-HEP-7910/Exp (1979)

Høg 78 H. Høgaasen and P. Sorba, Nucl.Phys. <u>B145</u>, 119 (1978)

Høg 79 H. Høgaasen and P. Sorba, Nucl.Phys. <u>B150</u>, 427 (1979)

Hoh 78 G. Höhler, F. Kaiser, R. Koch and E. Pietarinen, in *Handbook of pion-nucleon scattering*, ZAED Physics Data 12-1 (1979); updated and extended version of section 9, University of Karlsruhe report no TKP 79-15

Hoo 71 G. 't Hooft, Nucl.Phys. <u>B33</u>, 173 (1971)

Hor 73 R. Horgan and R.H. Dalitz, Nucl.Phys. <u>B66</u>, 135 (1973)

Hos 78 N. Hoshizaki, Prog.Theor.Phys. <u>60</u>, 1796 (1978)

Hos 79 N. Hoshizaki, Prog.Theor.Phys. <u>61</u>, 129 (1979)

Ike 79 H. Ikeda et al., Phys.Rev.Lett. <u>42</u>, 1321 (1979)

Ino 75 T. Inoue and T. Maskawa, Prog.Theor.Phys. <u>54</u>, 1833 (1975)

Isg 77   N. Isgur and G. Karl, Phys.Lett. 72B, 109 (1977); Phys.Rev.
          D 18, 4187 (1978); Phys.Lett. 74B, 353 (1978); Phys.Rev.
          D 19, 2653 (1979); Phys.Rev. D 20, 1191 (1979)

Itz 66   C. Itzykson and M. Nauenberg, Rev.Mod.Phys. 38, 95 (1966)

Jaf 76   R.L. Jaffe, in *Proceedings of the Topical Conference on
          Baryon resonances*, Oxford, 1976, edited by R.T. Ross and D.H.
          Saxon (Rutherford Laboratory, Chilton, Didcot, England, 1977)
          p. 455

Jaf 77.1 R.L. Jaffe, Phys.Rev.Lett. 38, 195 (1977)

Jaf 77.2 R.L. Jaffe, Phys.Rev. D 15, 267 (1977)

Jaf 77.3 R.L. Jaffe, Phys.Rev. D 15, 281 (1977)

Jaf 78   R.L. Jaffe, Phys.Rev. D 17, 1444 (1978)

Jaf 79.1 R.L. Jaffe and F.E. Low, Phys.Rev. D 19, 2105 (1979)

Jaf 79.2 R.L. Jaffe, in *Proceedings of the 1979 Erice Summer School*,
          Erice, 1979, edited by A. Zichichi (Plenum Press, New York,
          to be published), MIT report no CTP-814

Joh 76   K. Johnson and C.B. Thorn, Phys.Rev. D 13, 1934 (1976)

Joh 79.1 K. Johnson and C. Nohl, Phys.Rev. D 19, 291 (1979)

Joh 79.2 K. Johnson, MIT report no CTP-766 (1979)

Kad 71   J.A. Kadijk et al., Nucl.Phys. B27, 13 (1971)

Kam 77.1 T. Kamae et al., Phys.Rev.Lett. 38, 468 (1977)

Kam 77.2 T. Kamae and T. Fujita, Phys.Rev.Lett. 38, 471 (1977)

Kan 79   K. Kanai, A. Minaka, A. Nakamura and H. Sumiyoshi, Prog.
          Theor.Phys. 62, 153 (1979)

Kar 68   G. Karl and E. Obryk, Nucl.Phys. B8, 609 (1968)

Kec 56   J.C. Keck and A.V. Tollestrup, Phys.Rev. 101, 360 (1956)

Kib 67   T.W. Kibble, Phys.Rev. 155, 1554 (1967)

Klo 77   W.M. Kloet, R.R. Silbar, R. Aaron and R.D. Amado, Phys.Rev.
          Lett. _39_, 1643 (1977)

Kro 78   P. Kroll, in _Proceedings of the 13. Rencontre de Moriond_,
          France, 1978, edited by J. Tran Thanh Van (Université Paris
          Sud, 91405 Orsay, France, 1978)

Lam 66   R.C. Lamb et al., Phys.Rev.Lett. _17_, 100 (1966)

Lan 76   K. Lanius, in _Proceedings of the XVIII. International
          Conference on High Energy Physics_, Tbilisi, 1976, edited by
          N.N. Bogolubov et al. (JINR, Dubna, U.S.S.R., 1977), vol. I,
          p. C45

LB 68   _Landolt-Börnstein vol. 3_, by H. Appel; edited by H. Schopper,
          Springer-Verlag, New York, 1968

Lic 78   D.B. Lichtenberg, E. Predazzi, D.H. Weingarten and J.G. Wills,
          Phys.Rev. _D 18_, 2569 (1978)

Lit 50   D. Littlewood, _Theory of group characters and matrix repre-
          sentations_, Oxford University Press, New York, 1950

Lon 77   R.S. Longacre and J. Dolbeau, Nucl.Phys. _B122_, 493 (1977)

Mar 78   W. Marciano and H. Pagels, Phys.Rep. _36C_, 137 (1978)

Mat 77   V. Matveev and P. Sorba, Lett.Nuov.Cim. _20_, 425 (1977)

Mul 78.1 P.J. Mulders, A.T. Aerts and J.J. de Swart, Phys.Rev.Lett.
          _40_, 1543 (1978)

Mul 78.2 P.J. Mulders, A.T. Aerts and J.J. de Swart, University of
          Nijmegen report no THEF-NYM-78.3, submitted to XIX. Inter-
          national Conference on High Energy Physics, Tokyo, 1978

Mul 78.3 P.J. Mulders, A.T. Aerts and J.J. de Swart, in _Proceedings
          of the meeting on exotic resonances_, Hiroshima, Japan, 1978,
          edited by I. Endo et al. (Dept. of Physics, Hiroshima Univer-
          sity, Hiroshima, 1978)

Mul 78.4   P.J. Mulders, A.T. Aerts and J.J. de Swart, in *Proceedings of the international meeting on frontiers of physics*, Singapore, 1978, edited by K.K. Phua, C.K. Chew and Y.K. Lim (Singapore National Academy of Science, Singapore, 1978), vol. 2, p. 863

Mul 79.1   P.J. Mulders, A.T. Aerts and J.J. de Swart, Phys.Rev. D 19, 2635 (1979)

Mul 79.2   P.J. Mulders, A.T. Aerts and J.J. de Swart, University of Nijmegen report no THEF-NYM-79.19, submitted to Phys.Rev. D

Nag 75   M.M. Nagels, T.A. Rijken and J.J. de Swart, Phys.Rev. D 12, 744 (1975)

Nag 78   M.M. Nagels, T.A. Rijken and J.J. de Swart, Phys.Rev. D 17, 768 (1978)

Nam 66   Y. Nambu, in *Preludes in Theoretical Physics*, edited by A. de Shalit, H. Feshbach and L. van Hove (North Holland, Amsterdam, 1966), p. 133

Nee 61   Y. Ne'eman, Nucl.Phys. 26, 222 (1961)

Oza 78   S. Ozaki, in *Proceedings of the XIX. International Conference on High Energy Physics*, Tokyo, 1978, edited by S. Homma, M. Kawaguchi and H. Miyazawa (Physical Society of Japan, Tokyo, 1979), p. 101

PDG 78   Particle Data Group, Phys.Lett. 75B, 1 (1978)

Pol 73   H.D. Politzer, Phys.Rev.Lett. 30, 1346 (1973)

Pro 79   S.D. Protopopescu et al., Phys.Rev. D 7, 1279 (1973)

Reb 76   C. Rebbi, Phys.Rev. D 14, 2362 (1976)

Rei 78   L.J. Reinders, J.Phys. G 4, 1241 (1978)

Roi 79   C. Roiesnel, Phys.Rev. D 20, 1446 (1979)

Ruj 75   A. De Rújula, H. Georgi and S.L. Glashow, Phys.Rev. D 12, 147 (1975)

Sal 68   A. Salam, *Elementary particle theory. relativistic groups and analyticity* (Nobel symposium no 8), edited by N. Svartholm (Almqvist and Wiksell, Stockholm, 1968), p. 367

Sax 80   D.H. Saxon et al., Nucl.Phys. $\underline{B162}$, 522 (1980)

Sha 73   B.A. Shahbazian and A.A. Timonina, Nucl.Phys. $\underline{B53}$, 19 (1973); B.A. Shahbazian, N.A. Kalinina and A.A. Timonina, Lett.Nuov. Cim. $\underline{6}$, 63 (1973), B.A. Shahbazian, P.P. Temnikov, A.A. Timonina and A.M. Rozhdestvensky, in *Proceedings of the Tblisi Conference* (see Lan 76), Vol. I, p. C35

Sha 78   B.A. Shahbazian, P.P. Temnikov and A.A. Timonina, JINR report no E1-11839

Sha 79   B.A. Shahbazian et al., JINR report no E1-11877; in *Proceedings of the International Symposium on New Particle Problems in Nuclear Physics*, Dubna, 1979; in *Proceedings of the 1979 International Conference on Hypernuclear and Low Energy Kaon Physics*, Jabłonna, Poland, 1979

Sim 71   W.H. Sims et al., Phys.Rev. $\underline{D\ 3}$, 1162 (1971)

So   79   S.I. So and D. Strottman, J.Math.Phys. $\underline{20}$, 153 (1979)

Som 78   L.J.A.M. Somers, $Q^2\bar{Q}^2$ *and* $Q^4\bar{Q}$ *s-wave hadrons in the bag model*, scriptie University of Nijmegen, 1978

Som 80   L.J. Somers and J.J. de Swart, University of Nijmegen report no THEF-NYM-80.1

Str 79   D. Strottman, Phys.Rev. $\underline{D\ 20}$, 748 (1979)

Swa 62   J.J. de Swart and C.K. Iddings, Phys.Rev. $\underline{128}$, 2810 (1962), G. Fast, J.C. Helder and J.J. de Swart, Phys.Rev.Lett. $\underline{22}$, 1453 (1966); M.M. Nagels, T.A. Rijken and J.J. de Swart, Phys.Rev. $\underline{D\ 20}$, 1633 (1979)

Swa 66   J.J. de Swart, in *Proceedings of the 1966 CERN School of Physics* (CERN report no 66-29), vol. II

Swa 79.1 J.J. de Swart, G. Austen, P.J. Mulders and T.A. Rijken, University of Nijmegen report no THEF-NYM-79.15, in *Proceedings of the Dubna conference* (see Sha 79)

Swa 79.2 J.J. de Swart, University of Nijmegen report no THEF-NYM-79-16, in *Proceedings of the Jabłonna Conference* (see Sha 79)

Tan 69   T.H. Tan, Phys.Rev.Lett. 23, 395 (1969)

Ued 78   T. Ueda, Phys.Lett. 79B, 487 (1978)

Wei 67   S. Weinberg, Phys.Rev.Lett. 19, 1264 (1967)

Wyb 74   B.G. Wybourn, *Classical Groups for Physicists*, Wiley, New York, 1974

Yan 54   C.N. Yang and H. Mills, Phys.Rev. 96, 192 (1954)

Zra 79   M. Zrałek et al., Phys.Rev. D 19, 820 (1979)

Zwe 64   G. Zweig, CERN reports no TH-401 and TH-412 (1964)

163

In 1964 werden "quarks" geïntroduceerd om op een natuurlijke wijze het grote aantal hadronen te verklaren. Hadronen zijn deeltjes die sterke wisselwerkingen voelen; de bekendste zijn de nucleonen, proton en neutron. De in 1964 bekende hadronen waren deeltjes opgebouwd uit een quark en een antiquark ($Q\bar{Q}$), mesonen of deeltjes opgebouwd uit drie quarks (Q^3), baryonen. Deeltjes met zodanige eigenschappen dat het onmogelijk $Q\bar{Q}$- of Q^3-toestanden konden zijn, werden *exotische* deeltjes genoemd. Echt exotische deeltjes waren er niet; het deuteron bijvoorbeeld is geen exotisch deeltje met zes quarks, maar een gebonden toestand van een proton en een neutron ten gevolge van attraktieve meson-uitwisselings-krachten.

In de afgelopen vijf jaren is de situatie sterk veranderd. Allereerst kwam het "MIT bag model". Dit model maakte kwantitatieve voorspellingen mogelijk voor veel-quark toestanden. Jaffe liet zien dat de $J^{PC} = 0^{++}$ mesonen, $\epsilon(760)$, $S^*(980)$ en $\delta(980)$ *crypto-exotische* deeltjes zijn. Ze hebben een exotische quark-inhoud, namelijk $Q^2\bar{Q}^2$ maar ze hebben quantumgetallen die ook voor $Q\bar{Q}$-mesonen mogelijk zijn. Jaffe voorspelde ook echte exotische deeltjes opgebouwd uit zes quarks (Q^6). Naast deze kwantitatieve voorspellingen is er het toenemende aantal experimenten die aanwijzingen geven voor exotische Q^6 toestanden in baryon-baryon kanalen en exotische $Q^4\bar{Q}$ toestanden, bijvoorbeeld baryonen met hyperlading $Y = 2$ (Z^*'s).

Het "MIT bag model" is een fenomenologische toepassing van Quantum-Chromo-Dynamika (QCD) dat de kleur-wisselwerkingen tussen gekleurde quarks beschrijft, zoals Quantum-Elektro-Dynamika (QED) de

elektromagnetische wisselwerkingen tussen geladen deeltjes beschrijft.

Een mogelijk, nog niet bewezen gevolg van QCD is de permanente opslui-
ting van quarks in het hadron. In het "MIT bag model" is dit a priori
ingebouwd. Het model heeft succes geoogst met de berekening van de
massa's van de lichte hadronen ($Q\bar{Q}$ en Q^3) en met de beschrijving van
de laagstgelegen $Q^2\bar{Q}^2$ mesonen. Deze laatste berekening toonde de
betrouwbaarheid van berekeningen voor hadronen waarvoor het aantal
quarks en antiquarks groter dan drie is.

Bij kollektieve rotaties worden de veel-quark "bags" sigaarvormig.
Aan beide einden van de sigaarvormige "bag" bevinden zich een aantal
quarks, voor baryonen bijvoorbeeld twee aan de ene kant en een aan de
andere kant (Q^2-Q). De beide groepen van quarks aan de uiteinden hebben
een kleurlading die een sterke aantrekkende (kleur-elektrische) kracht
veroorzaakt. Het kleur-elektrische veld in de cylindervormige "bag" is
homogeen en geeft een konstante kracht. Dit leidt tot een lineair
verband tussen het kwadraat van de energie van de "bag" en het impuls-
moment ℓ. Tussen de quarks in de uiteinden werken alleen zwakkere
kleur-magnetische wisselwerkingen die een fijnopsplitsing van de
rotatieniveaux geven.

Bovenstaande aannamen maken het mogelijk zonder parameters te
introduceren de massa's van roterende veel-quark systemen te berekenen.
Het blijkt echter voor het laagste rotatieniveau ($\ell = 1$) van de
baryonen nodig enkele fenomenologische bijdragen in rekening te
brengen. Deze zijn het gevolg van het feit dat voor lichte deeltjes met
een klein impulsmoment de bag nog maar weinig van de bolvorm afwijkt
en een quark gemakkelijk van de ene naar de andere kant kan tunnelen.

Het onderzoek naar de massa's, stabiliteit en vervalswijzen van

$Q\bar{Q}$, $Q^2\bar{Q}^2$, Q^3, $Q^4\bar{Q}$ en Q^6 systemen is uitgevoerd samen met A.Th.M. Aerts. De resultaten voor $Q\bar{Q}$-, $Q^2\bar{Q}^2$- en ($\ell = 0$) Q^6-systemen staan beschreven in het proefschrift van A.Th.M. Aerts, terwijl die voor Q^3, $Q^4\bar{Q}$ en Q^6 systemen staan beschreven in dit proefschrift.

Curriculum Vitae

Ik werd geboren op 22 september 1953 te Veulen-Venray, waar ik van september 1959 tot augustus 1965 lager onderwijs genoot aan de St. Anthoniusschool. De opleiding Gymnasium B volgde ik van 1965 tot 1971 aan het Boschveldcollege te Venray. Vanaf september 1971 studeerde ik natuurkunde aan de Katholieke Universiteit te Nijmegen. Na het kandidaatsexamen (maart 1974) koos ik theoretische hoge-energiefysika als specialisatie. Sinds mijn doctoraal-examen op 8 april 1976 ben ik als wetenschappelijk medewerker in dienst van de Stichting voor Fundamenteel Onderzoek der Materie (F.O.M.) en verbonden aan het Instituut voor Theoretische Fysika te Nijmegen.

STELLINGEN

I

Een analyse van de effecten die lange-dracht interakties in het $\pi\pi$-kanaal (ρ uitwisseling) hebben, laat zien dat deze interakties weinig invloed hebben op de posities van de polen in de P-matrix (Jaffe en Low); eenzelfde analyse laat zien dat voor het NN-kanaal (π uitwisseling) grote verschuivingen in de posities van de polen te verwachten zijn.

R.L. Jaffe en F.E. Low, Phys.Rev. D 19, 2105 (1979)

II

De D15(1920) baryon resonantie in de reaktie $\pi^- p \to K\Lambda$ (Saxon et al.) koppelt relatief sterk aan het ΛK-kanaal. In πN analyses (Hohler et al.) is een D15(2180) resonantie gevonden. Het grote massaverschil tussen deze resonanties en de koppeling aan het ΛK-kanaal geeft aanleiding bovengenoemde resonanties als twee verschillende $\ell = 3$ Q^2-Q baryon toestanden te klassificeren.

D.H. Saxon et al., Nucl.Phys. B162, 522 (1980)
G. Hohler et al., ZAED Physics Data 12-1 (1979)
dit proefschrift, H. 3

III

Bij het gebruik van fantasie-namen voor deeltjes en hun eigenschappen, zoals quark, smaak, vreemdheid, tover, kleur, technicolor, is soms een sceptische houding te bespeuren bij op andere terreinen werkzame fysici; deze houding is onterecht.

De drie-deeltjes golffunkties die gebruikt worden in niet-relativisti-
sche potentiaalmodellen om de baryon resonanties te klassificeren in
"flavor-spin" SU(6) multipletten, zijn niet bruikbaar in geexciteerde
"bags" door de extra vrijheidsgraad, die door de gluon-velden geintro-
duceerd wordt.

G. Karl en E. Obryk, Nucl.Phys. B8, 609 (1968)

V

Het meten en analyseren van de hoekverdeling van pionen in de reaktie

$$K^- d \rightarrow \pi^- D$$
$$\quad\quad \hookrightarrow \Lambda N$$
$$\quad\quad\quad \hookrightarrow N\pi$$
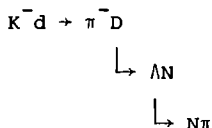
met een gepolariseerd deuteron "target", kan aanwijzingen geven voor
de spin en pariteit van de ΛN resonanties met massa's M = 2129 en
2139 MeV.

T.H. Tan, Phys.Rev.Lett. 23, 395 (1969)

VI

Bij in de toekomst te bouwen versnellers dient men mede in verband met
de kosten te overwegen of het bereiken van een hogere bundel-intensi-
teit niet moet prevaleren boven het bereiken van hogere energieen.

R.R. Wilson, Sci.Am. 242, no. 1, 26 (1980)

Eén-gluon uitwisseling en quark verwisselingen geven geen volledige beschrijving van nucleon-nucleon wisselwerkingen. Hieruit volgt dat de berekening van de energie van een gedeformeerde zes-quark bag niet het meson-uitwisselingsdeel van de NN potentiaal bevat, afgezien van de moeilijkheden deze energie te relateren aan het NN systeem.

> *S.J. Brodsky, C.E. Carlson en H. Lipkin, Phys.Rev. <u>D 20</u>, 2278 (1979)*
>
> *C. DeTar, Phys.Rev. <u>D 17</u>, 323 (1978)*

VIII

Een veelvoorkomende misvatting is dat de bandenstruktuur in vaste stoffen een gevolg is van de roosterperiodiciteit.

IX

Het is hypocriet het opschrift "Atoomenergie - nee bedankt" op een auto aan te brengen.

2 mei 1980   P.J.G. Mulders